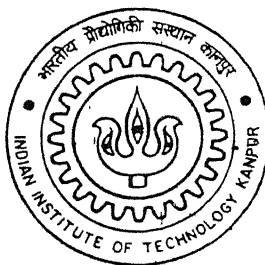


Y010646

QUANTITATIVE CHARACTERIZATION OF SILICON CARBIDE PARTICULATE REINFORCED ALUMINIUM MATRIX COMPOSITES.

By

Sudin Chatterjee



TH
MME/2001/M
C.3029

DEPARTMENT OF MATERIALS AND METALLURGICAL ENGINEERING

Indian Institute of Technology Kanpur

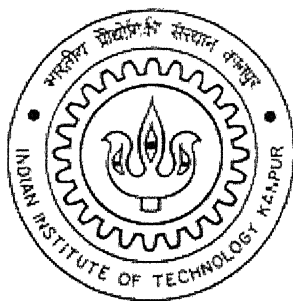
DECEMBER, 2001

**QUANTITATIVE CHARACTERIZATION OF SILICON CARBIDE
PARTICULATE REINFORCED ALUMINIUM MATRIX
COMPOSITES.**

A Thesis Submitted in
Partial fulfillment of the requirements for the degree of
Masters of Technology.

By

Sudin Chatterjee



**DEPARTMENT OF MATERIALS AND METALLURGICAL ENGINEERING
INDIAN INSTITUTE OF TECHNOLOGY
KANPUR**

- 5 MAR 2002/MMA

पुरुषोत्तम राजे राधे केशव पृथ्वी नारायण

भारतीय प्रौद्योगिकी संस्थान कानपुर

प्राप्ति क्र० A.13.7.9.5.5.....



A137955



CERTIFICATE

It is certified that the work contained in this thesis entitled
“*Quantitative Characterization of Silicon Carbide Particulate Reinforced
Aluminium Matrix Composites*” by Sudin Chatterjee, has been carried out
under my supervision and this work has not been submitted elsewhere for
any degree.

Asim Tewari
Dr. Asim Tewari
Asst. Professor
Dept. of Materials and Metallurgical Engineering
Indian Institute of Technology
Kanpur

December, 2001

ACKNOWLEDGEMENT

I would like to express my sincere thanks to my thesis supervisor Dr. Asim Tewari for giving me the opportunity to work on this project. I am extremely thankful to him for his guidance, fruitful suggestions and inspiration.

I would like to thank all laboratory staff members for helping me in conducting various experiments during my course work.

Last but not the least, I am grateful to Dr. M.N. Mungole for the cooperation and suggestions provided in conducting some of the experiments during the entire course of this work.

Sudin Chatterjee

LIST OF SYMBOLS

| | |
|------------------------------------|----------------------------------|
| <i>MMC</i> | Metal Matrix Composites |
| <i>CMC</i> | Ceramic Matrix Composites |
| <i>PMC</i> | Polymeric Matrix Composites |
| <i>PM</i> | Powder Metallurgy |
| <i>VIIP</i> | Vacuum Hot Pressed |
| <i>PVD</i> | Physical Vapor Deposition |
| <i>OA</i> | Over Aged |
| <i>UA</i> | Under Aged |
| <i>PFZ</i> | Precipitate Free Zone |
| <i>Ti</i> | Titanium |
| <i>Fe</i> | Iron |
| <i>Cu</i> | Copper |
| <i>Pb</i> | Lead |
| <i>Zn</i> | Zinc |
| <i>Mg</i> | Magnesium |
| <i>Si</i> | Silicon |
| <i>Al</i> | Aluminium |
| <i>SiC</i> | Silicon Carbide |
| <i>SiCp</i> | Silicon Carbide Particulate |
| <i>SiCw</i> | Silicon Carbide Whisker |
| <i>Al₄C₃</i> | Aluminium Carbide |
| <i>MgSi₂</i> | Magnesium Silicide |
| <i>E</i> | Elastic Modulus |
| <i>W</i> | Weight |
| <i>V</i> | Velocity |
| <i>L</i> | Length |
| <i>TS</i> | Tensile Strength |
| <i>MP</i> | Melting Point |
| <i>CTE</i> | Coefficient of Thermal expansion |
| <i>TC</i> | Thermal Conductivity |

| | |
|-----------------|--|
| σ | Stress |
| σ_{fat} | Fatigue Strength |
| $\sigma_{0.2}$ | Proof Stress |
| ε | Strain |
| a | Crack Length |
| N | Number of Cycles to Failure |
| ΔK | Stress Intensity factor Range |
| ΔK_{th} | Threshold value of Stress Intensity factor Range |
| r_Y | Plastic zone size |
| K_m | Elastic bulk modulus (matrix) |
| μ_{ms} | Elastic Strain modulus (matrix) |
| K_p | Elastic bulk modulus (particle) |
| μ_p | Elastic Strain modulus (particle) |
| ρ | Density |
| V_v | Volume Fraction |
| S_v | Surface area per unit volume |
| P_L | Points of intersection per unit length |
| P_P | Point Fraction |
| λ | Mean Free Distance |
| D | Particle Size. |

CONTENTS

| | |
|---|----|
| LIST OF FIGURES | i |
| LIST OF TABLES..... | v |
| ABSTRACT..... | vi |
| <u>CHAPTER 1</u> INTRODUCTION | 1 |
| <u>CHAPTER 2</u> LITERATURE REVIEW | 2 |
| 2 1. COMPOSITES | 2 |
| 2.1.1. Classification of Composite Materials:..... | 3 |
| 2 2.METAL MATRIX COMPOSITES..... | 4 |
| 2.2.2.Types of Metal Matrix Composites.. | 5 |
| 2.3.SILICON CARBIDE PARTICULATE REINFORCED ALUMINIUM MATRIX COMPOSITES | 8 |
| 2.4. PROCESSING OF METAL MATRIX COMPOSITES | 8 |
| 2.4.1. Primary Liquid Phase Processing..... | 9 |
| 2.4.2. Primary Solid State Processing | 13 |
| 2.4.3. Secondary Processing..... | 14 |
| 2.5. MECHANICAL BEHAVIOUR OF Al-SiCp METAL MATRIX COMPOSITES | 15 |
| 2.5.1. Stress-Strain Curve..... | 15 |
| 2.5.2.Factors Affecting Modulus of Elasticity | 17 |
| 2.5.3.Factors Influencing Strength | 17 |
| 2.6.FAILURE PROCESS AND FRACTURE TOUGHNESS OF ALUMINIUM- SILICON CARBIDE METAL MATRIX COMPOSITES | 19 |
| 2.6.1. Micro-Damage Process | 19 |
| 2.7.FATIGUE PROPERTIES OF PARTICULATE METAL MATRIX COMPOSITES | 22 |
| 2.8.EFFECTS OF MICROSTRUCTURAL VARIABLES ON THE FRACTURE AND FATIGUE PROPERTIES OF ALUMINIUM SILICON CARBIDE PARTICULATE MMCs | 24 |

| | |
|--|----|
| 2.9 EFFECT OF MATRIX AGEING ON THE PROPERTIES OF <i>Al-SiCp</i> METAL MATRIX COMPOSITES..... | 28 |
| 2.10.EFFECT OF PROCESSING ON THE MICROSTRUCTURE AND..... | 28 |
| PROPERTIES OF <i>Al-SiCp</i> METAL MATRIX COMPOSITES | 28 |
| 2.10.1. Effect of Primary Liquid Processing Technique..... | 28 |
| 2.10.2. Effect of Solid State Processing and Secondary Processing technique | 30 |
| 2.11. QUANTITATIVE STEREOLOGY | 31 |
| 2.11.1. Measurement of Volume Fraction (V_v)..... | 31 |
| 2.11.2. Measurement of Surface Area per unit Volume (S_v) | 31 |
| 2.11.3. Measurement of Mean Free Distance (λ) | 32 |
| 2.11.4. Measurement of Particle Size (D) | 32 |
| 2.11.5. Error Analysis | 32 |
| 2.12.TABLES | 34 |
| 2.13.FIGURES..... | 36 |
| <u>CHAPTER 3. EXPERIMENTAL DETAILS</u> | 50 |
| 3.1. Material..... | 50 |
| 3.2. Density Measurement..... | 50 |
| 3.3. Measurement of Elastic Modulus..... | 50 |
| 3.4. High Temperature Compression Testing..... | 51 |
| 3.5. Micro-Hardness Test | 51 |
| 3.6. Specimen Preparation for Metallographic Observations..... | 52 |
| 3.7. Quantitative Stereology | 53 |
| 3.8.TABLES | 54 |
| 3.9.FIGURES..... | 55 |
| <u>CHAPTER 4. RESULTS AND DISCUSSION</u> | 57 |
| 4.1. QUALITATIVE RESULTS | 57 |
| 4.1.1. Microstructure | 57 |
| 4.1.2. Stress-Strain Plots | 57 |
| 4.1.3. Effect of Temperature on Flow Stress..... | 57 |
| 4.2. QUANTITATIVE ANALYSIS..... | 58 |
| 4.2.1.Quantitative Stereology..... | 58 |

| | |
|--|----|
| 4.2.2.Effect of Volume Fraction (V_v) and Particle Size (D) on Mean Free Distance (λ) | 58 |
| 4.2.3.Effect of Volume Fraction on Elastic Modulus (E) | 58 |
| 4.2.4.Effect of Volume Fraction (V_v), and Mean Free Distance (λ) on the Flow Stress | 59 |
| 4.2.5.Variation of Stress Ratios ($\sigma_{350}^{\circ}\text{C} / \sigma_{150}^{\circ}\text{C}$) with Strain | 60 |
| 4.2.6. Micro-Hardness | 60 |
| 4.3.TABLES ... | 61 |
| 4.4.FIGURES | 65 |
| <u>CHAPTER 5. CONCLUSION.</u> | 85 |
| REFERENCE | 86 |

LIST OF FIGURES

| | |
|--|----|
| Figure 2.1 Schematic illustration of an apparatus used for squeeze infiltration [4] | 36 |
| Figure 2.2. Schematic illustration of Osprey spray casting arrangement [4]..... | 36 |
| Figure 2.3. Schematic section through a plasma spray torch [4]..... | 37 |
| Figure 2.4. Schematic of Lanxide Process [7] | 37 |
| Figure 2.5. Schematic of XD Process [7]. | 38 |
| Figure 2.6 Stress Strain curves for <i>Al</i> (A356) alloy and 15% particulate <i>SiC/Al MMCs</i> [9] | 38 |
| Figure 2.7. Optical micrograph of a cast <i>SiC_p/Al</i> (A356) <i>MMCs</i> [9] | 39 |
| Figure 2.8. Schematic figure showing the role of reinforcing particles in resisting slip behavior of the <i>MMCs</i> [9]. | 39 |
| Figure 2.9. Effect of reinforcement content on modulus of elasticity of discontinuous <i>SiC/6061 Al</i> composites [13]..... | 40 |
| Figure 2.10. Effect of <i>Al</i> matrix alloy on the stress strain behavior of composites with 20 vol% <i>SiC_w</i> reinforcement [13]..... | 40 |
| Figure 2.11. Effect of <i>SiC</i> reinforcement type and content on the tensile properties of discontinuous <i>SiC/Al</i> composites [13]..... | 41 |
| Figure 2.12. Stress-Strain curves of <i>SiC/6061 Al</i> composites [13]..... | 42 |
| Figure 2.13. Fractography of the tensile sample, showing tear ridges, isolated patches of very small dimples, and broken <i>SiC</i> particles [17]..... | 42 |
| Figure 2.14. Typical microcracks observed inside specimens of <i>SiC/6061Al</i> (a) Interface debonding (b) particle cracking [18]..... | 43 |
| Figure 2.15. Schematic representation of fatigue cracks growth behavior in a non- aggressive environment [24]. | 43 |
| Figure 2.16. Typical fatigue curves for ferrous and non-ferrous metals [24]..... | 44 |

| | |
|--|----|
| Figure 2.17. Schematic depiction of fatigue crack growth rate as a function of the applied stress intensity factor for a typical discontinuous MMC and the corresponding unreinforced alloy [4]. | 44 |
| Figure 2.18. Effect of SiC reinforcement volume fraction on the fatigue life of Al/SiCp MMCs [25]. | 45 |
| Figure 2.19. Effect of volume fraction on the frequency of particle fracture [26]. | 45 |
| Figure 2.20. Effect of different uniform particle sizes on the flow behavior of Al-15vol% SiC composites [29]. | 46 |
| Figure 2.21. Effect of particle size on frequency of particle fracture as a function of K_{max} [26]. | 46 |
| Figure 2.22. Effect of reinforcement particle size on the fatigue life of 20 vol% SiCp/Al MMC [25]. | 47 |
| Figure 2.23. Correlation between the clustering parameter and tensile ductility [33]. | 47 |
| Figure 2.24. The influence of particle clustering on fracture toughness of Al-SiCp MMCs [34]. | 48 |
| Figure 2.25. Representative micrographs of (a) 2124 Al/10vol% SiCp and (b) 2124 Al/ 30 vol% SiCp composites; VHP condition [50]. | 48 |
| Figure 2.26. Representative micrographs of (a) 2124 Al/ 10 vol% SiCp and (b) 2124 Al / 30 vol% SiCp composites; VHP+extruded condition [50]. | 49 |
| Figure 2.27. Representative micrographs of (a) 2124 Al/ 10 vol% SiCp and (b) 2124 Al / 30 vol% SiCp composites; VHP+extruded +section rolled condition [50]. | 49 |
| Figure 3.1. Schematic Sketch of Ultrasonic Flaw Detector. | 55 |
| Figure 3.2. Schematic Sketch of Material Test System (MTS). | 56 |
| Figure 4.1. Optical Micrograph for Specimen 1 at 50X. | 65 |
| Figure 4.2. Optical Micrograph of Specimen 1 at 125X. | 65 |

| | |
|---|----|
| Figure 4.3. Optical Micrograph of Specimen 2 at 50X..... | 66 |
| Figure 4.4. Optical Micrograph of Specimen 2 at 125X..... | 66 |
| Figure 4.5. Optical Micrograph of Specimen 3 at 50X..... | 67 |
| Figure 4.7. Optical Micrograph of Specimen 4 at 50X..... | 68 |
| Figure 4.8. Optical Micrograph of Specimen 4 at 125 X..... | 68 |
| Figure 4.9. Optical Micrograph of Specimen 5 at 50X..... | 69 |
| Figure 4.11. Optical Micrograph of Specimen 6 at 50X..... | 70 |
| Figure 4.13. Optical Micrograph of Specimen 7 at 50X..... | 71 |
| Figure 4.14. Optical Micrograph of Specimen 7 at 125X..... | 71 |
| Figure 4.15. Optical Micrograph of Specimen 8 at 50X..... | 72 |
| Figure 4.16. Optical Micrograph of Specimen 8 at 125X..... | 72 |
| Figure 4.17. Optical Micrograph of Specimen 9 at 50X..... | 73 |
| Figure 4.18. Optical Micrograph of Specimen 9 at 125X..... | 73 |
| Figure 4.19. Optical Micrograph of Specimen 5 showing clusters of SiC particles at (a)12.5X, (b)25X, (c)50X, (d)125X. | 74 |
| Figure 4.20. True Stress-Strain Curves at 150 ⁰ C..... | 75 |
| Figure 4.21. True Stress-Strain Curves at 250 ⁰ C..... | 75 |
| Figure 4.22. True Stress-Strain Curves at 350 ⁰ C..... | 76 |
| Figure 4.23. True Stress vs True Strain at Different Temperatures..... | 76 |
| For Specimen 1 | 76 |
| Figure 4.24. True Stress vs True Strain at Different Temperatures..... | 77 |
| For Specimen 2. | 77 |
| Figure 4.25. True Stress vs True Strain at Different Temperatures..... | 77 |
| For Specimen 3. | 77 |
| Figure 4.26. True Stress vs True Strain at Different Temperatures..... | 78 |
| For Specimen 4. | 78 |
| Figure 4.27. True Stress vs True Strain at Different Temperatures..... | 78 |
| For Specimen 5. | 78 |

| | |
|---|----|
| Figure 4.28. True Stress vs True Strain at Different Temperatures | 79 |
| For Specimen 6. | 79 |
| Figure 4.29. True Stress vs True Strain at Different Temperatures | 79 |
| For Specimen 7. | 79 |
| Figure 4.30. True Stress vs True Strain at Different Temperatures | 80 |
| For Specimen 8. | 80 |
| Figure 4.31. True Stress vs True Strain at Different Temperatures | 80 |
| For Specimen 9. | 80 |
| Figure 4.32. Variation of Stress with Temperature at a strain of 0.015 mm (the flat portion of the stress-strain curves). | 81 |
| Figure 4.33. Comparison between Calculated density and Experimentally measured density. | 82 |
| Figure 4.34. Variation of Elastic Modulus with Volume Fraction. | 82 |
| Figure 4.35. Variation of True Stress at 350 ⁰ C at a strain of 0.015 (corresponding to the flat region of the stress-strain curves) with Volume Fraction. | 83 |
| Figure 4.36. Variation of stress at a strain of 0.015 (corresponding to the flat region of the stress-strain curves) with Mean Free Distance (λ). | 83 |
| Figure 4.37. Variation of Stress with Particle Size (D) of SiC particles at a strain of 0.015 (corresponding to the flat region of the stress-strain curves) | 84 |
| Figure 4.38. Variation of Stress Ratios ($\sigma_{350}^{\circ}\text{C} / \sigma_{150}^{\circ}\text{C}$) with increase in strain..... | 84 |

LIST OF TABLES

| | |
|---|----|
| Table 2.1. Mechanical Properties [4] | 34 |
| Table 2.2. Tensile properties of reinforced and unreinforced 2080 <i>Al</i> alloy [23] | 34 |
| Table 2.3. Effect of reinforcement volume fraction on the fatigue properties of 2080 <i>Al</i> alloy [23] | 35 |
| Table 2.4. Monotonic Tensile Properties of 2124 <i>Al-SiCp</i> Composite..... | 35 |
| Table 2.5. Effect of reinforcement size on the fatigue properties of 2080 <i>Al-SiCp</i> composites | 35 |
| Table 3.1. Samples used for investigation. | 54 |
| Table 3.2. Polishing Steps | 54 |
| Table 4.1. Results of Density Measurements..... | 61 |
| Table 4.2. Results of Elastic Modulus Measurements | 62 |
| Table 4.3. Quantitative Stereological Measurements. | 63 |
| Table 4.4. Mechanical Properties..... | 64 |

ABSTRACT

Silicon Carbide particulate reinforced Aluminium matrix composites comprise a new generation materials whose properties can be tailor made for a particular application. These composites not only possess high specific strength and modulus at room and elevated temperatures but also have excellent wear resistance, high thermal conductivity, low coefficient of thermal expansion, good dimensional stability and low density. These materials also exhibit isotropy unlike continuous fibre reinforced composites. These are much easier and less expensive to fabricate through conventional casting and rolling process. The potential applications for such composites include aerospace, automobile, electronic packaging and sporting goods. Some typical applications include missile fins, inertial guidance control components, precision laser mirror substrate, piston in diesel engines, brake calipers, electronic packaging materials etc.

One of the major concerns to these materials is the variability in the properties. For example, two composites with same volume fraction may have different mechanical properties, especially the extreme properties like ultimate tensile strength and fracture toughness. This has been attributed to the fact that the flow properties of the matrix are altered by the presence of second phase particles (silicon carbide). Hence the volume fraction, size, shape and spatial distribution (for instance clustering or patches of matrix) of the *SiC* particles have a considerable effect on the flow properties of the matrix. Some of these microstructural parameters, especially the particle distribution depends on the type of processing used. In order to predict the extreme properties a detailed microstructural characterization is needed.

The present research work involves quantitative microstructural characterization and correlation with the mechanical properties of these materials. High temperature compression test and measurement of elastic modulus were performed to determine the mechanical properties of the composites. Microstructure was analyzed using optical microscope and stereological measurements including volume fraction, surface area per unit volume were carried out.

The composites used for investigation were provided by three US industries and were manufactured by patented processes by two different routes- Permanent Mold

Casting and Sand Casting. The samples were provided by Prof. P.K. Rohatgi (The University of Wisconsin-Milwaukee). Densities for the sample have been measured using an Analytical Balance by the concept of Archimedes Principle. An Ultrasonic Flaw detector (KRAUTKRAMER-BRANSON USI P12) was used to determine the elastic modulus of the samples. High temperature compression tests were carried out using Material Test System (MTS). The samples were tested at three temperatures of 150⁰C, 250⁰C, and 350⁰C and Stress-Strain Plots were obtained. The specimens were prepared by metallographic specimen preparation techniques for microstructural characterization. The microstructural parameters that have been measured include volume fraction (V_v), surface area per unit volume (S_v), connectivity, mean free path, and particle size.

All these parameters have been measured using Digital Image Analysis (Image Pro-Plus). The project work aims at correlating the above mentioned microstructural parameters with Elastic Modulus and Flow Stress of the composites under study. Regression analysis was performed and equations were derived to correlate the microstructural parameters with the modulus and flow stress for the composites. It was found that Elastic Modulus was a strong function of volume fraction. The flow stress at high temperature was also dependent on the volume fraction. The mean free distance between *SiC* particles had a little effect on the flow stress at high temperatures.

CHAPTER 1

INTRODUCTION

Metal matrix composites (*MMCs*) are promising new materials for advanced engineering applications because of their high specific stiffness and strength and their high temperature stability. The development of metal matrix composites has been catalyzed by the need for structural materials, materials for aerospace and automobile industry. Reinforcements may be continuous in the form of fibers or discontinuous in the form of whiskers or particulates. Discontinuous (whisker or particulate) reinforced metal matrix composites have attracted more and more attention from both academic institutions and industries. In addition to their superior mechanical properties to conventional metals and alloys, these types of *MMC* materials can now be produced economically by conventional metallurgical techniques (casting, rolling, forging etc), and they are usually machinable after fabrication. Furthermore, they can be isotropic in mechanical properties, whereas continuous fibre- reinforced *MMCs* are usually anisotropic. Among all the *MMCs*, of particular interest are the *Al* and *Al* alloys reinforced with discontinuous *SiC*, either as particulate or whisker. The improved mechanical properties, such as elastic moduli and strength, are governed by the properties of continuous phases as well as shape, orientation and volume fraction of the reinforcing phase. The size, shape and orientation of *SiC* particles have a major effect on the properties of *Al/SiC* composites. The overall properties also depend on the manufacturing process of these composites, since the manufacturing process determines the orientation of the particles and may produce internal defects, such as porosities etc. Thus, a proper correlation between the manufacturing process, microstructure, and properties of these grades of composites materials is needed. The main aim of the present thesis is to study the effect of various microstructural parameters on the mechanical properties of *Al-SiCp* metal matrix composites.

CHAPTER 2

LITERATURE REVIEW

2.1. COMPOSITES

Unfortunately there is no widely accepted definition of what a composite material is. A dictionary defines a composite as something made up of distinct parts (or constituents). At the atomic level materials such as some metals, alloys and polymeric materials could be called composite materials since they consist of distinct atomic groups. At the microstructural level a metal alloy such as a plain carbon steel containing ferrite and pearlite could be called a composite material since the ferrite and pearlite are distinctly visible constituents as observed in the optical microscope. At the macrostructural level a glass fiber reinforced plastic, in which the glass fiber are distinctly recognized by the naked eye could be considered a composite material. Now we see that the difficulty in defining a composite material is the size limitations we impose on the constituents that make up the material. In engineering designs a composite material usually refers to a material consisting of constituents in the micro-macro size range, and even favors the macro-size range.

One can define a composite material as a material system composed of a mixture or combination of two or more micro- or macro-constituents that differ in form and chemical composition and which are essentially insoluble in each other.

The engineering importance of the composite materials are that two or more distinctly different materials combine together to form a composite material, which possesses properties that are superior, or important in some other manner to the properties of the individual components.

2.1.1. Classification of Composite Materials:

There are many ways for classification of composite materials based on type of matrix and type of reinforcement.

I. Classification based on type of matrix

Composites can be classified into three major groups depending on the type of matrix used.

- i. Metal Matrix Composites (*MMCs*): Matrix is a metal or an alloy of two or more metals such as *Al*, *Ti*, *Fe*, *Cu*, etc.
- ii. Ceramic Matrix Composites (*CMCs*): Matrix is a ceramic compound such as Alumina (Al_2O_3).
- iii. Polymeric Matrix Composites (*PMCs*): Matrix is a polymer such as epoxy resins.

II. Classification based on type of reinforcement:

Composites can be classified into three major types based on the type of reinforcement used.

i. Fibrous Composites

These are composed of reinforced fibres in a matrix. Fibers are small in diameter and when pushed axially, bend easily. Although they may have outstanding tensile strength, they must be supported to keep individual fibers from bending and buckling. These composites can be further classified into three types.

Uniaxial Fibre Composites: Fibres are oriented in a single direction.

Laminar Composites: These are composed of layers of materials held together by the matrix binder. They include the clad metals, often where a more corrosion resistant metal is bonded to a stronger one. Wooden laminators, plywood, glasses, some ceramic and metallic composites also fall under this category.

Complex 3D: Here the fibres are oriented randomly in all possible directions.

ii. Particulate Composites:

Particulate composites consist of particles dispersed in a matrix. They have no distinct arrangement of the phases or components and the properties tend to be more isotropic than the fiber or laminar composites, e.g. cemented carbides, *Al/SiC_p* composites.

iii. Whisker or Short Fibre Composites:

These composites consist of short fibres or whiskers distributed randomly in the matrix. The whiskers have a very small diameter and length as compared to long fibres in fibrous composites.

2.2.METAL MATRIX COMPOSITES

Metal matrix composites, in general consist of at least two components; one obviously is the metal matrix (in most cases, an alloy is the metal matrix), and the second component is a reinforcement (e.g. an intermetallic compound or a ceramic [1].

2.2.1. Constituents of Metal Matrix Composites

i. Matrix metal:

The metal matrix, in general, is an alloy. The alloy can be relatively simple, but, in general, it is a multielement alloy. There are a number of phases that can exist within the alloy.

The matrix metal provides sufficient amount of toughness and ductility to the composites. The metals that have been used as the matrix include *Al*, *Cu*, *Fe*, *Mg*, *Ti*, and *Pb* [1]. The chemistry of the alloy used as matrix material is important because of interfacial properties.

ii. Reinforcements:

Reinforcement in a composite provides higher modulus, strength and wear resistance. The reinforcements can be divided into two major groups,

discontinuous and continuous. The most prominent discontinuous reinforcements have been SiC , Al_2O_3 etc. in both whisker and particulate forms [1].

2.2.2.Types of Metal Matrix Composites

Metal matrix composites can be reinforced by strong second phases of three-dimensional shapes (particulates), two-dimensional shapes (laminar) or one-dimensional shapes (fibrous). Each of these classes of reinforcement has it's own advantages and characteristics. Generally, these classes of composites fall into considerably different areas of application, not only because of the differing mechanical properties of the classes but also because of the contrast in fabrication techniques [2].

i. Particle Reinforced MMCs:

Particle reinforced composites include those composites having more than 20v/o of the hard reinforcing dispersed phase and do not include the class of dispersion hardened metals, which have considerably lower volume fraction of the dispersoid [2]. In addition, the diameter of the particles and the interparticle spacing are much greater in the composites, normally of the order of $10\mu m$. With particle-reinforced composites such as $Al-SiCp$, the reinforcing phase is the principal load-bearing phase, and the matrix is used for transferring the load. The three dimensional reinforcement leads to isotropic material properties, since the material is symmetrical across the three orthogonal planes. Strength of particulate composites normally depends on the volume fraction of the reinforcement, diameter of particles, and interparticle spacing.

ii. Laminated MMCs:

Laminated composites are reinforced by a repeating layer of reinforcement of high modulus and strength, which is contained in more ductile and formable metallic matrix material. The in-plane properties of laminated composites are a strong function of laminate orientation. The low strain to failure of brittle reinforcements limits the elongation and ductility of the composite in all directions in the plane of reinforcements. The reinforcement strength and modulus, however, are present in all directions of the plane through a function of

laminate orientation and offer a significant advantage compared to the unidirectional reinforcement of a filament array [2].

iii. Fibre-Reinforced *MMCs*:

Fibre composites derive most of their properties from the reinforcing fibres. The reinforcing phase in fibre composite materials spans the entire size range, from 0.1 to 250 μm in length to continuous fibres, and spans the entire range of volume concentrations from a few percent to greater than 70% [2]. These composites have high strength and modulus values in the fibre direction. At angles of 10° from the fibre direction, the strength values of the composite are approximately 50% of the 0° values. At 90° from the fibre direction, the strength values are less than 10% of the 0° values [3].

iv. Whisker-Reinforced *MMCs*:

Whisker reinforced *MMCs* consist of short fibres or whiskers randomly distributed in the matrix alloy. Typical fibre diameters are a few microns and they are initially produced in lengths of several hundred microns. However, they are often broken up during fabrication [4]. Short fibre *MMCs* can offer some attractive combination of properties. However, their formability is in general markedly inferior to that of particulate *MMCs*.

However, while excellent properties have been reported for whisker reinforced *MMCs* and there is still some interest in them, there has been little commercial exploitation. This is largely a consequence of handling difficulties. These commonly arise with very fine fibres, which tend to form ball like structures, and are difficult to orient in a controlled way. The most significant problem of this type of *MMCs* concerns perceived health hazards. Whiskers and Whisker fragments in slightly sub-micron size range are likely to reach the lungs through air. They tend to evade the natural protective mechanisms

2.2.3. Properties of Metal Matrix Composites

MMCs include the combinations of the following properties [2]:

- i. High strength;
- ii. High modulus;
- iii. High toughness and impact properties;
- iv. Low sensitivity to changes in temperature or thermal shock;
- v. High surface durability and low sensitivity to surface flaws;
- vi. High electrical and thermal conductivity;

2.2.4. Engineering Applications of MMCs

Metal matrix composites have the potential to be used for many structural applications. However, due to their higher cost as compared to a monolithic metal alloy, their use is restricted to cost effective applications. Metal matrix composites have been so intensely researched over the past decades that many new high strength-to-weight ratio materials have been produced. Most of these materials have been developed for aerospace industries, but some are being used in other applications such as automobile industry.

2.3.SILICON CARBIDE PARTICULATE REINFORCED ALUMINIUM MATRIX COMPOSITES

In recent years much of the research has been carried out on particle reinforced metal matrix composites due to the combination of high strength-to-weight ratios, high stiffness, and the ability to be formed by conventional metal processing techniques. The most commonly used composites consist of Aluminium based alloys reinforced with ceramic particles, usually silicon carbide. These materials have been shown to have different strengthening mechanisms from conventional precipitation hardened alloys or continuous fibre-reinforced composites. Thus much research, both experimental and analytical, has been performed to gain a better understanding of the mechanical behavior of these materials. *Al-SiCp* reinforced composites comprise a class of new generation materials whose properties can be tailor made to suit a particular application. These composites not only possess high specific strength and modulus at room temperature and elevated temperatures, but also have excellent wear resistance, high thermal conductivity, low coefficient of thermal expansion and good dimensional stability. These materials also exhibit isotropy unlike continuous fibre reinforced composites and are much easier and less expensive to fabricate. The potential applications for such composites are concentrated into three market sectors; namely aircraft, automobile, and sporting goods. Some typical applications include missile fins, inertial guidance control components, precision laser mirror substrater, piston in diesel engines, brake calipers.

2.4. PROCESSING OF METAL MATRIX COMPOSITES

A variety of processes have been and are being developed for the manufacture of metal matrix composites. These may be divided into primary material production, and secondary consolidation or forming operation. A further important distinction can be drawn for the primary processes depending on whether the matrix becomes liquid at any stage. Each technique has it's own limitations in terms of component size and shape, and change certain micro-structural features on the product. Before looking in details at the various processing options, it is worthwhile dwelling for a moment on selection of the reinforcement. Clearly, the size, shape and strength of reinforcing particles or fibres are

of central importance. Often the choice between the continuous and discontinuous options is relatively straightforward, both in terms of performance and processing cost.

Fabrication of metal matrix composites can be divided into three categories-

1. Primary Liquid Phase Processing.
2. Primary Solid State Processing.
3. Secondary Processing.

2.4.1. Primary Liquid Phase Processing

Various techniques have been developed, which involve the matrix becoming at least partially molten as it is brought into contact with the ceramic reinforcement. This generally favors intimate interfacial contact and hence a stronger bond. Various processing techniques developed under this category are-

- i. Compocasting (Rheocasting / slurry casting)
- ii. Squeeze casting or Squeeze Infiltration.
- iii. Spray Deposition.
- iv. Reactive Processing ('In-situ Composites').

i. Compocasting or Slurry Casting:

Compocasting refers to the casting of composites using semisolid alloys (rheoslurry with a temperature between solidus and liquidus) [5]. Arguable the simplest and most economically attractive method of *MMC* manufacture is to simply stir mix the liquid metal with solid ceramic particles and then allow the mixture to solidify. The slurry can be continuously agitated when the ceramic is progressively added. This can in principal be done using fairly conventional processing equipment and can be carried out on a continuous or semi-continuous basis. This type of processing is now in commercial use for *Al-SiCp* composites [4].

In this method, the liquid alloy at a temperature 30 to 50 K above liquidus is vigorously agitated and allowed to slowly cool to semisolid range. The continued agitation breaks up the solidifying dendrites into fine spherical particles and prevents a rise in viscosity of the slurry. While the stirring continues, reinforcement particles or whiskers or chopped fibres are added to the semisolid slurry. The composite mixture, with relatively low viscosity can be directly cast into simple billet; this is termed as rheocast composite and the process is known as Rheocasting [5]. Alternatively, the

semisolid composite mixture can be reheated to just above liquidus and die-cast into net shape components; this process is termed Compocasting [5].

Compocasting (or Rheocasting) is useful for fabricating composites because it allows uniform distribution of the reinforcement in the metal matrix. The solid in the semisolid slurry entraps the reinforcement and it is prevented from agglomerating, settling, or floating to the top [5].

ii. Squeeze Casting or Squeeze Infiltration:

The term squeeze casting has come to be applied to various processes in which pressure is imposed on a solidifying system, usually via a single hydraulically activated ram [4]. The primary distinction between this and conventional pressure die-casting is that the ram continues to move during solidification, deforming the growing dendrite array and compensating for the freezing contraction (which is typically about 5%). In addition to this, the ram movement is usually slower, and the application of pressure often greater than in typical die casting. Squeeze casting can be applied to *MMCs*, as reheated powder mixtures or stir cast material, but the most common pressure assisted solidification process for *MMC* production is properly termed squeeze infiltration [4]. This involves the injection of liquid metal into the interstices of an assembly of short fibres, usually called a 'preform'. While preforms can be prepared in various ways, they are commonly fabricated by sedimentation of short fibres from liquid suspension. Preforms can also be prepared from particulate or aligned long fibre reinforcements. The main problem in these cases is usually that the volume fraction of reinforcement becomes very high when pressure is applied, which may be undesirable in itself and can also cause problems of premature solidification and very high pressure needed for infiltration [4].

In order for the preform to retain its integrity and shape, it is often necessary for a binder to be used, particularly if a relatively high volume fraction of fibre ($\geq 10\%$) is required. Unbound short fibres tend to peak naturally with a very low volume fraction. Either fugitive binders, which set at relatively low temperature, or agents requiring a high temperature firing operation, or some combination of the two types may be used. Various silica and Alumina based mixtures have been popular as high temperature binders. The binding agents are normally introduced via the suspension liquid. Infiltration is usually carried out with equipment of the type shown in Figure 2.1 [4].

iii. Spray Deposition:

A number of processes have evolved in which a stream of metallic droplets impinge on a substrate in such a way as to build up a composite deposit. Spray deposition is an attractive method for applying matrix material to fibres. Fibre alignment is easily controlled and the rapid solidification of molten matrix material minimizes, fibre degradation while producing unique matrix microstructure. Composite monolayers and continuously and discontinuously reinforced composites, have been fabricated by this technique [6].

The technique employed fall into two distinct classes, depending whether the droplet stream is produced from a molten bath, or by continuous feeding of cold metal into a zone of rapid heat injection [4].

The Osprey Process (melt atomization):

Figure 2.2 shows the schematic illustration of an Osprey spray casting arrangement for composite manufacture. Ceramic particles are injected into the spray cone and become incorporated into the deposited ingot. The substrate is continuously rotated and withdrawn, keeping the flight distance approximately constant. The metal droplet size depends on nozzle design and flow rates of metal and atomizing gas.

Thermal Spraying:

Thermal spraying involves the feeding of powder, or in some cases wire, into the hot zone of a torch, where it is heated and accelerated as separate particles by the rapid expansion of gas. The heating is usually generated by an electric arc or by gas combustion. Particularly good process control is possible with plasma spraying. A typical design for plasma spray torch is shown in Figure 2.3 [4].

iv. In-Situ Reinforcement of MMCs:

Direct Metal Oxidation:

There has been considerable interest recently in the family of processes developed by the Lanxide Corporation, in which metal is directionally oxidized so as to produce a near net shape component containing metal and ceramic [4]. A typical process involves raising an aluminium melt to high temperature, with addition such as Mg, so that the

aluminium skin becomes unstable and the metal moves by capillary action into an array of ceramic particles, such as alumina. Figure 2.4 shows a schematic of Lanxide Process for directed oxidation of Al to produce an Al_2O_3 composites.

Directional Solidification of Eutectics:

Directional solidification has long been used to produce anisotropic material, often with a high degree of microstructural regularity and perfection. In certain special cases, this procedure can be used to produce castings, which are in effect metal matrix composites [4]. A binary alloy melt of exactly the eutectic composition normally freezes at a congruent temperature to form an aligned two-phase structure. If the volume fraction of one of the phases is sufficiently low, it is energetically favorable for it to solidify in the form of fibres, rather than the more commonly observed lamellae. The critical volume fraction depends on the interfacial energy and solute diffusion characteristics but it is typically about 5% [4]. The fibres may be intermetallic compounds of high strength and stiffness, with a strong fibre/matrix interface. Furthermore, by selecting the growth conditions, the fibre diameter and spacing can be controlled to some extent.

Exothermic reaction Process:

The XD process, developed by Martin Marietta Corporation around 1983, differs somewhat from the Lanxide Process. Where the Lanxide process is typically used to produce the final part directly, the XD process is a means for making the starting materials for conventional metal working technologies- casting, forging, extrusion, rolling. In the XD process the powder of elemental components of various reinforcing phases are mixed with or incorporated into metallic or intermetallic matrix material. When this mixture is heated to a high temperature, typically above the melting point of the metal, or to a point where a self-propagating reaction takes place, the elemental constituents react exothermically to form a dispersion of submicroscopic reinforcing particles in the matrix [7]. An example of this process is shown in Figure 2.5.

2.4.2. Primary Solid State Processing

This process involves producing metal matrix composites without the matrix ever becoming even partially liquid while in contact with the ceramic. The techniques that comes under this category are –

- Powder Blending and Pressing
- Diffusion Bonding of Foils.
- Physical Vapor Deposition.

i. Powder Blending And Pressing:

This process involves mixing of metallic powders and ceramic fibres or particulates. The blending can be carried out dry or in liquid suspension. This is usually followed by cold compaction, canning, evacuation (degassing) and a high temperature consolidation stage such as hot isostatic pressing or extrusion [4].

Diffusion Bonding:

Diffusion bonding is a solid state welding technique, which can be used to join the same or dissimilar metals. As the name implies, interdiffusion of atoms from clean metal surfaces in contact at elevated temperature is responsible for creating the joint [8].

Diffusion bonding has been successfully used to fabricate *MMCs*. While many processes, from vacuum hot pressing to roll bonding, have been developed, which employ diffusion bonding to form composites, all share the common feature of application of pressure for a given time at an elevated temperature.

ii. Physical Vapor Deposition:

Three basic *PVD* processes can be utilized to form metal matrix composites:

- Evaporation.
- Ion Plating.
- Sputtering.

PVD is a vapor deposition process, the primary difference being in how the vapors are created. Vapor sources and process geometries vary, depending on the characteristics desired in the coating. Multiple sources can be used with any of the techniques to produce alloy, multilayered, or graded composition films. Evaporation generally has the fastest deposition rates since materials can be evaporated or sublimed in high vacuum ($\leq 1 \times 10^{-4}$

torr) [6]. Vapor sources for evaporation may include resistance heating in crucible, electron beam evaporation, arc evaporation, radiation heating, or laser ablation.

Ion plating involves passing the vapor through a gas (usually *Ar*) glow discharge around the substrate, leading to the bombardment by ions of both *Ar* and the coating material. This gives a denser deposit than the evaporation, but slower deposition rates [4].

Sputter deposition, in which a target of the coating material is bombarded by ions of a working gas (*Ar*) and the atoms are ejected towards the substrate, is still slower, but has the advantage of being applicable to virtually all materials- even those with very low vapor pressures [4].

2.4.3. Secondary Processing

A number of secondary processes can be applied to *MMC* material, usually with the objective of consolidation (porosity elimination), generating fibre alignment and/or forming into required shape. This involves high temperatures and large strain deformations and includes processes like:

- Extrusion and Drawing.
- Rolling, Forging, and Hot Isostatic Pressing.
- Superplastic Forming and Sheet Forming [4].

2.5. MECHANICAL BEHAVIOUR OF Al-SiCp METAL MATRIX COMPOSITES

Silicon Carbide (SiC), either as particulate (also nodules) or whisker additions to Al and Al -alloys, has been the metal matrix composites most widely studied. This section illustrates the mechanical behavior of Al - $SiCp$ metal matrix composites and mechanism of strengthening of these materials. Table 2.1 shows the various mechanical properties of Al , Al -alloys, $SiCp$, and $SiCw$.

2.5.1. Stress-Strain Curve

Figure 2.6 shows the typical stress-strain curves obtained from Uniaxial tension tests carried out by Wang and Zhang on SiC (particulate)/ Al (A356) composites [9]. The composites used for the study were fabricated by direct casting using the molten metal mixing method. The two curves are for 15 vol% SiC particulate reinforced Al alloy (A356) metal matrix composites and monolithic Al alloy (A356). It is apparent that the slope of the linear portion of the MMC curve is higher than that of the matrix material. The increase of the elastic constant of the composite is caused by the addition of the high stiffness SiC particles.

Stress-Strain Behavior:

From the stress strain curve shown in Figure 2.6 it can be also seen that the influence of the addition of the reinforcing SiC particles on the hardening behavior of the studied MMC material appears differently at different stages of deformation. The considerable increase of the strain-hardening rate in the beginning of plastic deformation, i.e., immediately after the onset of the plastic deformation, marked by 'A' in Figure 2.6 is rationalized by the strong resistance of the hard reinforcing particles to the slip behavior of the Al -matrix [9].

Figure 2.7 shows the optical micrograph of $SiCp/Al$ (A356) MMC . As seen from the figure, most dendrite branches of the Al matrix are surrounded by the SiC particles as well as the eutectic Si particles. The slip behavior of each dendrite branch, if considered as an Al matrix grain, is highly constrained by the surrounding particles. Any deformation in these Al grains, therefore, would require corresponding deformation in the surrounding particles, which would be unlikely to occur since the particles formed in the eutectic reaction also act as a kind of reinforcement, since their strengths are much higher than that of Al . To keep the continuity of the composite material under external load, which

requires no formation of any voids and cracks along the particle- matrix interface, a strong internal stress develops between SiC particles and the matrix. This type of internal stress resists the slip behavior in the metal matrix, and hence the strain-hardening rate increases [9]. The phenomenon of the particle matrix interaction is schematically illustrated in Figure 2.8, where the clustered SiC particles and eutectic Si particles along the dendrite boundaries act as barriers in the slip behavior of the matrix, and hence strengthen the composite material. This strengthening mechanism is similar to the conventional theory of grain boundary strengthening in which the grain boundaries block the dislocation movement during plastic deformation; however, this effect of reinforcing SiC particles along the grain boundaries is much stronger [9]. Similar results were also obtained by Yang et al [10], where hardening was due to formation of $MgSi_2$ precipitates and SiC particles.

The Yield Point:

Historically, the difficulties involved in the definition of a yield are well exemplified by the widespread adoption of ‘proof stress’ measured at a somewhat arbitrary plastic strain offset. The use of such a definition causes considerable confusion in the comparison of materials, such as *MMCs*, which have differing degrees of inhomogeneity in their early flow behaviors. The problem lies in the fact that *MMCs* characteristically exhibit a progressive transition from local plastic flow to bulk flow, with a very high initial work hardening rate. Pragnell et al [11] proposed a new method of defining the onset of yielding in the *MMCs*. It has been demonstrated that the definition of a yield point as the stress and strain at which the third derivative of the stress-strain response ($\partial^3\sigma / \partial\epsilon^3$) has its first minimum, is useful in describing the mechanical response of an *MMC*. Its value indicates the stress at which there is a significant, but small, departure from elastic behavior and thus it also quantifies the proportional regime [11].

In hard particle/ ductile matrix system yielding of the matrix generally takes place at a lower applied load than for the unreinforced matrix alloy, despite the proof stress often being higher for the composite material, because the proof stress fails to differentiate between the initiation of yielding and the high rate of initial work hardening of such systems. The proof stress is thus unrepresentative of the elastic working range of

an *MMC* and could potentially be dangerous if used as a design parameter in this context [11].

2.5.2. Factors Affecting Modulus of Elasticity

The modulus of elasticity of a composite is strongly dependent upon the mode of measurement. In general, if the modulus is measured dynamically, it is higher than that determined from the initial slope of the stress-strain curve [12].

Mc Danels [13] investigated composites having three different *SiC* morphologies, whiskers ($1/d \approx 2-3d \approx 0.5\mu\text{m}$), nodules (flattened spheres 1-5 μm in diameter), and particulates (2-7 μm in diameter) in the platelet form.

The modulus of elasticity of 6061 *Al* matrix composites increases with increasing reinforcement content as shown in Figure 2.9. The reinforcement content is the dominant factor in the improvement of the modulus of elasticity in these *SiC/Al* composites. For a given reinforcement content, the modulus tends to be isotropic, with nearly equal values obtained from tests in both the longitudinal and transverse directions. In addition, the modulus appears to be independent of the type of reinforcement, with modulus values being within 5% of the average value for all composites tested at any given reinforcement content, regardless of the type of reinforcement [13].

2.5.3. Factors Influencing Strength

The factors influencing the yield and tensile strength of *Al/SiC* composites are complex and interrelated, and the best way to evaluate this behavior is through isolation of variables and analysis of stress-strain curves and fracture behavior [13].

Effect of *Al* Matrix Alloy:

The *Al* matrix used for the *SiC/Al* composites is one of the most important factor affecting yield strength and ultimate tensile strength of these composites. Figure 2.10 shows the effect of *Al* matrix alloy on the stress strain behavior of composites with 20 vol% *SiC_w* reinforcement [13]. These curves show that *SiC/Al* composites with higher strength aluminium alloys, such as 2024/2124 or 7075 *Al*, have higher strengths but lower ductility. Composites with a 5083 *Al* matrix fail in a brittle manner. Similar trends of increased yield strengths were also observed for composites with these matrices using other types of *SiC* reinforcements.

Effect of Reinforcement Content:

Reinforcement content is another important factor controlling the strength of *SiC/Al* composites. The effect of reinforcement content of a given type of *SiC* reinforcement is shown in the yield/UTS histograms in Figure 2.11. These figures show that for a given matrix alloy and reinforcement, the yield and ultimate tensile strength generally increases with increasing reinforcement content. The increase in strength with increase in reinforcement content can also be seen from the stress-strain curves for *SiC/6061 Al* composites containing different reinforcement types and contents in Figure 2.12. These curves show that the proportional limit stress, where the composite enters plastic flow increases as the reinforcement content increases. As the reinforcement content is increased the elastic modulus increases and causes the stress-strain curves to enter plastic flow at a higher flow stress. The slope of the stress-strain curve also increases as the composite enters plastic flow and a higher flow stress is required to reach a given plastic strain until either a stable plastic flow is reached (ductile failure) or the specimen fractures (brittle failure). This indicates that the strength increase is caused by closer packing of the reinforcement and smaller interparticle spacing in the matrix. This causes increase in interaction of dislocations with the *SiC* reinforcement, resulting in increase in strain hardening [13].

The strength increases with increasing reinforcement content only as long as the composite is able to exhibit enough ductility to attain full strength. As the content reaches 30-40 vol% *SiC*, the strength increase tends to taper off because the composite fails. In this region, the matrix probably doesn't have sufficient internal ductility to redistribute the very highly localized internal stresses, and that's why the composite fails before being able to reach stable plastic flow and normal ultimate strength [13-14].

One of the most important effect of adding stiff particles to soft matrix include introduction of matrix residual stresses and an increase in dislocation density in the matrix due to thermal expansion mismatch between particulate and matrix. Alteration of the recrystallization characteristics of the matrix during thermal treatment would control the size of grains and formation of subgrains, and the alteration of precipitate particles. This results in increase in the yield stress [14-16].

2.6.FAILURE PROCESS AND FRACTURE TOUGHNESS OF ALUMINIUM-SILICON CARBIDE METAL MATRIX COMPOSITES

The property improvements that composites offer over their monolithic metallic counter parts have generated much interest in the scientific and technical communities. In particulate reinforced metal matrix composites, the aim has been to combine the beneficial stiffness of ceramics with the superior ductility and toughness of metals. Typically, it has been found that additions of moderate amounts of reinforcement to a metal matrix can give significant modulus and strength increase in the resultant composite. However, this combination produces relatively lower ductility and toughness in the composite as compared to the matrix alloy. Maximizing these properties requires an understanding of the local micro-mechanical failure modes and their relation to macroscopic toughness.

With short-fibre or particulate reinforcement, failure processes are more complex than in long fibre *MMCs*. Fracture is thought to occur largely by the formation and link of voids within the matrix. Fracture is thought to occur largely by the formation and link-up of voids within the matrix. Classical treatments of fracture in metals containing isolated, poorly bonded inclusions allow predictions about the nucleation and growth of cavities, but this may be of limited relevance to *MMCs*, which contain closely spaced, well bonded fibres or particles.

2.6.1. Micro-Damage Process

Various workers [17-22] have tried to explain the mechanisms by which damage initiates at the microscopic level. According to these workers failure and fracture in particulate reinforced *MMCs* can occur in following ways:

- Formation and growth of microvoids.
- Formation of microcracks due to reinforcement cracking.
- Matrix failure due to addition of reinforcement.

Formation and Growth of Micro-voids:

Formation and growth of microvoids is one of the important energy absorption mechanisms. Voids that form during fracture are found as dimples on the fracture surface, where their diameters may be directly measured. The energy absorbed in void coalescence and growth is directly dependent on the size of the voids and their aspect ratio, or depth. Measurements of void size and shape are difficult because they are made

usually from fracture surfaces, which are rough, thereby requiring extensive analysis, such as that done by photogrammetry of stereopairs [15]. Evaluation of the importance of void mechanism to fracture toughness is done by determining the coverage and size of dimples from the fracture surfaces generated by rapid crack growth. Figure 2.13 shows the appearance of fracture surface of 2014 *Al*-15 vol% *SiC*. Davidson [17] found that a little difference is seen in fracture surface appearance between the tensile tests and the fast fracture regions of the fracture toughness tests.

Formation of Micro-cracks Due To Reinforcement Cracking and Interfacial De-bonding:

The particle reinforced *MMCs* consist of a ductile matrix metal, together with hard particles and their interfaces, and is subjected to various types of loading during the deformation process. The internal stress and strain distributions under external loading would therefore be much more complicated as compared with conventional, and the complicated internal stresses gives rise to microstructural degradation. Failure in the particle reinforced *MMC* is believed to be due to cavity formation at the particle/matrix interface or particle cracking [18]. Kanetake et al [18] observed the microstructural degradation during tensile loading of particle reinforced aluminium matrix composites. Figure 15 shows micrographs of *Al/SiCp* composites under tensile loading. Typical microcracks due to interfacial debonding [Figure 2.14(a)] and particle cracking [Figure 2.14(b)] are seen inside the specimen. The microcracks produced by interfacial debonding and particle cracking do not immediately lead to failure of the material. The microcracks do not propagate with increasing external loading because of the ductility of the matrix, but a number of new microcracks develop just before failure. Most microcracks are due to interfacial debonding rather than particle cracking [18].

Interfacial strength plays a very role in the failure process of the particulate reinforced *MMCs*. If the interface between particle and matrix is very weak, particle debonding takes place and hence there is no load transfer from the matrix to the particle. On the other hand, if the interface is very strong particle fracture occurs without any debonding. Maximum amount of energy is absorbed when debonding and particle cracking takes place simultaneously. Hence an optimum amount of interfacial strength is necessary to cause debonding and particle cracking to take place simultaneously [18].

According to Davidson [15] magnitude of the effect of debonding of particle/matrix interface can be largely controlled by the size of the particles and their bonding with the matrix. Location of the microcracks is also important. If the microcracks are confined to particle-matrix interface, and if the particles are small, the effect may be promotion of microvoid initiation, which has a potent influence on the fracture toughness. However, the influence of particulate fracture on composite fracture toughness has been the subject of considerable debate [15]. When the particles break, the energy of new surface formation is absorbed but, because this energy is so low, the effect on fracture toughness is negligible. If the particle is small and contains a large enough flaw to break far enough ahead of the crack tip to form a microvoid, then the energy effect would be greater. It might also be argued that the effect of particle fracture would be to increase surface roughness, and that would in turn, enhance fracture toughness because of the increase in the fracture surface area created [15].

Matrix Failure Due To Addition of Reinforcement:

Bernstein et al [19] have proposed that matrix failure may play a significant role in the failure mechanism of *Al/SiCp* composites. The reinforcement particles contribute to the failure process primarily by imposing high levels of constraint on matrix deformation and by raising the stress in the matrix to a level significantly greater than that normally associated with matrix failure. Due to addition of hard particles to ductile alloy, the slip characteristics of the matrix alloy are altered. Particles will have the primary effect of blocking slip lines, but there may also be secondary effects, such as limiting the operation of secondary dislocation sources and limiting the extent of cross-slip. These effects will have such consequences as limiting the size of the plastic zone surrounding a crack-tip, thereby decreasing the volume of deforming material within it. Since the volume of deforming material is at least partly responsible for the magnitude of the fracture toughness, this would be a major effect of decreasing the fracture toughness.

2.7.FATIGUE PROPERTIES OF PARTICULATE METAL MATRIX COMPOSITES

The use of discontinuous reinforcements to improve the mechanical properties of metallic alloys has provided a relatively less expensive means of producing materials with improved stiffness, strength, wear, and high temperature resistance for applications where the very highly directional properties of continuous fiber-reinforced composites are not required.

Whether their primary use is with aerospace or automotive applications, the resistance of *MMCs* to failure under cyclic or otherwise varying loads is of paramount importance. However, whereas the addition of particulate reinforcements such as *SiC* can lead to acceptably low ductility and fracture toughness properties, the fatigue properties of *MMCs* are compatible and in many cases exceed that of their respective unreinforced matrices [23].

Fatigue Crack Propagation:

Fatigue crack propagation behavior is generally characterized in terms of fracture mechanics; crack growth rate (da/dN) data are displayed as a function of the applied stress intensity range ($\Delta K = K_{max} - K_{min}$), where K_{max} and K_{min} are the extremes of stress intensity in the fatigue cycle. Such results are often described by equations of the form,

$$\frac{da}{dN} = \beta * \Delta K^n \rightarrow (2.1)$$

Where, β is a constant. Hence, a plot of crack growth rate (m/cycle) against ΔK , with log scales, should give a straight line in the Paris regime, with a gradient equal to n . At low stress intensities, there will be a threshold, ΔK_{th} , below which no crack growth occurs, while the crack growth rate usually accelerates as the level for fast fracture, K_c , is approached [Figure 2.15].

Fatigue data are sometimes presented in the form of S-N curves, showing the number of cycles to failure (N) as a function of the stress amplitude (S) [Figure 2.16]. Many materials show a roughly sigmoidal curve, with very rapid crack growth when the stress amplitude is high, a central portion corresponding to the Paris regime and a fatigue limit, which is stress amplitude below which failure does not occur even after large numbers of cycles. This corresponds to stress intensity below ΔK_{th} .

Closure is the term used to describe phenomenon, which prevent attainment at the crack tip of the K_{min} , and thus reduce the crack propagation rate through a failure to attain the full ΔK range. Three types of closure are commonly encountered-

- Roughness induced closure.
- Oxide induced closure.
- Plasticity induced closure.

All the three limit the actual K_{min} attained by holding open the crack tip. For *MMCs*, the effect of closure has been found to be reduction of about $1.5 \text{ MPa m}^{-1/2}$ in ΔK for K_{max} in the range of $4\text{-}8 \text{ MPa m}^{-1/2}$ [4]. Closure is generally reduced at greater R ratios,

$$R = \frac{\text{min load}}{\text{max load}} = \frac{K_{min}}{K_{max}} \rightarrow (2.2)$$

because the crack is then held more widely open throughout the cycle [4].

Fatigue Crack Propagation in Particulate *MMCs*:

The fatigue response of discontinuous *MMCs* is best considered by relating the magnitude of ΔK to the plastic zone size (r_Y), the scale of the microstructure, and the failure mechanism. Figure 2.17 shows a schematic depiction of the fatigue crack growth rate as a function of the applied stress intensity factor for a typical discontinuous *MMC* and the corresponding unreinforced alloy [4]. Below ΔK_{th} cracks are unable to grow at all. For *Al-SiCp MMCs*, ΔK_{th} is typically around $2\text{-}4 \text{ MPa m}^{-1/2}$, which is double that of the unreinforced alloys ($1\text{-}2 \text{ MPa m}^{-1/2}$) [4].

Because of the relatively low fracture toughness of *MMCs*, the Paris regime is usually short. The exponent n is often around $5\text{-}6$, which is higher than those typical of unreinforced systems (~ 4) [4]. In this regime ($\Delta K \sim 8 \text{ MPa m}^{-1/2}$), a number of particles are encompassed by the plastic zone ($r_Y \sim 50 \mu\text{m}$), so that the crack tip sees a continuum with a higher yield stress. At high ΔK ($>12 \text{ MPa m}^{-1/2}$, $r_Y > 100 \mu\text{m}$), many particles are within the plastic zone, fast fracture failure modes become operative and the fatigue resistance of *MMCs* becomes appreciably worse than that of unreinforced alloys, reflecting their generally inferior fracture toughness [4].

2.8.EFFECTS OF MICROSTRUCTURAL VARIABLES ON THE FRACTURE AND FATIGUE PROPERTIES OF ALUMINIUM SILICON CARBIDE PARTICULATE *MMCs*

The fracture toughness and fatigue behavior of *MMCs* can be quite sensitive to the microstructural details. This sensitivity covers the reinforcement, the interface and the matrix. Microstructural factors that affect the properties of *Al-SiCp* composites are mainly the volume fraction, the particle size, shape, and distribution.

Effect of *SiC* Volume Fraction:

Generally, tensile and yield strengths increases over the unreinforced matrix alloy with the addition of *SiC* particles. This is shown in Table 2.2. The results have been taken from the investigations of Chawla et al [23].

Similar trends have been reported by Hall et al [25]. Various authors [26-27] have suggested various explanations for the increase in the yield strength with increase in volume fraction of *SiC* particles. Most of the workers have suggested that much of the strengthening comes from load transfer from the matrix to the reinforcements [25-27]. Arsenault [26, 12] has suggested that the increase in strength is due to increase in dislocation density that arises from thermal mismatch between the composite constituents. It has been also investigated that increasing volume fraction results in an increase in fatigue resistance of these materials [23]. Table 2.3 shows the effect of reinforcement volume fraction on the fatigue properties of 2080 *Al* alloy.

Figure 2.18 shows stress amplitude vs cycles to failure for the unreinforced and composite materials with varying reinforcement volume fractions. Both Table 2.4 and Figure 2.18 show that increasing *SiC* volume fraction results in higher fatigue strength. Similar trends were shown by Hall et al [25]. It has been suggested that the higher fatigue strengths of the composites is largely due to lower total strain as a result of load transfer to the high modulus reinforcement [23]. The addition of *SiC* particles reduces the effective stress concentration on intermetallic inclusions in the matrix of the composites, increasing fatigue life over the unreinforced alloy, where the inclusions have a higher stress concentration. Increasing *SiCp* volume fraction results in smaller inclusion sizes in the composites. This is attributed to breaking of the brittle inclusions by the reinforcing particles during extrusion and rolling process before testing. The lower inclusion size in the composites with higher reinforcement loading may indirectly

contribute to higher fatigue lives in these composites [23]. Hall et al [25] have suggested that the increased fatigue life due to increasing volume fraction of *SiC* particles is attributed to the increased modulus of the composite.

Volume fraction also has an effect on the frequency of particle fracture during fatigue crack propagation. This has been illustrated in Figure 2.19. The results show that the amount of particle fracture increases with increase in volume fraction. In addition during fatigue crack propagation the frequency of the particle fracture increases with increasing stress intensity. Increased particle fracture with increased crack tip stress intensity is due to the increase in plastic zone size, which samples a statistically greater number of particles [25].

Effect of Particle Size:

Considerable effort has been expended in investigating the size dependence of fracture toughness and fatigue properties for the *Al-SiCp* composites [23,25, 28-30]. Nan and Clarke [28] predicted for the effect of different uniform particle sizes on the flow behavior of the *Al*-15 vol% *SiC* composite. The results are shown in Figure 2.20. Table 2.4 shows the effect of *SiC* particle size on the monotonic tensile properties of 2124 *Al-SiCp* composites.

From Figure 2.20 and Table 2.4 it can be seen that tensile strengths and yield strengths increases with decreasing particle size. Nan and Clarke [28] have suggested that when particle size is large, e.g. $d > 10\mu\text{m}$, there is only a slight dependence of the behavior on the particle size and so continuum plasticity dominates. In contrast, when the particle size is small, e.g. $d < 0.5\mu\text{m}$, the dislocation strengthening dominates and the mechanical behavior has a strong dependence on the particle size. In the intermediate particle size range, both mechanisms play a significant role in the deformation process of these *MMCs*. The dependence of fracture toughness on the particle size is not clearly understood. Flom and Arsenault [29] found that fracture toughness is largely independent of particle size. However, it has also been mentioned that it is better to go for finer particles for higher fracture toughness [31].

Figure 2.21 shows the effect of particle size on the probability of particle fracture, with the frequency of particle fracture increasing as the particle size increases. This is because crack tends to avoid the smaller particles. On the other hand it gets arrested by

the bigger particles and passes only when the particle fractures. Hence the probability of particle fracture is greater in the case of bigger particles. Increased particle fracture with increased crack tip stress intensity has been attributed to be the result of increased plastic zone size, which samples a statistically greater number of particles [25].

The effect of reinforcement size on the fatigue properties of 2080 *Al*-20 vol% *SiC* composites are shown in Table 2.5 and Figure 2.22. This has been attributed to the fracture of the coarser particles during working operation prior to testing [23].

Effect of Particle Shape:

Particle shape effects on fracture and ductility of 20 vol% *Al₂O₃*-6061 *Al* composites were studied by Song et al [32]. It has been concluded that the spherical particle reinforced composites exhibit lower yield strength, a slightly lower work hardening rate, but considerably higher ductility than the angular particle reinforced composites. Fracture of the angular particulate reinforced composites proceeds through particle fracture, where as failure of the spherical particle reinforced composite is demonstrated by void nucleation, growth and coalescence in the matrix near the reinforcement [32].

Effect of Reinforcement Distribution or Clustering:

Recent advances in the quantification of the effects of local reinforcement arrangements have been stimulated by improved quantification of spatial distributions via Dirichlet Tessellations using image analysis [33-38]. Particle clustering does not have an influence on the global properties, such as the young's modulus, but it does affect those properties that are susceptible to microstructural inhomogeneity, such as strength and ductility [33].

According to Nan and Clarke [28], the macroscopically averaged stress and strain on a perfectly bonded isotropic metal matrix composite can be expressed as

$$\sigma_y = \int \sigma_y^m \left(1 + f \frac{y_{ms}}{\mu_{ms}} \frac{\mu_p - \mu_{ms}}{\mu_p + y_{ms}} \right) + \frac{\delta_y}{3} \sigma_{kk}^m \left(1 + f \frac{4\mu_{ms}}{k_m} \frac{k_p - k_m}{3k_p + 4\mu_{ms}} \right) p(d') \delta d' \rightarrow (2.3)$$

$$\varepsilon_y = \int \left[\varepsilon_y^m \left(1 - f \frac{\mu_p - \mu_{ms}}{\mu_p - y_{ms}} \right) + \frac{\delta_y}{3} \varepsilon_{kk}^m \left(1 - 3f \frac{k_p - k_m}{3k_p + 4\mu_{ms}} \right) \right] p(d') \partial d' \rightarrow (2.4)$$

$$\text{With } y_{ms} = \mu_{ms} (9k_m + 8\mu_{ms}) / (6k_m + 12\mu_{ms}) \rightarrow (2.5)$$

Where k_m and μ_{ms} are the elastic bulk and secant shear moduli of metal matrix, k_p and μ_p are the elastic bulk and shear moduli of the particles, and f is the volume fraction of the particles; δ_{ij} is the Kronecker delta; σ_y^m and ε_y^m are the respectively hydrostatic and deviatoric parts of the stress and strain in the metal matrix. The integrals in eq (2.3) and (2.4) are over all possible particle sizes in the composite, and here $P(d')$ is a function of particle size distribution. In the previous simulations this distribution function has been taken as the lognormal number frequency function, namely,

$$P_N(d') = \frac{1}{d\sqrt{2\pi}\delta} \exp \left\{ - \left[\frac{\ln\left(\frac{d'}{d}\right)}{\sqrt{2\delta}} \right]^2 \right\} \rightarrow (2.6)$$

Where d is the geometric mean particle size and δ is the standard deviation. The macroscopically averaged stress and strain are volume weighted average one and thus $P(d')$ denotes a volume frequency function, $P_v(d')$, which is related to $P_N(d')$ through

$$P_v(d') = \left(\frac{d'}{d} \right)^3 \exp \left(- \frac{9\delta^2}{2} \right) P_N(d') \rightarrow (2.7)$$

Experimental studies show that with increasing degree of particle clustering or non-uniform distribution of particles there are only small increase in the flow stress and work hardening rate but there is a large decrease in ductility [33-38]. Figure 2.23 shows one such result. The influence of particle clustering on fracture toughness is shown in Figure 2.24. This shows the decrease in fracture toughness with increasing particle clustering in A356 Al alloy/SiCp, where Clustering is represented as the standard deviation in the frequency distribution of the nearest neighbor edge-to-edge spacing. Fracture in particulate reinforced metal matrix composites involves damage initiation by cracking or particle- matrix decohesion, followed by damage accumulation process of void growth, with possible further damage initiation, until the critical damage state is reached and

fracture occurs. When the particle distribution is non-uniform, damage is concentrated in particle clusters and fracture occurs by linking of the “damage clusters” [33].

2.9. EFFECT OF MATRIX AGEING ON THE PROPERTIES OF *Al-SiCp* METAL MATRIX COMPOSITES

The magnitude of stress that can be supported within the matrix is of great importance when considering failure by void nucleation, as well as its ability to flow under highly constrained conditions. Many studies have been undertaken on the effect of ageing condition on the properties of *Al-SiCp* metal matrix composites. Lewandoski et al [39-40] have reported that the changes in the ageing condition can bring about significant changes in the fracture micro-mechanics. They studied over aged (*OA*) and under aged(*UA*) *Al-Zn-Mg-Cu* alloy containing 0, 15, 20% by volume of *SiCp* composites. In the *UA* composites, the area fraction of the particles at the fracture surface was approximately equal to that expected if the fracture were to take place by particle cracking, whereas in the *OA* composite it was significantly less, indication of fracture predominantly in the matrix. This has been attributed to the weakening of the interfacial bonding, or of the matrix near the reinforcement, due to a precipitate free zone (*PFZ*) in the *OA* material.

2.10.EFFECT OF PROCESSING ON THE MICROSTRUCTURE AND PROPERTIES OF *Al-SiCp* METAL MATRIX COMPOSITES

The processing techniques involved in the manufacturing of *Al-SiCp MMCs* has already been discussed previously in this section. Each processing technique results in a characteristic microstructure and thus properties.

2.10.1. Effect of Primary Liquid Processing Technique

As discussed earlier in this paper, the main primary liquid processing techniques involve Compocasting, squeeze casting, spray deposition and reactive processing. When the metal matrix composites are produced by molten metal methods there are some unique factors which have to be considered. One of the important factors is the change in the microstructure. The effect of microstructure on the properties of *MMCs* has already been discussed earlier. The microstructural feature that is greatly affected by processing via molten metal route is the reinforcement distribution in composites processed in the molten state, the reinforcement distribution is influenced by several factors [41]:

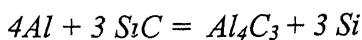
- i. distribution in the liquid as a result of the mixing.
- ii. distribution in the liquid after mixing but prior to solidification.
- iii. redistribution as a result of solidification.

The distribution during mixing will depend on the mixing process used, and it is essential to produce as uniform a distribution as possible without any gas entrapment, since any gas bubble will be lined with reinforcing particles. After mixing and prior to solidification, the particles will settle and segregate due to gravity. The settling rate will be a function of the particle density and size, and there is also the possibility that particle shape will play a role. Particles of different sizes and shapes will settle at different rates producing agglomeration and this can produce clusters which settle as a cluster rather than individual particles.

The third factor which influences reinforcement distribution is the solidification process itself. Reinforcing particles do not generally nucleate the primary solidifying phase(aluminium dendrites). If solidification nucleation does not occur, the reinforcing particles are rejected at the solid-liquid interface, and segregate to the interdendritic regions which solidify last. However, particle segregation due to particle rejection at the solidification front can be minimized by using a high solidification rate casting process such as twin roll casting [41].

During solidification two phenomenon occurs simultaneously. Firstly, the solidifying interface tend to push a freely suspended particle in the melt. Secondly, particles are captured by solidifying dendrites from the opposite directions. Particle distribution in the solidifying melt depends on the rate of particle pushing and particle capture by the growing dendrites [42].

Another important phenomenon encountered with molten metal processing route is the reaction of SiC with molten aluminium to form Al_4C_3 [41] as follow:



This reaction has several detrimental effects which are as follows:

- a. it produces the reaction product Al_4C_3 at the interface between the reinforcement and the matrix, which could result in a degradation of the reinforcement strength and the interfacial strength;

b. the reaction product Al_4C_3 is unstable in some environments, so it increases the corrosion susceptibility of the alloy;

c. the reaction increases the silicon content of the alloy and have the matrix composition of the alloy may be changed significantly if extensive reaction occurs [42-49]. Though partial reaction is helpful as it results in SiC wetting and causes proper interfacial bonding. However, if the reaction is more interfacial bonding is very strong which is not desired. This reduces the fracture toughness of the material. This has been discussed earlier in this chapter.

2.10.2. Effect of Solid State Processing and Secondary Processing technique

The PM route has the advantage of reducing the interaction between the ceramic reinforcement and the matrix through semisolid and/or solid state processing [49].

Other attractive features include it's ability to

- i. combine various matrix reinforcements within the same composite;
- ii. utilize non-equilibrium matrix alloys produced by rapid solidification;
- iii. achieve high reinforcement volume fraction [49].

However,. the selection of suitable processing parameters in the processing of composites via *PM* route to ensure uniform and reproducible elastic and mechanical properties. Jain et al [50] have studied the effect of various processing parameters and steps on the microstructure and mechanical properties of 2124 *Al/SiCp* composites. The specimens were prepared by vacuum hot pressing(*VHP*). The effect of secondary processing treatment were also studied. Representative micrographs of the composites with 10 vol% *SiC* particles and 30 vol% *SiC* particles in the *VHP*, *VHP*+extruded and *VHP*+extruded +section rolled conditions are illustrated in Figure 2.25, 2.26, 2.27 respectively. it is seen that the level of porosity is highest in the *VHP* condition and the *SiC* particles appear to be clustered around the aluminium alloy particle boundaries. After subsequent processing by extrusion and section rolling the pores are healed and the *SiC* particles have a more uniform and homogeneous distribution. This is because extrusion and section rolling produce extensive shear deformation of the matrix, causing break up of the prior *SiC*-rich cermet network in the billet, resulting in a more uniform distribution[50].

2.11. QUANTITATIVE STEREOLOGY

Quantitative Stereology attempts to characterize numerically the geometrical aspects of those features of microstructure that interest us. The basic measurements in quantitative stereology are performed on two dimensional sections or projections. The main measurements that have been discussed in this section include measurement of volume fraction (V_v), surface area per unit volume (S_v), mean free distance (λ), and particle size (D). The former two (V_v and S_v) are measured quantities whereas the latter two (λ and D) are derived or calculated from V_v and S_v .

2.11.1. Measurement of Volume Fraction (V_v)

Volume Fraction can be defined as the fraction of volume of a particular phase or particle in the total volume. There are three different methods for measurement of volume fraction. One of the methods involves measurements of areas; another, the measurement of lineal intercepts; and a third, the counting of points. These three methods are called areal analysis, lineal analysis, and point counting, respectively. Of the three different methods for estimating the volume fraction, point counting is preferred [51]. Point counting requires the least effort to obtain an estimate with a given sampling error. In this method, a network of points is disposed uniformly over a sample area of the microstructure. The number of points that falls over the area of interest is counted for the first position of the grid. Then the grid is repositioned randomly, or translated in a particular direction. The number of points falling over the feature of interest is counted again. This process is repeated until a sufficient number of measurements have been obtained. The total number of points falling over the feature of interest is divided by the total number of grid points to give the Point Fraction (P_p). It has been proved theoretically that volume fraction equals point fraction [51]. Hence Volume Fraction (V_v) of a particular phase can be easily obtained through simple point counting.

2.11.2. Measurement of Surface Area per unit Volume (S_v)

Measurement of S_v also requires simple point counting. It involves counting the number of points (intersections) generated per unit length of test lines, P_L . A linear array or circular test array is applied randomly to the microstructure in the section plane. The points usually consist of intersections made by test lines with traces of surfaces on the plane of polish. The test arrays may be applied randomly or dispersed systematically over

the entire microstructure. The actual length of the lines (L) depends on the magnification of the microstructure. The value of L can be determined at a standard magnification with the help of a micron bar. The basic equation for calculating the area of surfaces in a volume is

$$S_v = 2P_L \rightarrow (2.6)$$

Which was derived by Saltikov in 1945, and later by Smith and Guttman in 1953 [51].

2.11.3. Measurement of Mean Free Distance (λ)

A spatial parameter of great importance in particulate systems is the mean free distance, λ , between particles. The mean free distance is essentially a mean edge-to-edge distance. It represents the uninterrupted interparticle distance through the matrix averaged between all possible pairs of particles. Although λ is measured on random section planes, it gives the true three-dimensional distance between particles. A truly random distribution of particles has the same mean interparticle distance on a plane as in a volume, since the geometric property is same in any direction [51].

It has been proved that

$$\lambda = \frac{4(1 - V_v)}{S_v} \rightarrow (2.7)$$

Where, V_v and S_v refer to the volume fraction and surface area per unit volume, respectively of phase or particle of interest [51].

2.11.4. Measurement of Particle Size (D)

An ASTM-E112 standard is used to measure grain size of polycrystalline material. An equivalent measure of size for SiC particles in this *MMC* can be expressed as follows [51]

$$D = 4 \frac{(V_v)}{(S_v)} \rightarrow (2.8)$$

2.11.5. Error Analysis

An estimate of microstructural parameters depends on the reliability of the measurements. It is just as important to be able to estimate the errors in an analysis as is to perform the analysis itself. There are three general types of errors to guard against [51]. First are the errors arising from the experimental limitations. These include resolution of the microscope, etching effects, uncertainties in the length of test figure, incorrect counting, and so on. The second major type of error is caused by improper

sampling techniques. During analysis it is essential that all randomization processes be executed in a truly random fashion. The test area should be selected at random and the test figure applied at random, preferably without looking. If the observer makes a subjective decision, then some degree of bias will almost always be introduced. A third error results from non-representative samples, whereby the areas selected for analysis are not exactly representative of the specimen as a whole. These sampling errors usually constitute the bulk of the total error.

It is expected that the greater the number of observations involved in measurement, the greater will be its accuracy. However, a compromise must be achieved between effort and accuracy.

The estimation of error for a particular measurement is done by the concepts of Central Limit Theorem of Statistical Estimates. According to this, the mean of a population is given as

$$\bar{X} = \langle X \rangle \pm 2\sigma \rightarrow (2.9) \text{ With 95\% confidence.}$$

Where,

\bar{X} is the population mean.

$\langle X \rangle$ is the sample mean.

σ is the standard deviation and is given by

$$\sigma^2 = \frac{\sum (\langle X \rangle - X_i)^2}{(N-1)\sqrt{N}} \rightarrow (2.10)$$

Where,

N is the total number of observations.

2.12.TABLES

Table 2.1. Mechanical Properties [4]

| Material | E (GPa) | Poisson Ratio | $T.S.$ (GPa) | Density (gm/cc) | MP (K) | CTE ($\mu\epsilon/K$) | TC (W/mK) |
|------------------------|--------------|------------------|-----------------|--------------------|-------------|------------------------------|----------------|
| <i>Al</i> (1100) | 70 | 0.33 | 0.17 | 2.7 | 933 | 23.6 | 230 |
| <i>Al-Cu</i> (2024) | 73 | 0.33 | 0.47 | 2.8 | 915 | 23.6 | 190 |
| <i>Al-Mg-Si</i> (6061) | 70 | 0.33 | 0.38 | 2.7 | 925 | 23.6 | 180 |
| <i>Al-Zn</i> (7075) | 72 | 0.33 | 0.57 | 2.8 | 925 | 22.0 | 130 |
| <i>Al-Li</i> (8090) | 80 | 0.33 | ---- | 2.55 | 930 | ---- | |
| <i>SiC</i> | 450 | 0.17 | ---- | 3.2 | ---- | 4.0 | ~11 |
| <i>SiC_w</i> | 450 | 0.17 | 3.1<2 1 | 3.2 | ---- | 4.0 | >16 |
| <i>SiC</i> (Nialon) | 180 | ----- | >2.4, 8.3 | 2.55 | 1095 | 3.0 | 16 |

Table 2.2. Tensile properties of reinforced and unreinforced 2080 *Al* alloy [23]

| Vol% <i>SiC</i> | Yield strength (M Pa) | Ultimate tensile strength (M Pa) | Elastic modulus (G Pa) | Strain to failure (%) |
|-----------------|--------------------------|-------------------------------------|---------------------------|--------------------------|
| 30 | 575 | 639 | 119 | 2.27 |
| 20 | 539 | 593 | 107 | 3.14 |
| 10 | 528 | 574 | 89 | 6.34 |
| 20 | 522 | 563 | 106 | 2.88 |
| 20 | 457 | 478 | 95 | 1.02 |
| Unreinforced | 490 | 525 | 75 | 9.0 |

Table 2.3. Effect of reinforcement volume fraction on the fatigue properties of 2080 Al alloy [23]

| Vol% SiC | Approximate fatigue strength (10^7 cycles), σ_{fat} (M Pa) | Yield strength (0.2 % offset), $\sigma_{0.2}$ (MPa) | Fatigue ratio ($\sigma_{fat}/\sigma_{0.2}$) |
|--------------|--|---|---|
| 30 | 250 | 575 | 0.43 |
| 20 | 230 | 539 | 0.42 |
| 10 | 210 | 528 | 0.4 |
| Unreinforced | 140 | 490 | 0.28 |

Table 2.4. Monotonic Tensile Properties of 2124 Al-SiCp Composite

| SiC particle size (μm) | Yield strength (MPa) | Ultimate tensile strength (MPa) | Total elongation (%) |
|-------------------------------------|----------------------|---------------------------------|----------------------|
| 2 | 479 | 628 | 2.9 |
| 5 | 471 | 612 | 3.6 |
| 9 | 460 | 580 | 2.3 |
| 20 | 425 | 500 | 2.2 |

Table 2.5. Effect of reinforcement size on the fatigue properties of 2080 Al-SiCp composites

| SiC particle size (μm) | Approximate fatigue strength (10^7 cycles), σ_{fat} (MPa) | Yield stress (0.2% offset), $\sigma_{0.2}$ (MPa) | Fatigue ratio ($\sigma_{fat}/\sigma_{0.2}$) |
|-------------------------------------|---|--|---|
| 5.18 | 230 | 539 | 0.42 |
| 6.4 | 220 | 522 | 0.42 |
| 23.26 | 150 | 457 | 0.33 |
| Unreinforced | 140 | 490 | 0.28 |

2.13.FIGURES

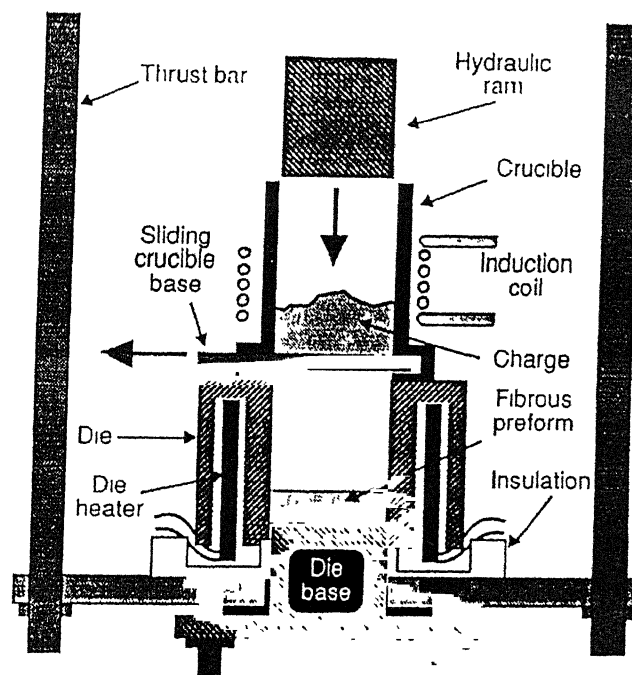


Figure 2.1 Schematic illustration of an apparatus used for squeeze infiltration [4]

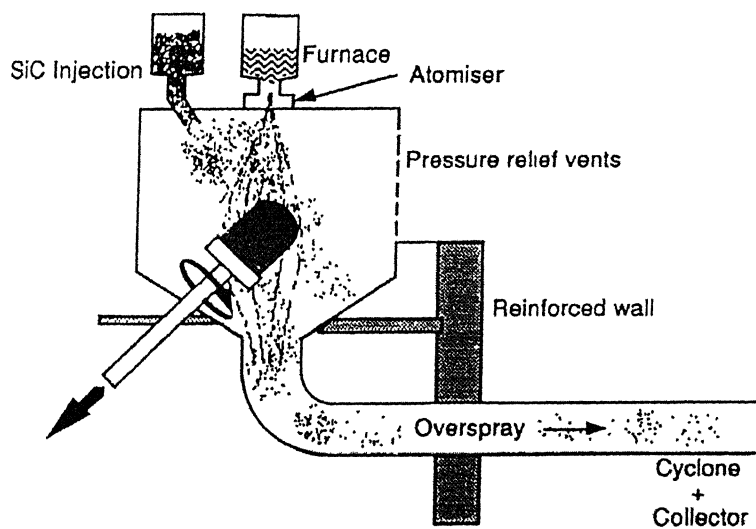


Figure 2.2. Schematic illustration of Osprey spray casting arrangement [4].

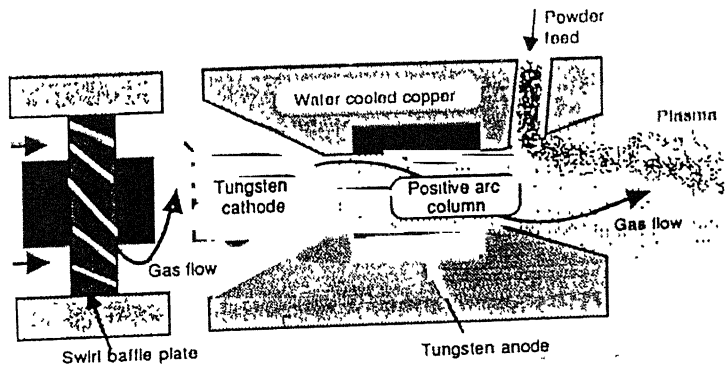


Figure 2.3. Schematic section through a plasma spray torch [4].

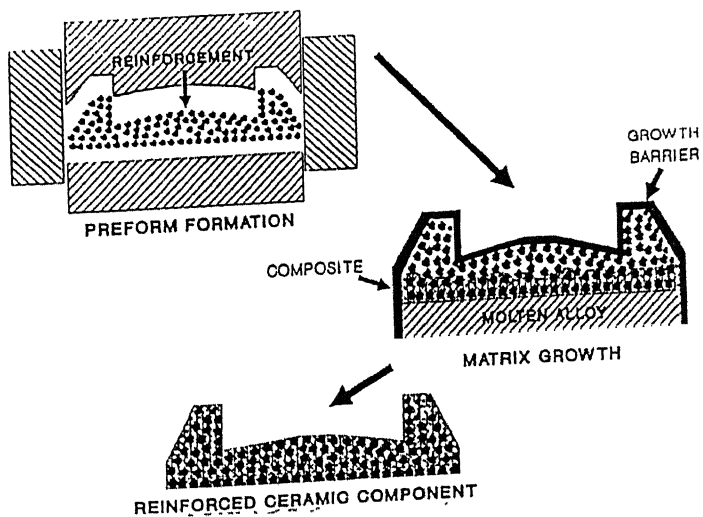


Figure 2.4. Schematic of Lanxide Process [7]

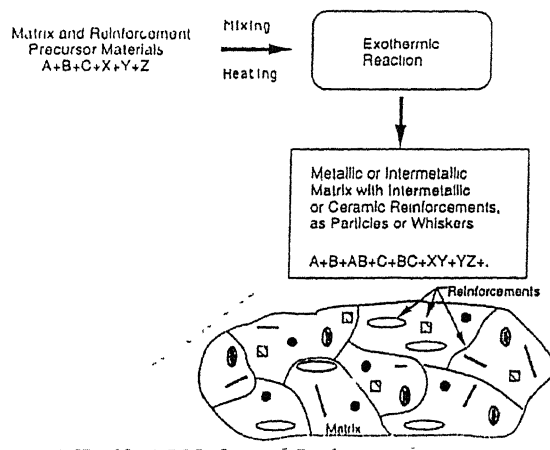


Figure 2.5. Schematic of XD Process [7].

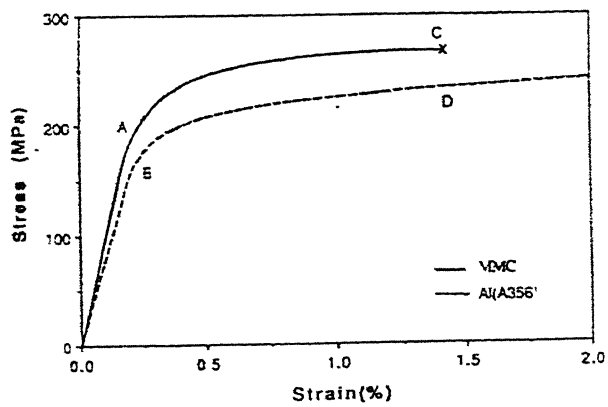


Figure 2.6 Stress Strain curves for Al (A356) alloy and 15% particulate SiC/Al MMCs [9]



Figure 2.7. Optical micrograph of a cast SiC_p/Al (A356) *MMCs* [9]

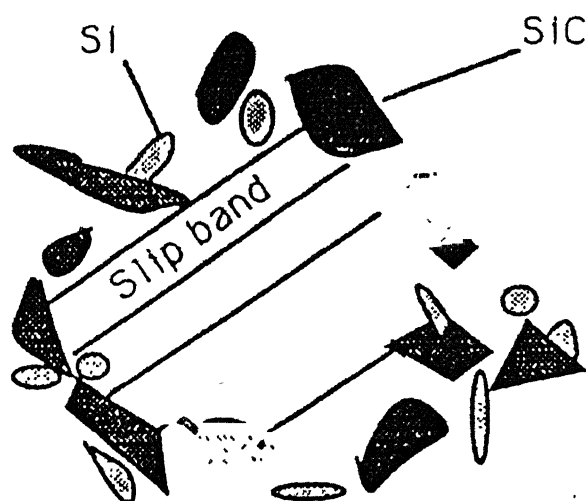


Figure 2.8. Schematic figure showing the role of reinforcing particles in resisting slip behavior of the *MMCs* [9].

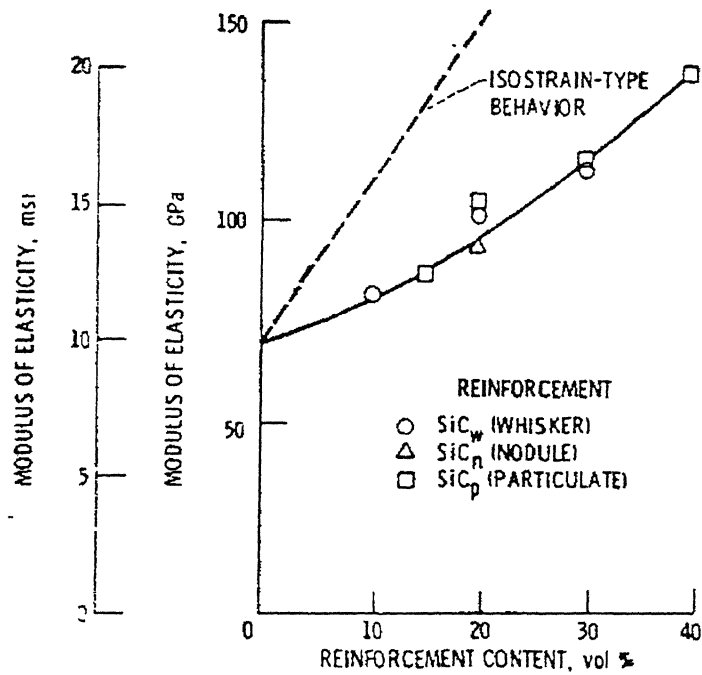


Figure 2.9. Effect of reinforcement content on modulus of elasticity of discontinuous *SiC/6061 Al* composites [13].

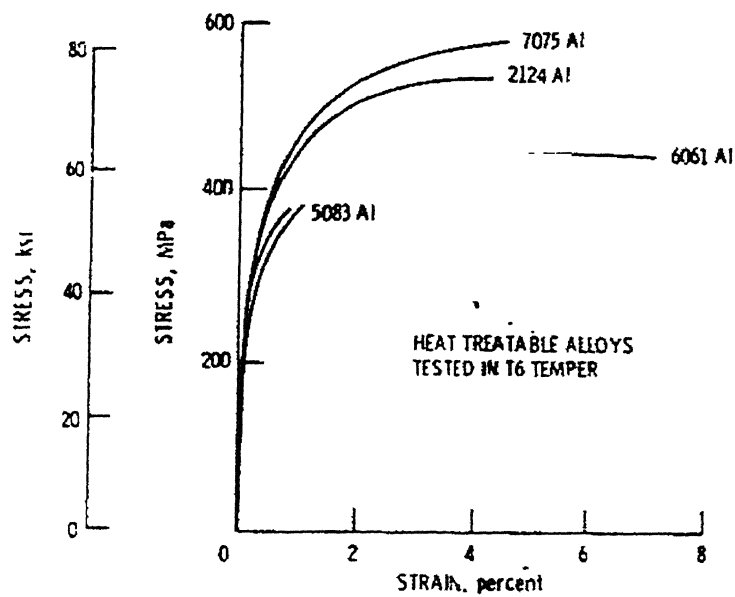


Figure 2.10. Effect of *Al* matrix alloy on the stress strain behavior of composites with 20 vol% *SiC_w* reinforcement [13].

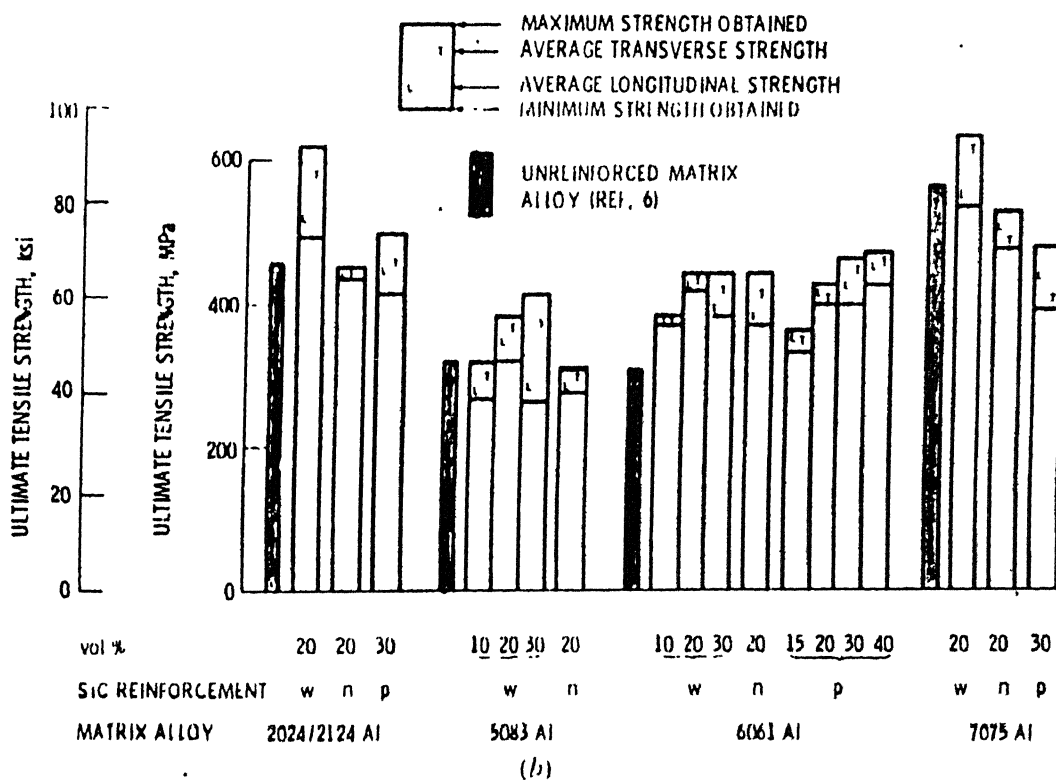
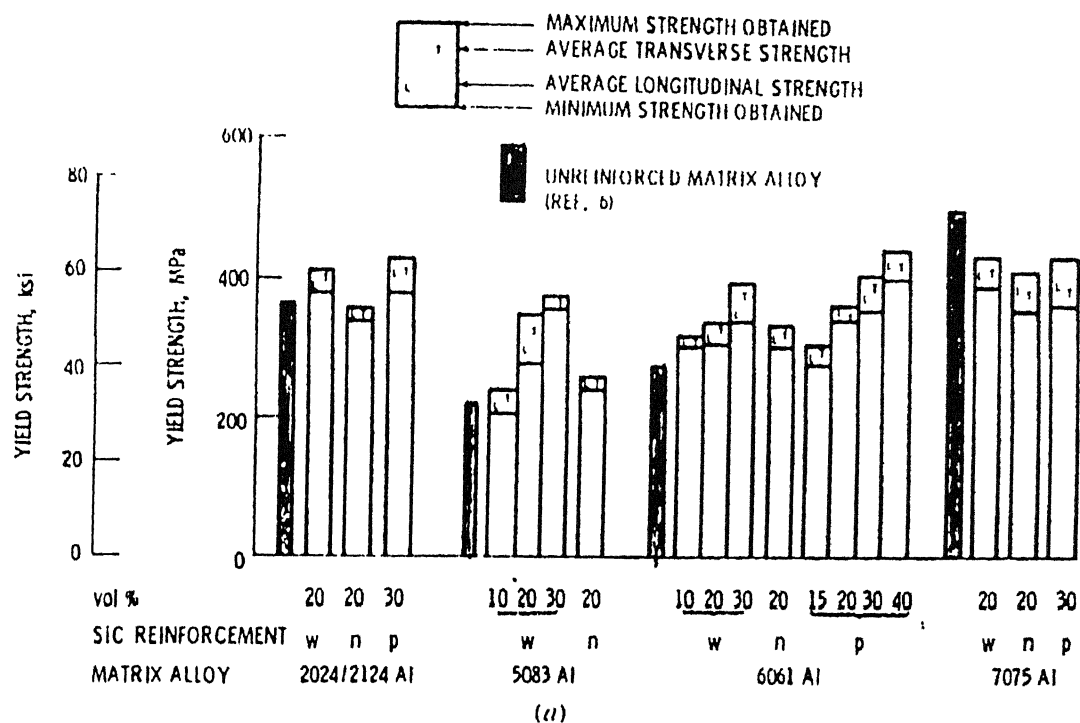


Figure 2.11. Effect of *SiC* reinforcement type and content on the tensile properties of discontinuous *SiC/Al* composites [13].

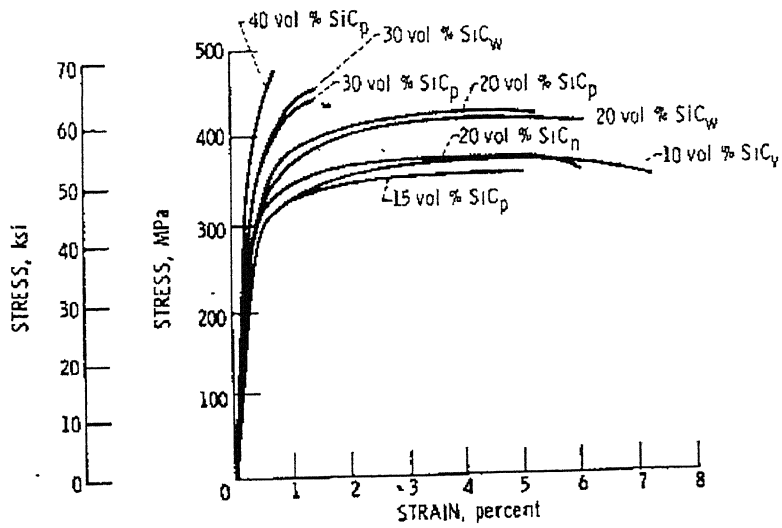


Figure 2.12. Stress-Strain curves of *SiC/6061 Al* composites [13].

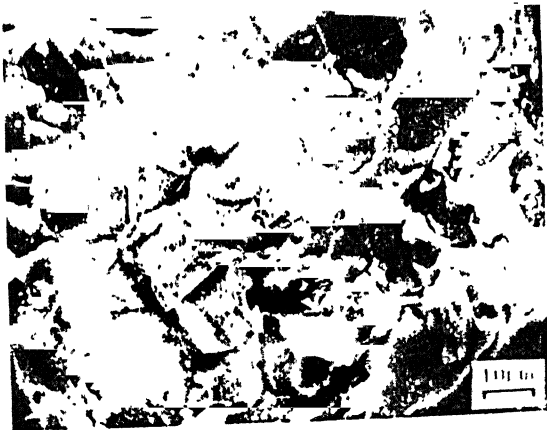


Figure 2.13. Fractography of the tensile sample, showing tear ridges, isolated patches of very small dimples, and broken *SiC* particles [17].

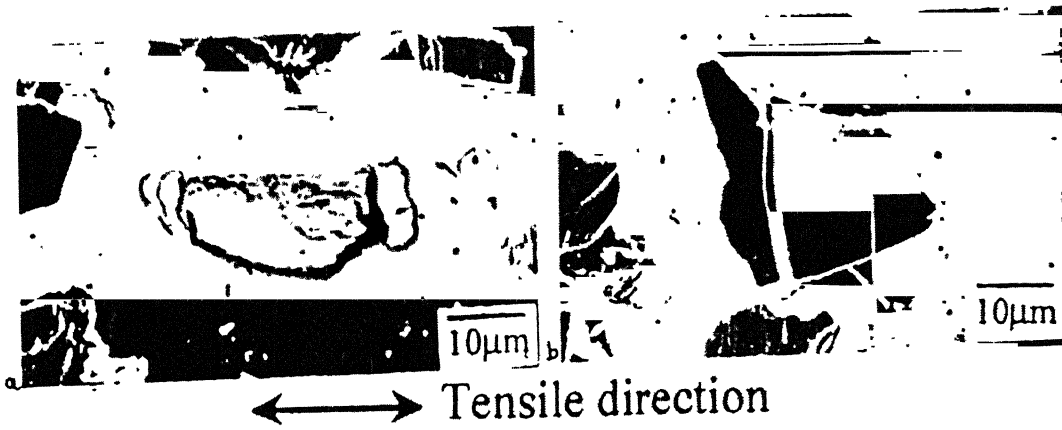


Figure 2.14. Typical microcracks observed inside specimens of *SiC/6061Al* (a) Interface debonding (b) particle cracking [18].

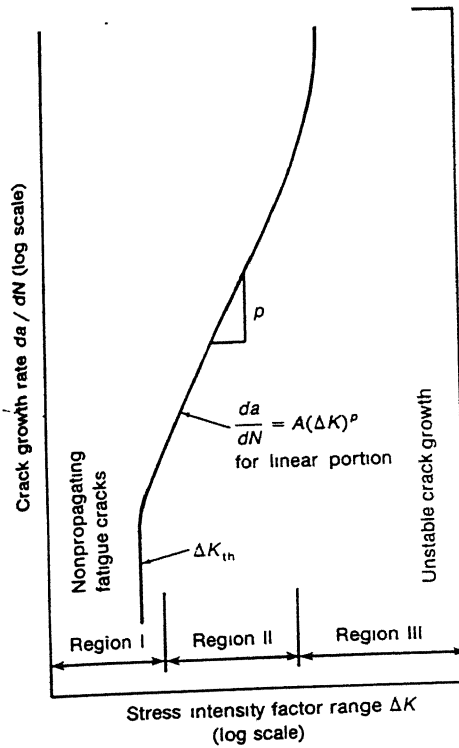


Figure 2.15. Schematic representation of fatigue cracks growth behavior in a non-aggressive environment [24].

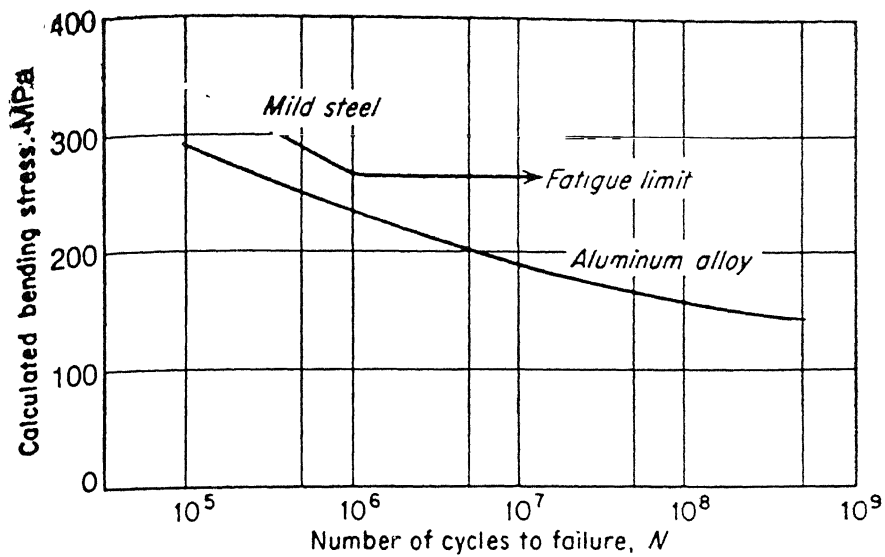


Figure 2.16. Typical fatigue curves for ferrous and non-ferrous metals [24].

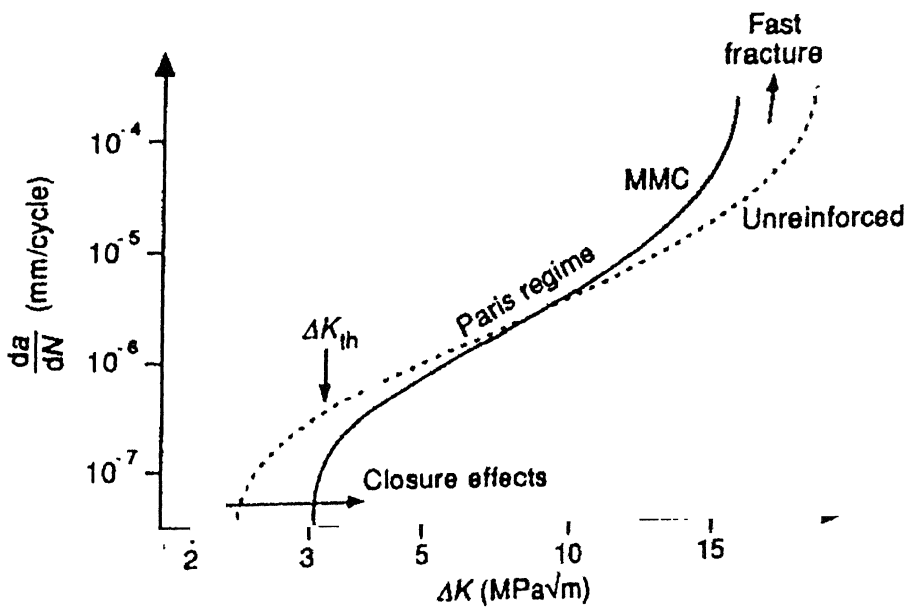


Figure 2.17. Schematic depiction of fatigue crack growth rate as a function of the applied stress intensity factor for a typical discontinuous MMC and the corresponding unreinforced alloy [4].

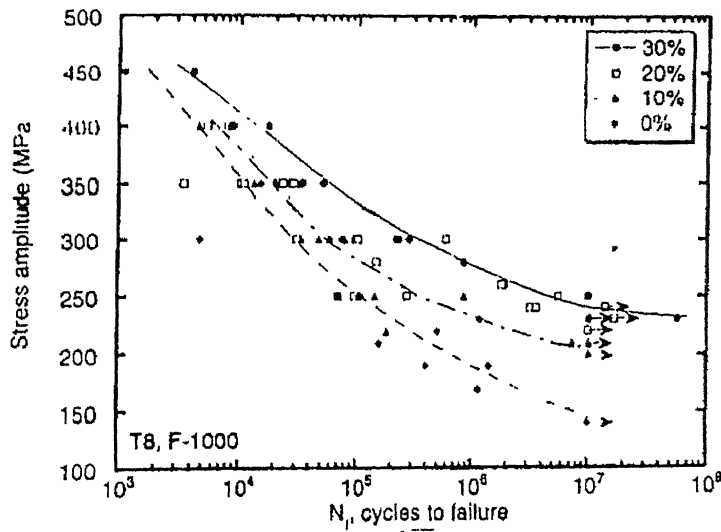


Figure 2.18. Effect of *SiC* reinforcement volume fraction on the fatigue life of *Al/SiCp* MMCs [25].

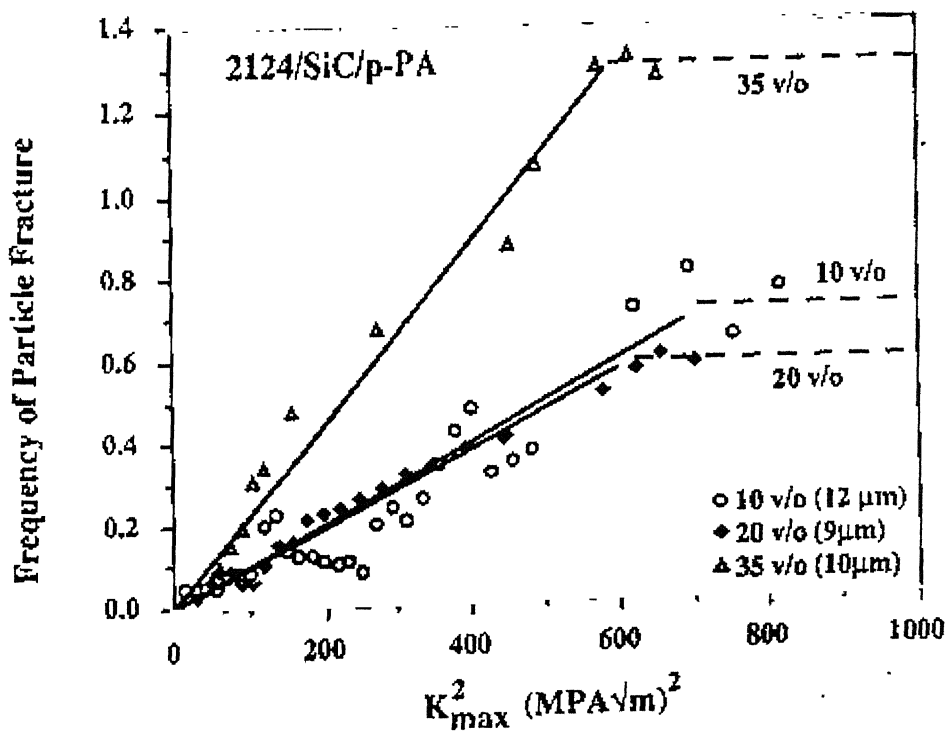


Figure 2.19. Effect of volume fraction on the frequency of particle fracture [26].

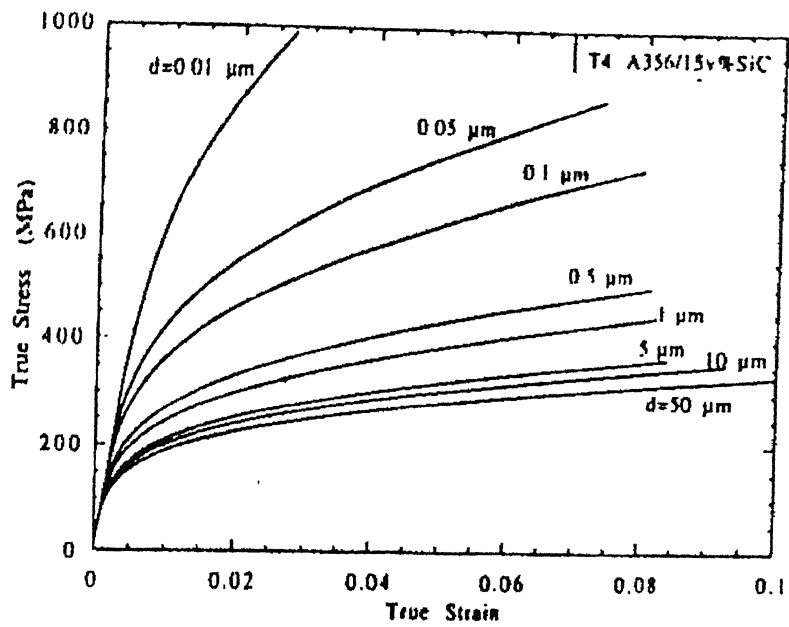


Figure 2.20. Effect of different uniform particle sizes on the flow behavior of Al-15vol% SiC composites [29].

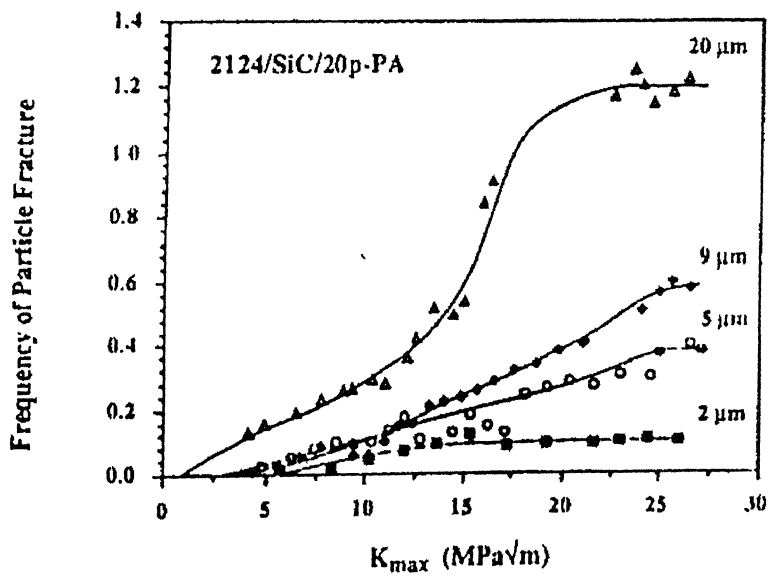


Figure 2.21. Effect of particle size on frequency of particle fracture as a function of K_{max} [26].

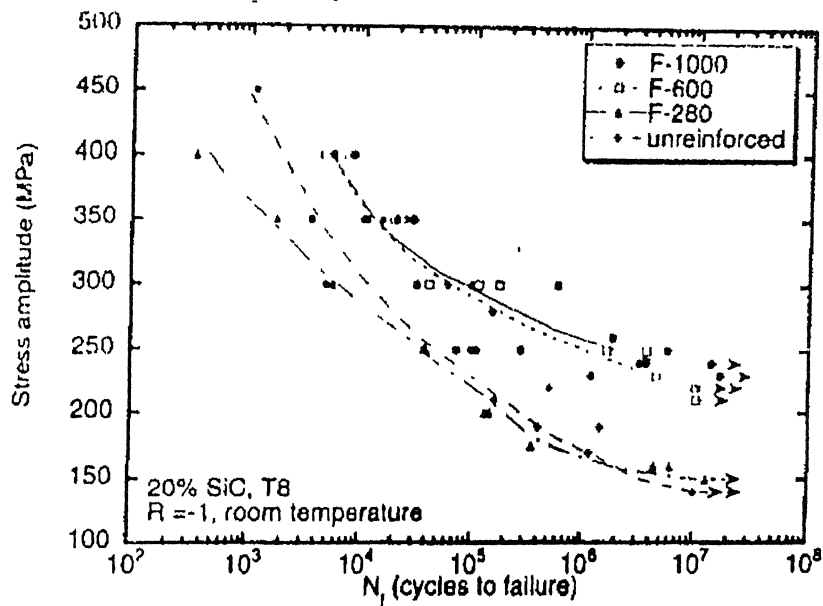


Figure 2.22. Effect of reinforcement particle size on the fatigue life of 20 vol% SiCp/Al MMC [25].

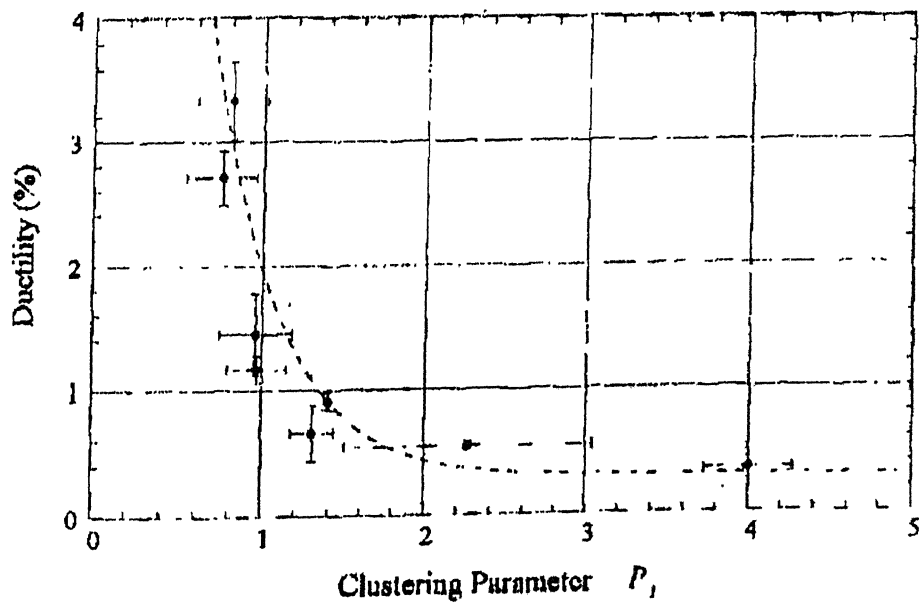


Figure 2.23. Correlation between the clustering parameter and tensile ductility [33].

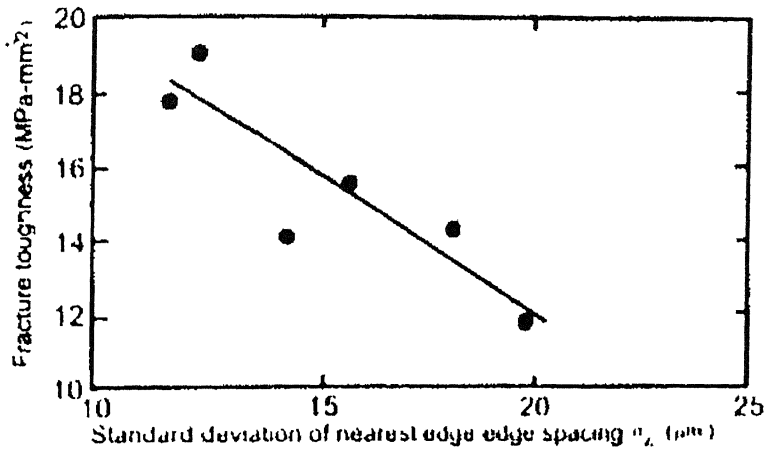


Figure 2.24. The influence of particle clustering on fracture toughness of *Al-SiCp MMCs* [34].

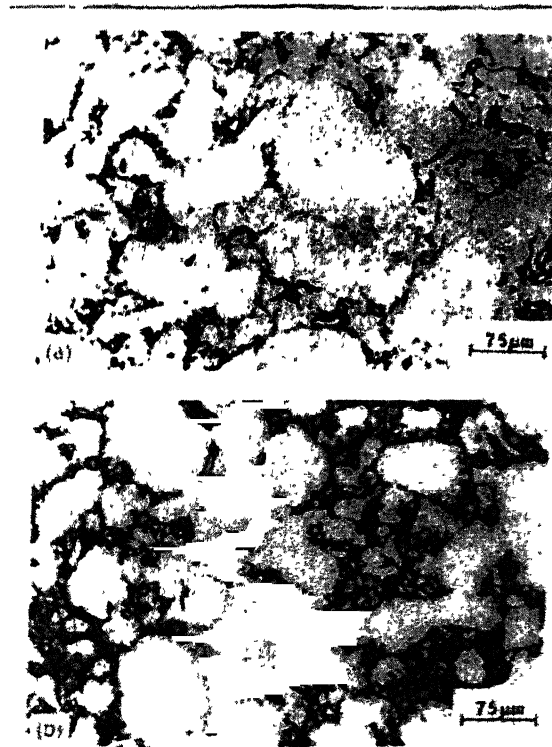


Figure 2.25. Representative micrographs of (a) 2124 *Al*/10vol% *SiCp* and (b) 2124 *Al*/30 vol% *SiCp* composites; *VHP* condition [50].

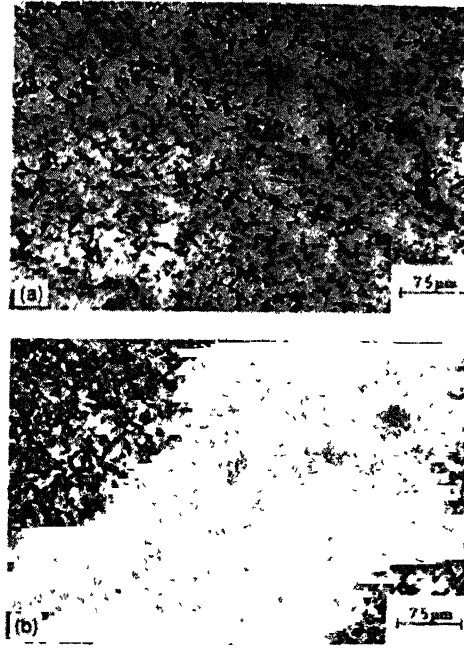


Figure 2.26. Representative micrographs of (a) 2124 *Al*/ 10 vol% *SiCp* and (b) 2124 *Al* / 30 vol% *SiCp* composites; *VHP*+extruded condition [50].

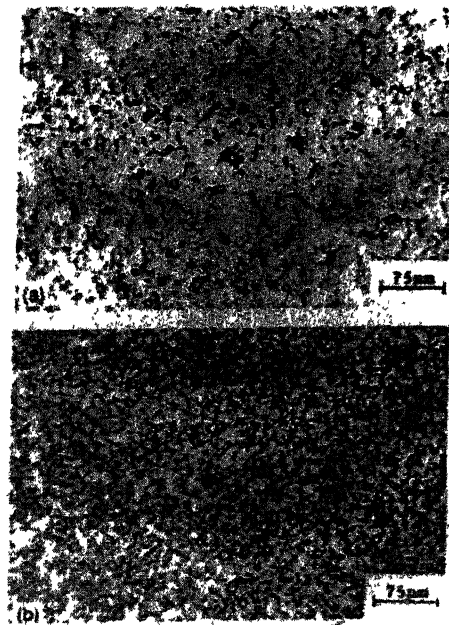


Figure 2.27. Representative micrographs of (a) 2124 *Al*/ 10 vol% *SiCp* and (b) 2124 *Al* / 30 vol% *SiCp* composites; *VHP*+extruded +section rolled condition [50].

CHAPTER 3

EXPERIMENTAL DETAILS

3.1. Material

The composites used for investigations were obtained from three different companies. Prof. P. K. Rohatgi provided the samples*. The matrix alloy used was *Al-Si* alloy. Two different techniques were used for manufacturing these composites. The specimens used along with their specification and processing techniques used are shown in Table 3.1.

3.2. Density Measurement

Density measurement for the samples was done using Archimedes Principle. Initially the weights for the samples were taken in air. Then the samples were immersed in pure distilled water and the weights were taken in water. An analytical balance was used for all the measurements.

The density was calculated using the following equation:

$$\rho_s = \frac{W_{SA}}{W_{SA} - W_{SW}} \rightarrow (3.1)$$

Where, ρ_s is the relative density of the sample.

W_{SA} is the weight of the sample in air,

W_{SW} is the weight of the sample in water.

3.3. Measurement of Elastic Modulus

An Ultrasonic Flaw detector (KRAUTKRAMER-BRANSON USI P12) was used to determine the elastic modulus of the samples. The instrument consisted of two Piezo electric probes as shown in Figure 3.1. One was the transmitting probe and the other was the receiving probe. The transmitting probe generated the ultrasonic wave and the receiving probe detected the signal. The length (L) of the specimens was measured and the time for travel of the ultrasonic wave was detected from the flaw detector. Dividing the length by the time of travel gave the velocity of travel. The elastic modulus was calculated using the following equation:

$$E = V^2 \rho \rightarrow (3.2)$$

Where, E is the Elastic Modulus of the sample,

V is the velocity of travel for the ultrasonic wave,

ρ is the density of the sample as measured using equation 3.1.

3.4. High Temperature Compression Testing

Material Testing System (MTS) was used for performing the compression tests. A schematic sketch of Material Test System is shown in Figure 3.2. Cylindrical specimens with length to diameter ratio of 1.5-2.5 were used for testing. Boron Nitride powder was applied between the punch and specimen as a dry lubricant to minimize friction. The equipment consisted of a furnace, which surrounded the specimen to be tested. The temperature was controlled with the help of three thermocouples attached at the top, middle and bottom of the furnace. Load was applied hydraulically in the furnace system apparatus. The strain rate used was 0.1mm/min. The samples were tested at three temperatures- 150⁰C, 250⁰C, and 350⁰C and load vs displacement curves were obtained. The load vs displacement curves were converted to stress-strain curves.

3.5. Micro-Hardness Test

MHP 160 Micro-Hardness Tester was used to perform the micro-hardness tests. Micro-Hardness Test was performed only on the matrix phase. The load used for indentation was 60 gm. A diamond pyramid indenter was used. The load was applied for a short period of around 3-4 seconds. The indentation was square shaped. The length of the two diagonals of square indentation was measured and their mean was taken. Micro-Hardness or Vickers Hardness Number (VHN) was measured using the following equation:

$$VHN = 1.854 \frac{P}{d^2} \rightarrow (3.3)$$

Where, P is the load applied, and d is the mean diagonal length of the indentation.

3.6. Specimen Preparation for Metallographic Observations

Metallographic techniques used for the preparation of these composites sectioning, mounting, grinding, and polishing.

Sectioning:

A diamond wheel was used for sectioning the specimens. The wheel was used at a very slow speed in order to avoid any particle pullouts or damage in the sample.

Mounting:

Specimens were cold mounted. Hot mounting was avoided because the temperature used in hot mountings may have resulted in a change in the microstructure. Care was taken while mounting to maintain the flatness of the sample and the mount.

Grinding:

Grinding is one of the steps, which induces considerable relief in the matrix or results in a dual plane structure. In other words, the two phases of the material being processed will be on two different levels. This is attributed to the fact that the emery paper used quickly grinds away the soft aluminium matrix while leaving the hard SiC particles practically untouched. Hence, the emery papers were only used for primary removal of the scratch. It is very difficult to avoid any relief, but it can be minimized. For these samples grinding was done in a series of emery papers starting from coarse grit to fine grit along with alcohol as lubricant. The alcohol helped in avoiding quick removal of aluminium along with preventing particle pullout.

Polishing:

Diamond abrasives were used for polishing of the samples. One of the critical factors is the choice of the polishing cloth. Soft cloths produce better surface finish, but at the expense of flatness and pullouts. Hard cloths maintain flatness but exhibit deeper scratches. Two grades of diamond suspensions, 15 micron and 3 microns were used for polishing. Rough cloth was used for polishing with 15 micron suspension, where as finer cloths were used for polishing with 3 micron diamond suspension. Final polishing was done with colloidal silica to enhance the contrast and bring about other microstructural

features. During final ten seconds of polishing, the cloth was rinsed with clean water to remove residual silica. Table 3.2 summarizes the polishing steps.

3.7. Quantitative Stereology

Quantitative Stereology involved the measurements of Volume Fraction of *SiC* particles (V_v) and Surface Area per unit Volume (S_v). Digital Image Analysis system was used to perform all the measurements.

In order to calculate the volume fraction a 6 by 5 grid was taken. Hence the total number of points was 30. The number of points falling in the feature of interest (*SiC* particles) was calculated manually and was divided by the total number of points. The result gave the volume fraction (V_v). Similarly, V_v of *Si*-rich phase was also estimated.

To calculate the S_v four lines of equal length and at equal spacing were taken. The total number of points of intersection with the *SiC* particle-matrix interface was calculated. This gave the points per unit length (P_L). The S_v was calculated as

$$S_v = 2 P_L \rightarrow (3.4)$$

The mean particle size (D) and mean free distance (λ) were calculated using the following equations:

$$\lambda = \frac{4(1 - V_v)}{S_v} \rightarrow (3.5)$$

$$D = 4 \frac{(V_v)}{(S_v)} \rightarrow (3.6)$$

3.8.TABLES

Table 3.1. Samples used for investigation.

| SPECIMEN NUMBER | SPECIMEN ID | PROCESSING TECHNIQUE | AIMED V_v |
|--------------------|-------------|-------------------------|----------------|
| 1 | C-3CP-50 | Permanent Mold Cast | 0.30 |
| 2 | C-2CP-21 | Permanent Mold Cast | 0.20 |
| 3 | C-3CS-7 | Sand Cast | 0.30 |
| 4 | C-2DP-25 | Permanent Mold Cast | 0.20 |
| 5 | C-1EP-18 | Permanent Mold Cast | 0.30 |
| 6 | G-4EP-31 | Permanent Mold Cast | 0.30 |
| 7 | G-2CS-29 | Sand Cast | 0.20 |
| 8 | G-4EP-3 | Permanent Mold Cast | 0.30 |
| 9 | G-2DS-32 | Sand Cast | 0.20 |

Table 3.2. Polishing Steps

| VARIABLE | Stage 1 | STAGE 2 | STAGE 3 |
|---------------|-------------|------------|------------------|
| Abrasive | Diamond | Diamond | Colloidal Silica |
| Abrasive Size | 15 microns | 3 microns | 0.04 microns |
| Speed, rpm | 300 | 150 | 150 |
| Pressure | Moderate | Moderate | Very low |
| Time. | Until Plane | 30 minutes | 45 seconds |

3.9.FIGURES

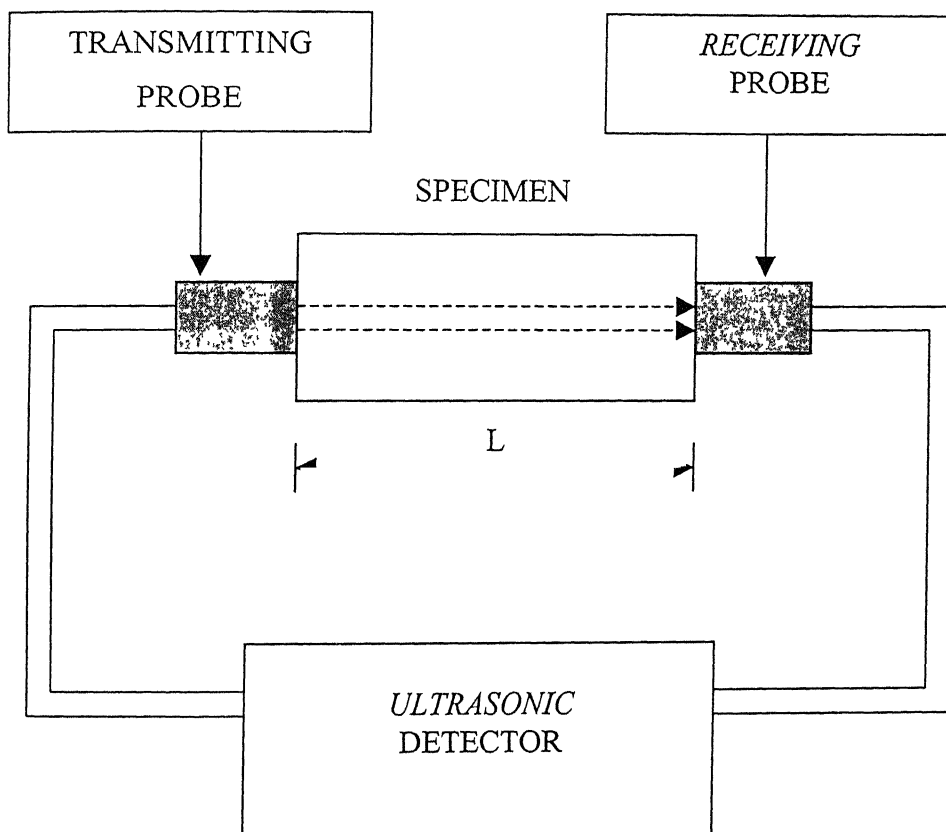


Figure 3.1. Schematic Sketch of Ultrasonic Flaw Detector.

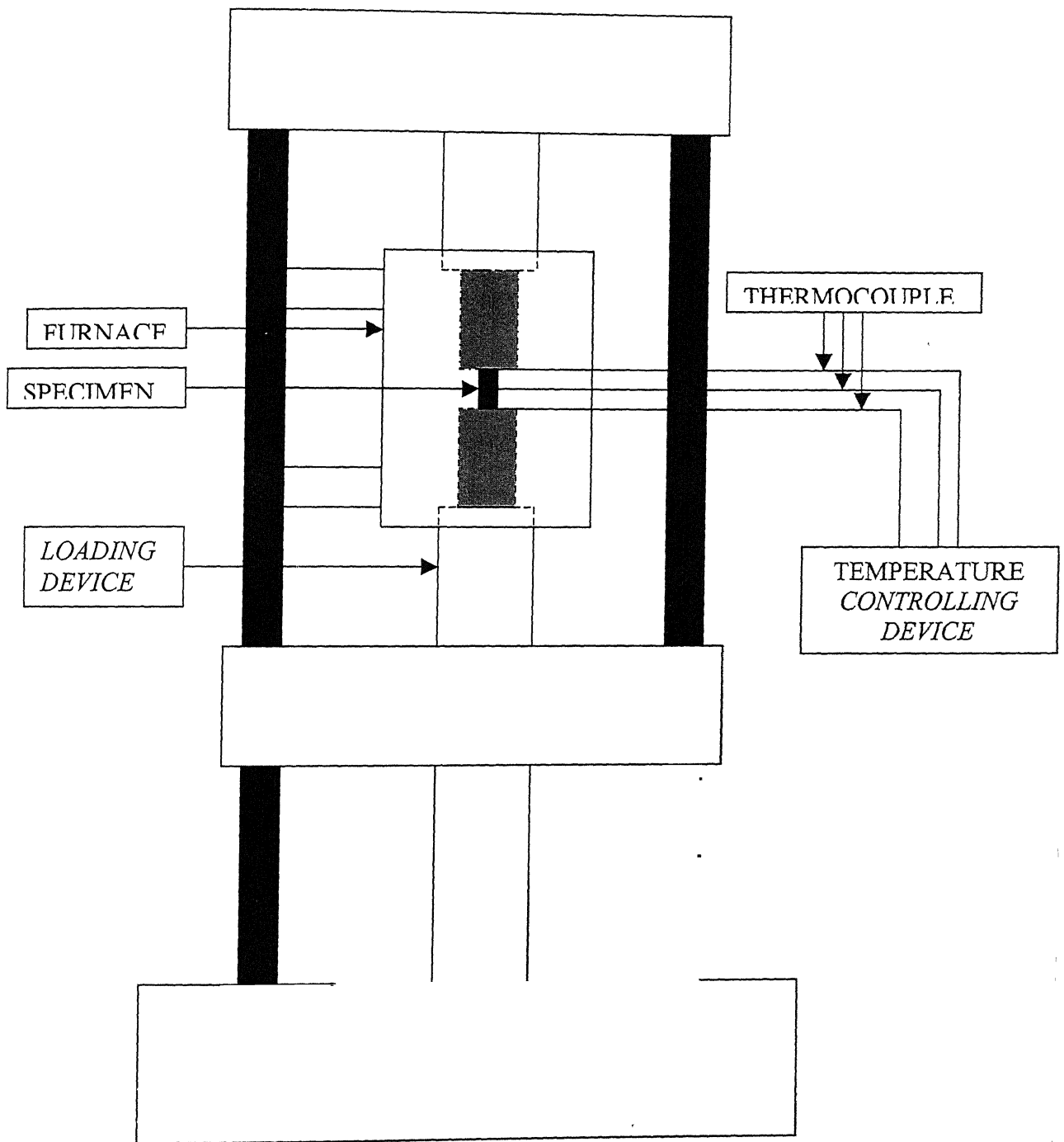


Figure 3.2. Schematic Sketch of Material Test System (MTS).

CHAPTER 4.

RESULTS AND DISCUSSION

4.1. QUALITATIVE RESULTS

4.1.1. Microstructure

As seen from the micrographs (Figure 4.1 to 4.18), the microstructures are free from porosity. In addition to this three phases are seen in the micrographs. The black irregular phases are the SiC particles (of the order of $10\mu m$ in size), the white part is the matrix (aluminium rich) and the grey phase is the Si rich phase (of the order of $1\mu m$ in size). Some of the micrographs show a non-uniform distribution of Silicon Carbide (SiC) particles. Some areas were empty or without any SiC particles where as some regions consisted of clusters of SiC particles. This is shown in Figure 4.19.

4.1.2. Stress-Strain Plots

The stress-strain curves obtained from the high temperature compression tests are shown in Figure 4.20 to 4.31. It has been found that stress value for samples with higher volume fraction is higher than for lower volume fraction. Exception is Specimen 7, which has a low volume fraction but a high value of stress. This may be attributed to the fact that it has a greater volume fraction of the Si -rich phase, which acts as another second phase particle apart from SiC particles for strengthening of the composite. Specimen 5 and 6 are also away from the trend. These samples have a high volume fraction but a low value of stress.

4.1.3. Effect of Temperature on Flow Stress

The variation of stress (at a constant value of strain of 0.015) with temperature is shown in Figure 4.32. Trend lines were added to see the effect of temperature on the true stress for all the samples. It is clear from Figure 4.32 that as the temperature increases the stress decreases. Also the difference in stress values for various specimens narrows down with increase in temperature. This shows that as temperature increases effect of reinforcement content decreases. This may be attributed to the fact that with the rise in temperature the material exhibit a progressive transition from local plastic flow to bulk flow [11]. Also the rate of strain hardening decreases with the rise in temperature due to increase in the dislocation mobility. In other words, the material at higher temperature undergoes rapid dynamic recovery.

4.2. QUANTITATIVE ANALYSIS

4.2.1. Quantitative Stereology

Quantitative Stereology included measurement of Volume Fraction (V_v), Surface Area Per Unit Volume (S_v), Connectivity, Mean free distance (λ) and Particle size (D). The results have been tabulated in Table 4.3. The Volume Fraction that was reported by the company was different from those obtained from the stereological measurements. To verify the correctness of the results obtained densities were measured both from the reported value of V_v and the measured value of V_v and compared with experimental measured density as shown in Figure 4.33. As seen from Figure 4.33, the density calculated from stereological measurements and experimentally measured density are well correlated where as those calculated from the reported values of V_v are away from the actual density. Hence it can be concluded that the aimed volume fraction could not be obtained.

4.2.2. Effect of Volume Fraction (V_v) and Particle Size (D) on Mean Free Distance (λ)

As seen from Table 4.3, as volume fraction increases, the value of mean free distance (λ) decreases and vice versa. Specimen 3 is an exception. It has a high volume fraction and also high λ . This is because Specimen 3 has a bigger particle size and λ is high for larger D values. Specimen 2 lies in between high and low.

4.2.3. Effect of Volume Fraction on Elastic Modulus (E)

The dependence of Elastic modulus on volume fraction is shown in Figure 4.34. Trend line was added using Regression Analysis. The Regression Analysis showed that the Elastic Modulus for the composites varied with Volume Fraction (V_v) according to equation 4.1 with a regression coefficient (R) of 0.87

$$E = 194.33V_v + 111.23 \rightarrow (4.1)$$

Equation 4.1 shows that Elastic Modulus is a strong function of V_v and Elastic Modulus increases with increase in volume fraction of SiC particles.

4.2.4. Effect of Volume Fraction (V_v), and Mean Free Distance (λ) on the Flow Stress

Flow Stress at high strain value (where yielding is seen with a flat region in the stress-strain curves) has been given in Table 4.4. Multiple Linear Regression Analysis was performed to see the combined effect of Volume Fraction (V_v) and Mean Free Distance (λ) on the Flow Stress of the material at 350°C. It was found that the Flow Stress of the material varied according to the following equation:

$$\sigma = 11.24V_v + 0.005\lambda \rightarrow (4.2)$$

$$R=0.73$$

Equation 4.2 shows that coefficient of V_v term is much higher as compared to λ and D term. Hence a slight change in the volume fraction will result in a considerable change in flow stress value as compared to λ .

The individual effects of Volume Fraction (V_v), Mean free distance (λ) between particles and Particle Size (D) is shown in Figure 4.35, 4.36, and 4.37, respectively. As seen from Figure 4.35, with increase in volume fraction the flow stress increases. Three points for specimen 5, 6, 7 are away from the trend. Specimen 7 has a low V_v but still a very high stress value. This may be probably due to the higher V_v of the *Si*-rich phase [see Table 4.3] in Specimen 7, which might have contributed to the strengthening effect. The rest two samples (Specimen 5 and 6) the stress values were low in spite of having high volume fraction. Reason for this discrepancy is unclear. Regression Analysis for the dependence of Flow Stress on the Volume Fraction (V_v) is shown in equation 4.3.

$$\sigma = 8.58V_v + 6.01 \rightarrow (4.3)$$

$$R=0.7$$

Equation 4.2 gives a better R-value as compared to Equation 4.2. This indicates that λ has some effect on the flow stress of the material. However, there is a very little change in the value of Flow Stress with λ . This has been shown in Figure 4.36. Similar is the case with D [as shown in Figure 4.37].

4.2.5. Variation of Stress Ratios ($\sigma_{350^{\circ}\text{C}} / \sigma_{150^{\circ}\text{C}}$) with Strain

Figure 4.38 shows the variation of Stress ratios ($\sigma_{350^{\circ}\text{C}} / \sigma_{150^{\circ}\text{C}}$) for strain values higher than 0.015 (corresponding to the flat portion of the stress strain curves) with increase in strain. Following conclusions can be drawn from Figure 4.38.

- i. The absolute value of ($\sigma_{350^{\circ}\text{C}} / \sigma_{150^{\circ}\text{C}}$) is always less than 1, which is expected as the material softens with increase in temperature.
- ii. ($\sigma_{350^{\circ}\text{C}} / \sigma_{150^{\circ}\text{C}}$) decreases as the strain increases. This indicates that the gap between stress-strain curves at temperatures 350°C and 150°C increases. This may be attributed to the fact that with the rise in temperature the material exhibit a progressive transition from local plastic flow to bulk flow [11]. Also the rate of strain hardening decreases with the rise in temperature due to increase in the dislocation mobility. In other words, the material undergoes dynamic recovery.
- iii. The slope of all the curves is similar. This indicates that similar mechanisms are operative for all the samples at higher temperatures.

4.2.6. Micro-Hardness

The results for the Micro-Hardness tests are shown in Table 4.4. The micro-hardness was only measured for the matrix phase (*Al*-rich). There is not much difference in the micro-hardness value for the matrix alloy (*Al*-rich phase) used for various samples. Only one of the sample (Specimen 4) had a low micro-hardness value.

4.3.TABLES

Table 4.1. Results of Density Measurements.

| Specimen No. | Specification | Weight in air (gms) | Weight in water (gms) | Density (gm/cc) | V_v (from density) |
|--------------|---------------|---------------------------|-----------------------------|--------------------|-------------------------|
| 1 | C-3CP-50 | 39.186 | 25.285 | 2.82 | 0.23 |
| 2 | C-2CP-21 | 37.505 | 23.959 | 2.77 | 0.13 |
| 3 | C-3CS-7 | 20.008 | 12.885 | 2.81 | 0.21 |
| 4 | C-2DP-25 | 33.968 | 21.671 | 2.76 | 0.12 |
| 5 | C-1EP-18 | 34.829 | 22.478 | 2.82 | 0.23 |
| 6 | G-4EP-31 | 35.625 | 23.015 | 2.82 | 0.24 |
| 7 | G-2CS-29 | 28.633 | 18.228 | 2.75 | 0.10 |
| 8 | G-4EP-3 | 34.983 | 22.623 | 2.83 | 0.25 |
| 9 | G-2DS-32 | 22.224 | 14.165 | 2.76 | 0.11 |

Table 4.2. Results of Elastic Modulus Measurements

| Specimen No. | Specification | Density (g/cc) | Length (in mm) | Time of Travel (nsec) | Velocity (m/s) | E (in GPa) |
|-----------------|---------------|-------------------|-------------------|-----------------------------|-------------------|--------------------|
| 1 | C-3CP-50 | 2.819 | 57.6 | 7530 | 7649.4 | 164.9 |
| 2 | C-2CP-21 | 2.768 | 53.5 | 7420 | 7210 | 143.9 |
| 3 | C-3CS-7 | 2.809 | 32.4 | 4400 | 7363.6 | 152.3 |
| 4 | C-2DP-25 | 2.762 | 26.72 | 3815 | 7003.9 | 135.45 |
| 5 | C-1EP-18 | 2.819 | 22.6 | 3060 | 7385.6 | 153.7 |
| 6 | G-4EP-31 | 2.852 | 21.7 | 2920 | 7431.5 | 156.01 |
| 7 | G-2CS-29 | 2.752 | 40.84 | 5760 | 7090 | 138.33 |
| 8 | G-4EP-3 | 2.830 | 25.8 | 3475 | 7424.4 | 155.99 |
| 9 | G-2DS-32 | 2.757 | 34.4 | 4920 | 6991.8 | 134.77 |

Table 4.3. Quantitative Stereological Measurements.

| Sl. No | Specification | V _v (SiC) | V _v (Si-rich phase) | S _v (M-S) | S _v (S-S) | Net S _v | Sp. S _v of SiC | Connectivity | λ (μm) | D (μm) |
|--------|---------------|-------------------------|-----------------------------------|-------------------------|-------------------------|-----------------------|---------------------------------|--------------|--------------------------------|------------------------|
| 1 | C-3CP-50 | 0.22 | 0.16 | 0.13 | 0.01 | 0.15 | 0.67 | 0.08 | 21.37 | 5.99 |
| 2 | C-2CP-21 | 0.16 | 0.14 | 0.12 | 0.01 | 0.14 | 0.90 | 0.14 | 23.32 | 4.46* |
| 3 | C-3CS-7 | 0.25 | 0.07 | 0.09 | 0.00 | 0.09 | 0.36 | 0.03 | 34.08 | 11 |
| 4 | C-2DP-25 | 0.14 | 0.17 | 0.12 | 0.00 | 0.12 | 0.86 | 0.02 | 27.65 | 4.65 |
| 5 | C-1EP-18 | 0.24 | 0.13 | 0.14 | 0.00 | 0.14 | 0.59 | 0.03 | 21.42 | 6.79 |
| 6 | G-4EP-31 | 0.22 | 0.12 | 0.15 | 0.00 | 0.15 | 0.70 | 0.02 | 20.75 | 5.68 |
| 7 | G-2CS-29 | 0.14 | 0.21 | 0.11 | 0.00 | 0.11 | 0.79 | 0.03 | 31.06 | 5.06* |
| 8 | G-4EP-3 | 0.22 | 0.15 | 0.15 | 0.00 | 0.15 | 0.69 | 0.03 | 20.68 | 5.76 |
| 9 | G-2DS-32 | 0.13 | 0.08 | 0.10 | 0.00 | 0.10 | 0.78 | 0.02 | 33.44 | 5.12 |

* The specimens had a Bi-Modal Size Distributions, i.e. from very particle size to coarse particle size. Hence, their mean diameter lies in between fine and coarse.

Table 4.4. Mechanical Properties.

| Sl. No. | Specification | Elastic Modulus (GPa) | True Stress (at 150 ⁰ C, 0.015 strain) | True Stress (at 250 ⁰ C, 0.015 strain) | True Stress (at 350 ⁰ C, 0.015 strain) | Micro Hardness (VHN) |
|---------|---------------|-----------------------|--|--|--|----------------------|
| 1 | C-3CP-50 | 164.9 | 13.1 | 10.36 | 8.76 | 81.39 |
| 2 | C-2CP-21 | 143.9 | 8.97 | 7.5 | 6.65 | 95.11 |
| 3 | C-3CS-7 | 152.3 | 12.6 | ----- | 7.78 | 61.73 |
| 4 | C-2DP-25 | 135.45 | 9.51 | 8.6 | 6.88 | 42.5 |
| 5 | C-1EP-18 | 153.7 | 7.18 | 6.87 | 5.6 | 79.43 |
| 6 | G-4EP-31 | 156.01 | 7.5 | 7.02 | 6.58 | 85.35 |
| 7 | G-2CS-29 | 138.33 | 15.55 | ----- | 7.5 | 72.75 |
| 8 | G-4EP-3 | 155.99 | 9.16 | 7.82 | 7.6 | 95.39 |
| 9 | G-2DS-32 | 134.77 | 14.09 | ----- | 7.42 | 71.29 |

4.4.FIGURES

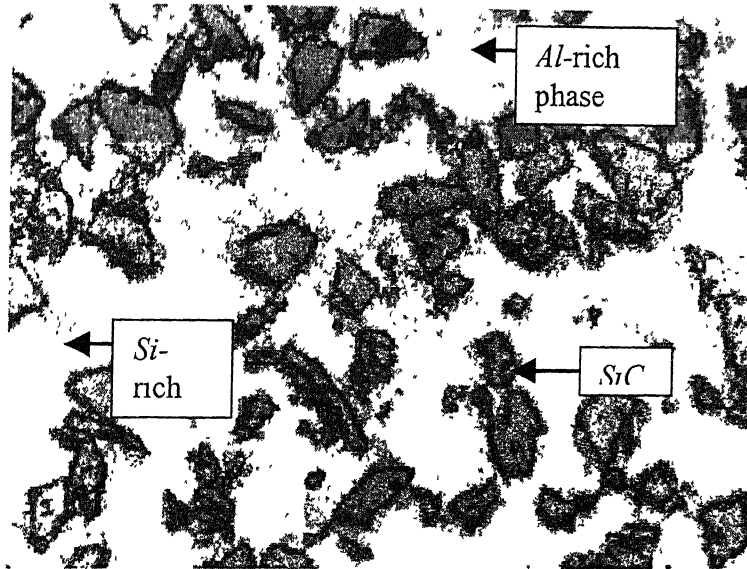


Figure 4.1. Optical Micrograph for Specimen 1 at 50X.

[The Figure shows a non-uniform distribution of SiC particles in the white matrix, which is the Al -rich phase. It also consists of Si -rich phase very finer in size around the particles]

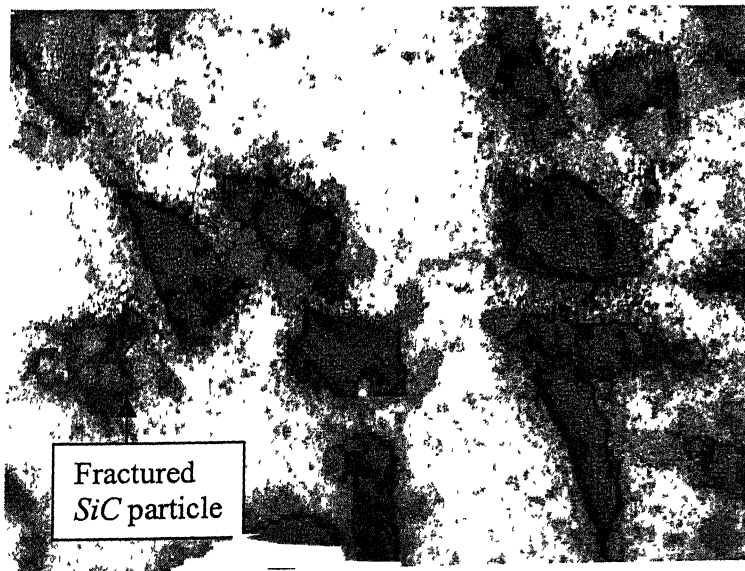


Figure 4.2. Optical Micrograph of Specimen 1 at 125X

[The Figure shows patches of matrix with irregular shape of SiC particles. Some particles also have a sharp corner. The particles are similar in size. Some particles seem to have fractured either during fabrication or during polishing stages]

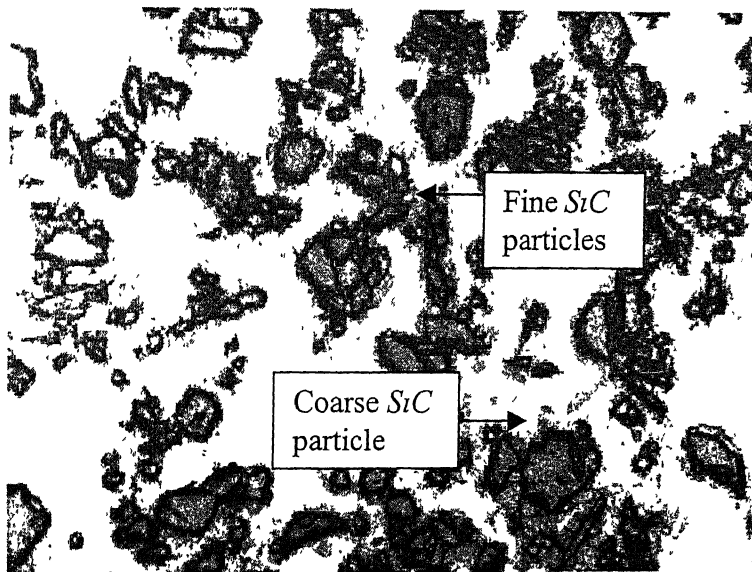


Figure 4.3. Optical Micrograph of Specimen 2 at 50X

[The SiC particles seem to have a bi-modal particle size distribution, that from very fine to coarse size. Si -rich phase is finer in size. The particles are also present in bunches]

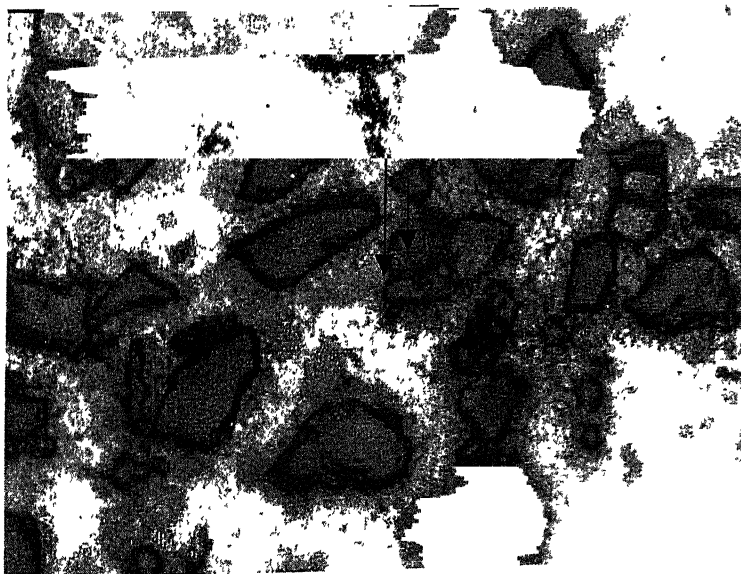


Figure 4.4. Optical Micrograph of Specimen 2 at 125X

[At higher magnification also the same thing is revealed. A bi-modal kind of particle size distribution is seen]

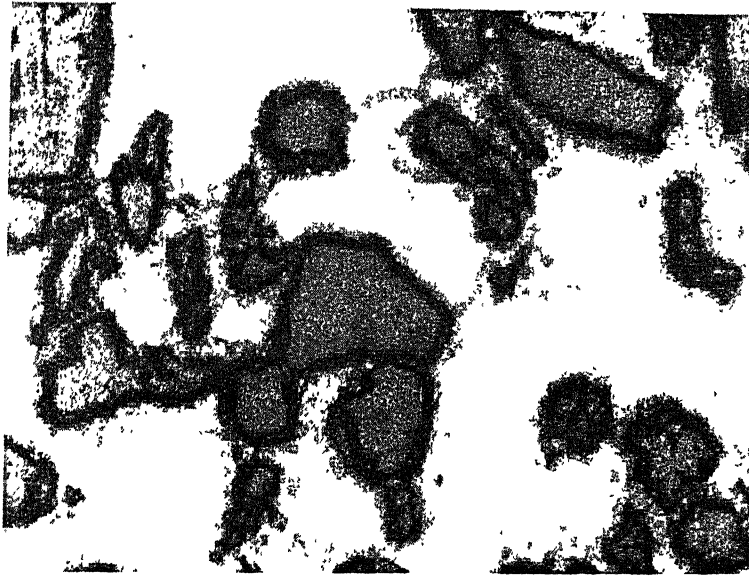


Figure 4.5. Optical Micrograph of Specimen 3 at 50X.

[The micrograph reveals that the SiC particle size is very coarse and the matrix has a very less volume fraction of Si -rich phase]

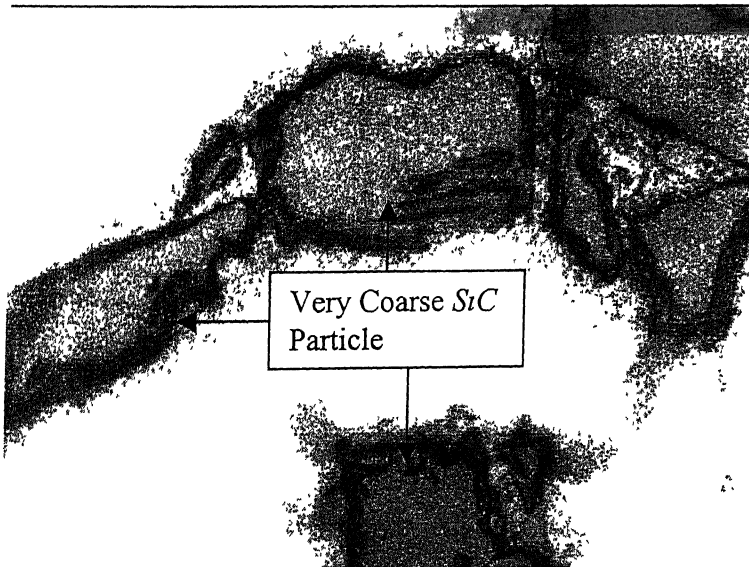


Figure 4.6. Optical Micrograph of Specimen 3 at 125X.

[At higher magnification it can be seen that the SiC particle size is very coarse]

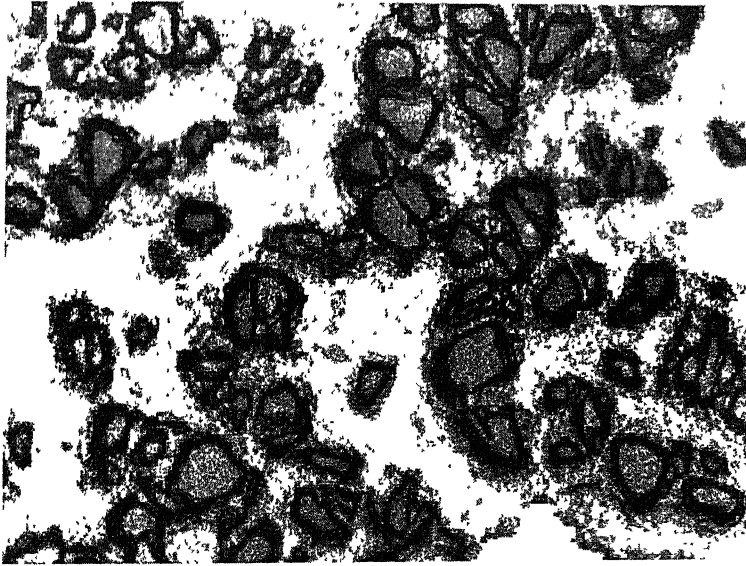


Figure 4.7. Optical Micrograph of Specimen 4 at 50X.

[The micrograph shows a non-uniform distribution of SiC particles. The size of the SiC particles is medium]

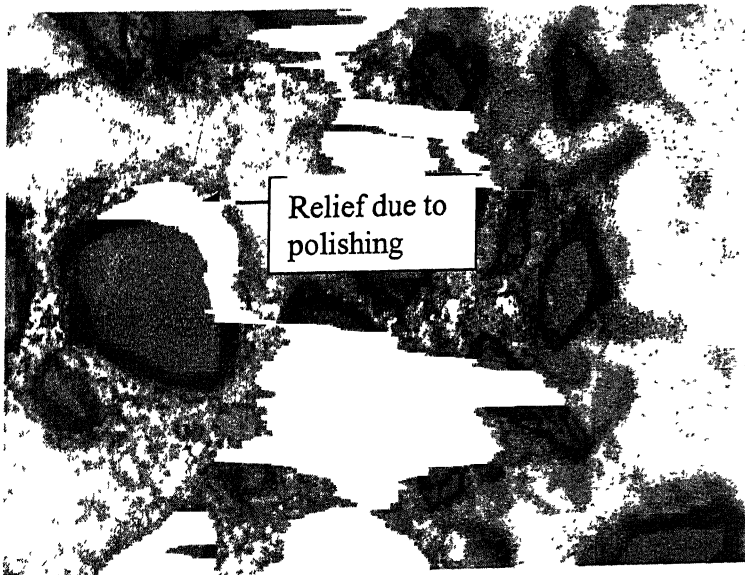


Figure 4.8. Optical Micrograph of Specimen 4 at 125 X

[The microstructure shows a considerable relief that has been produced due to polishing]

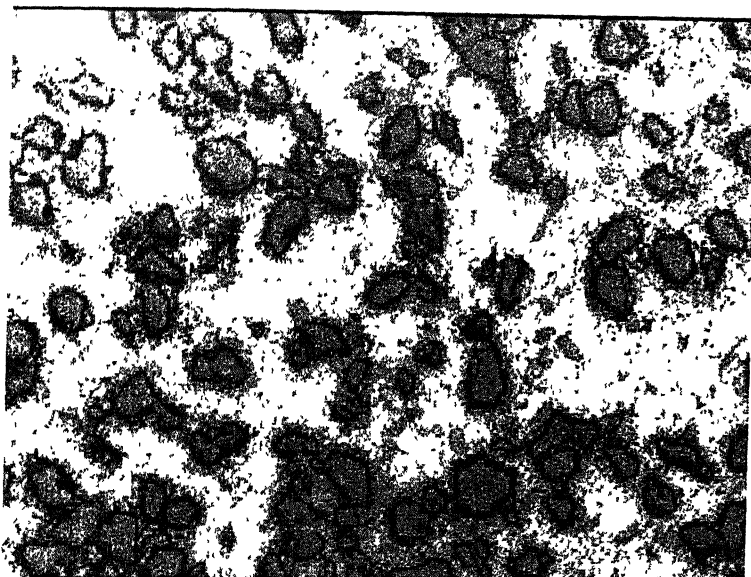


Figure 4.9. Optical Micrograph of Specimen 5 at 50X.

[The SiC particles are more homogeneously distributed. The SiC particles are almost of same size and more rounder in shape. The Si -rich phase is finer in scale and more uniformly distributed]

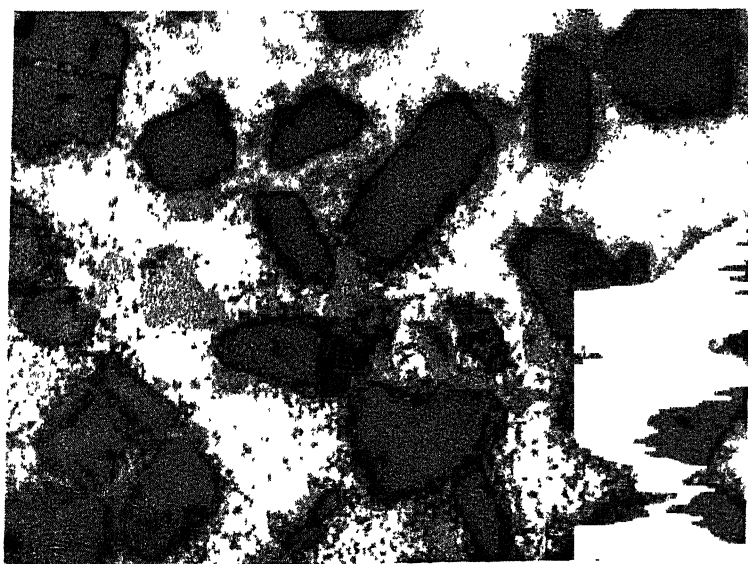


Figure 4.10. Optical Micrograph of Specimen 5 at 125X.

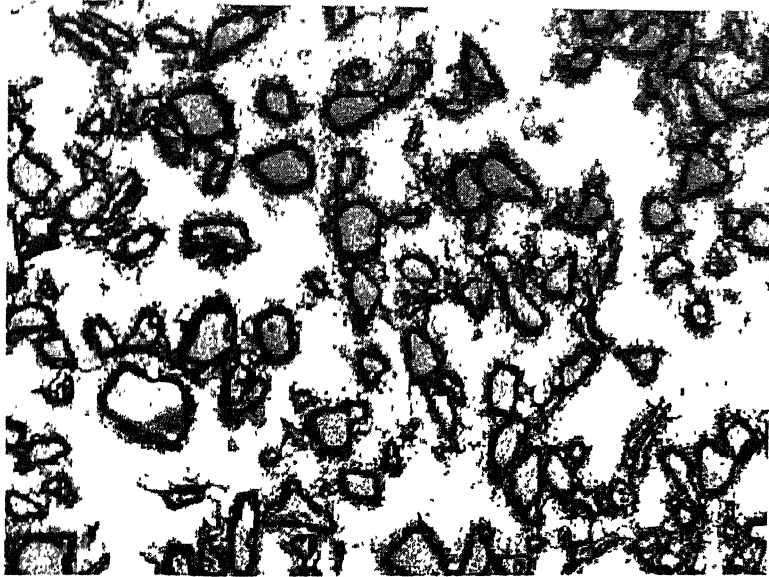


Figure 4.11. Optical Micrograph of Specimen 6 at 50X

[The micrograph shows a more uniform distribution of particle. The *Si*-rich phase is seen at the particle-matrix interface]

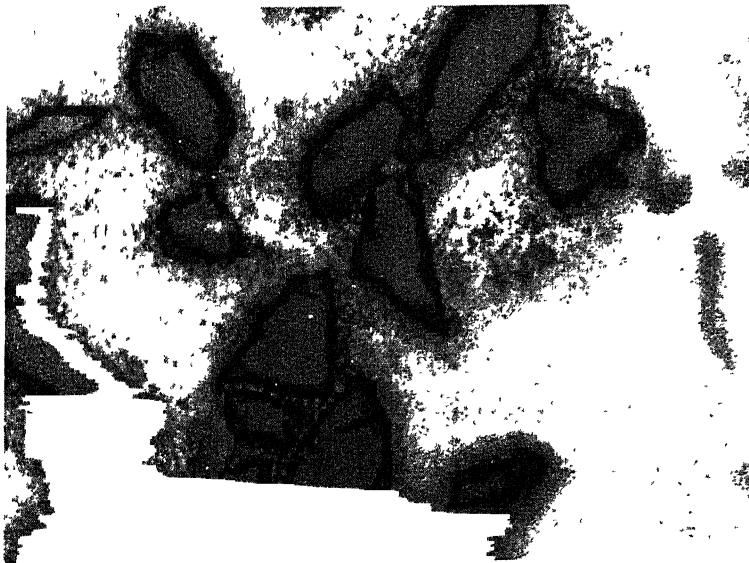


Figure 4.12. Optical Micrograph of Specimen 6 at 125X.

[At higher magnification it is seen that some portion of the micrograph is free from *SiC* particles. The particles are irregular in shape]

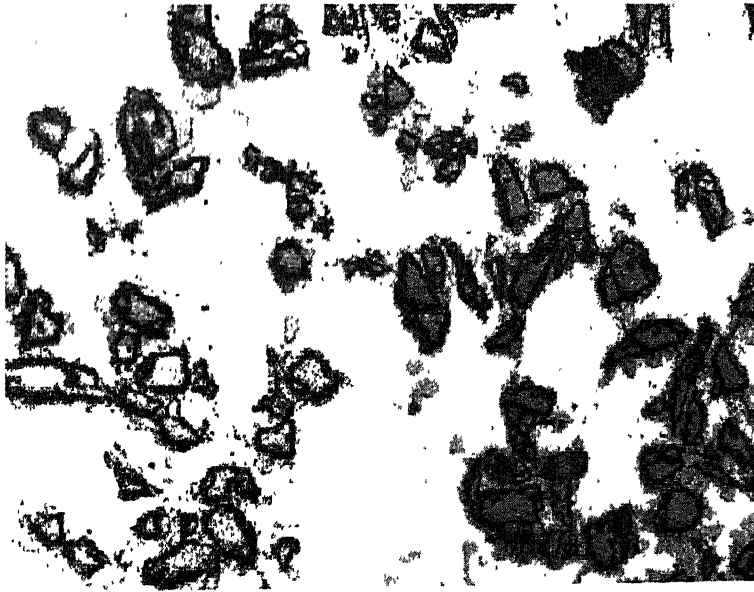


Figure 4.13. Optical Micrograph of Specimen 7 at 50X.

[The micrograph reveals a bi-modal size distribution of SiC particles. Patches of matrix is seen.]

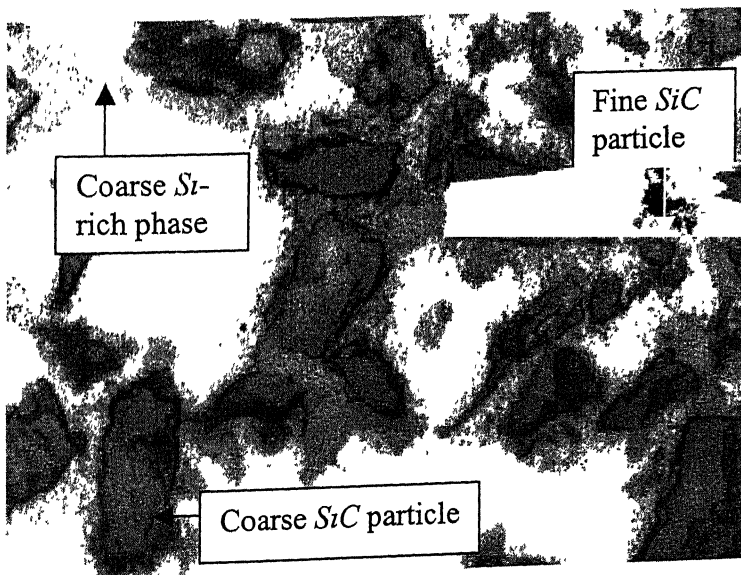


Figure 4.14. Optical Micrograph of Specimen 7 at 125X.

[At higher magnification a bi-modal particle size distribution is seen. The Si -rich phase has a higher volume fraction and is coarser in size]

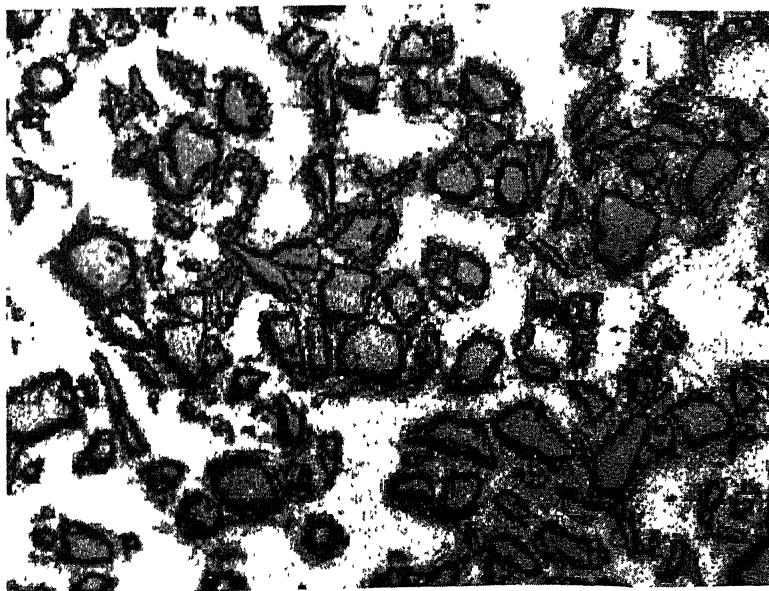


Figure 4.15. Optical Micrograph of Specimen 8 at 50X.

[A non-uniform distribution of particles is seen in the microstructure. Some portion of the material has a very high amount of *SiC* particles.]

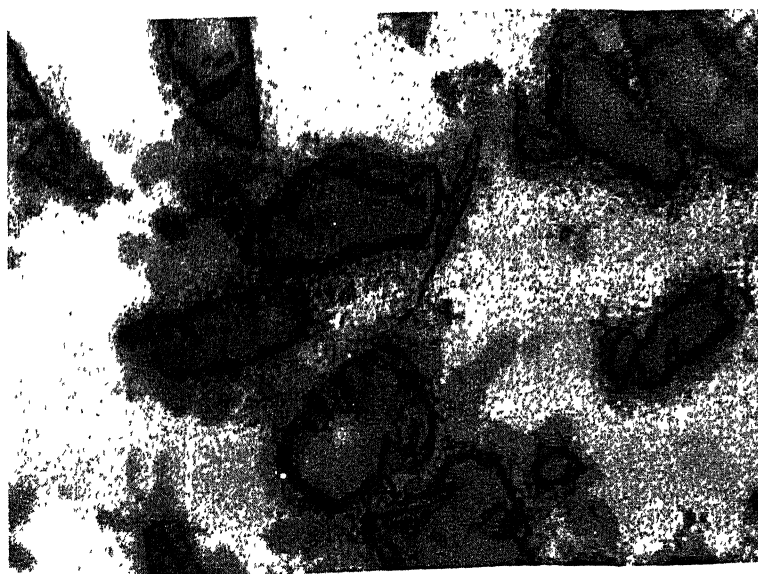


Figure 4.16. Optical Micrograph of Specimen 8 at 125X.

[The micrographs show patches of matrix. *Si*-rich phase is seen at the particle-matrix interface]

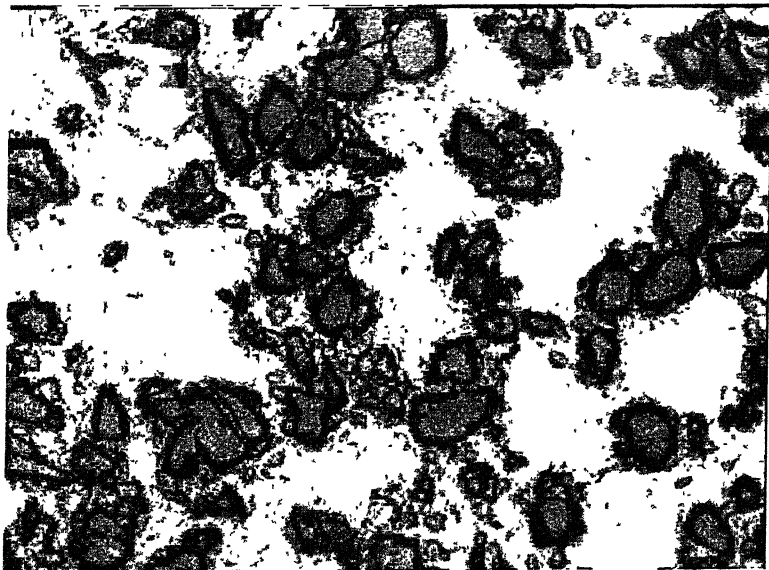


Figure 4.17. Optical Micrograph of Specimen 9 at 50X.

[The micrograph shows a bi-modal kind of particle size distribution. The *SiC* particles appear to form a chain like structure. This might have resulted during the fabrication process]

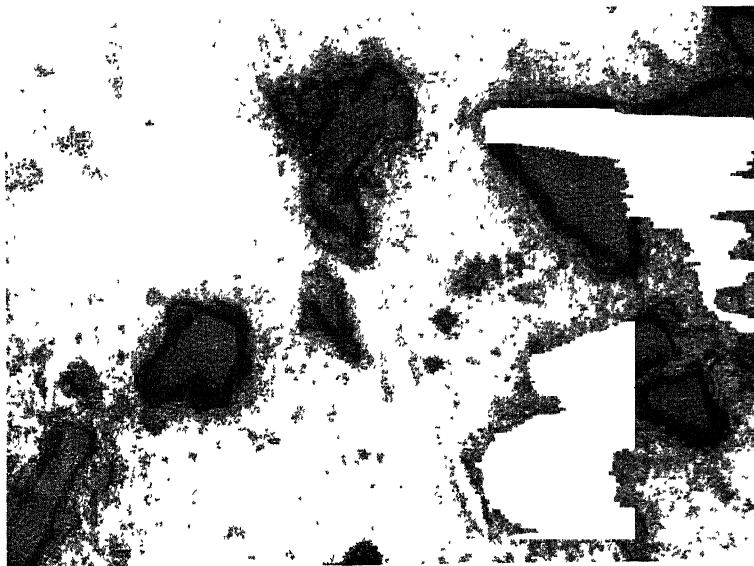
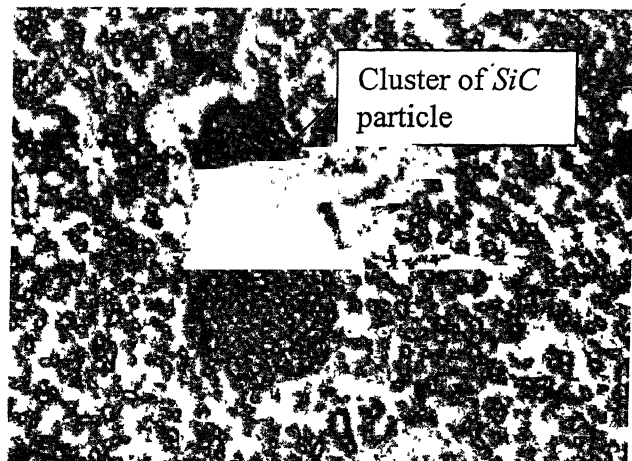


Figure 4.18. Optical Micrograph of Specimen 9 at 125X

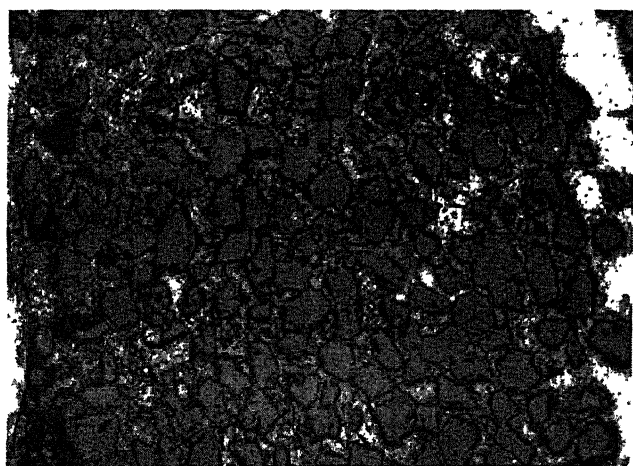
[The micrographs show large areas free of *SiC* particles]



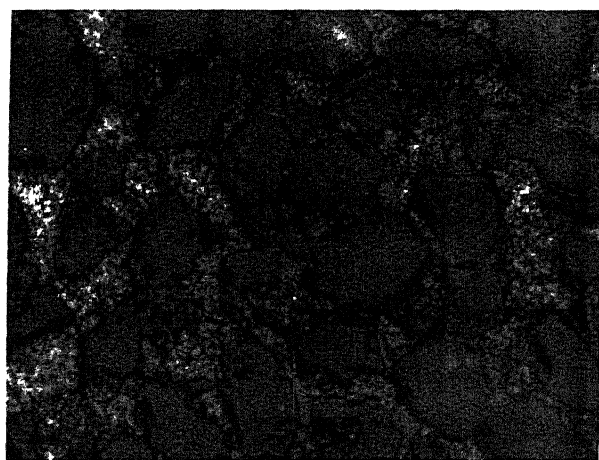
(a)



(b)



(b)



(d)

Figure 4.19. Optical Micrograph of Specimen 5 showing clusters of SiC particles at (a)12.5X, (b)25X, (c)50X, (d)125X.

[The micrographs show a region having a big cluster of SiC particles. Rest of the portions have a more homogeneous distribution of SiC particles]

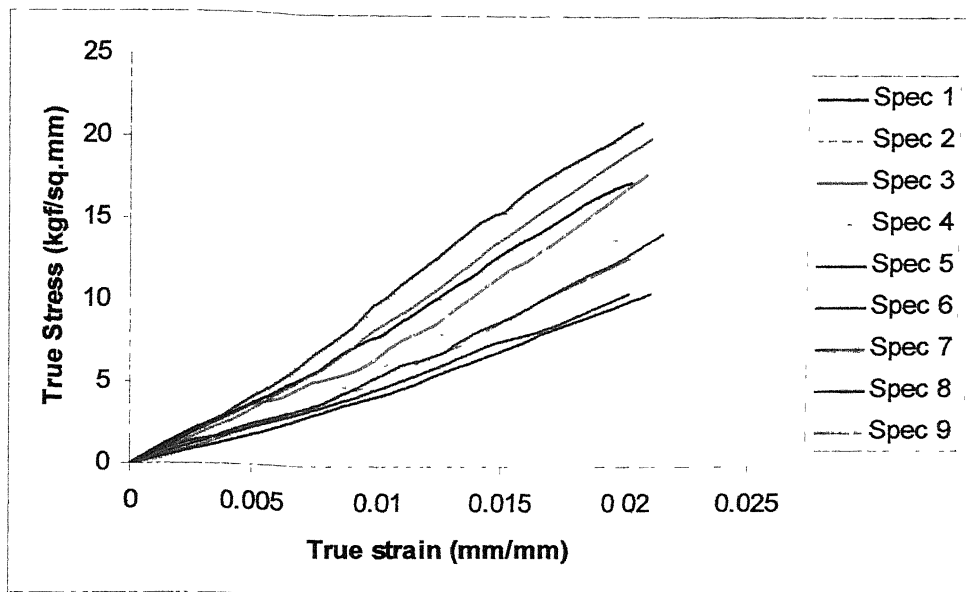


Figure 4.20. True Stress-Strain Curves at 150°C.

[Specimen 7, which has a low V_v seems to have a higher strength. Specimen 5 and 6 have a high V_v but still a lower strength]

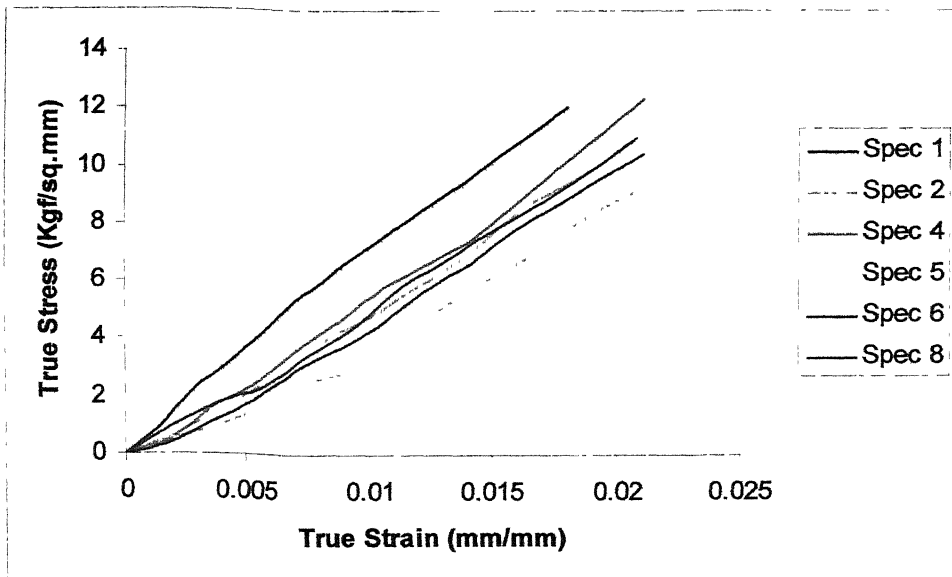


Figure 4.21. True Stress-Strain Curves at 250°C.

[At higher temperature also Specimen 5 and 6 have a lower strength values]

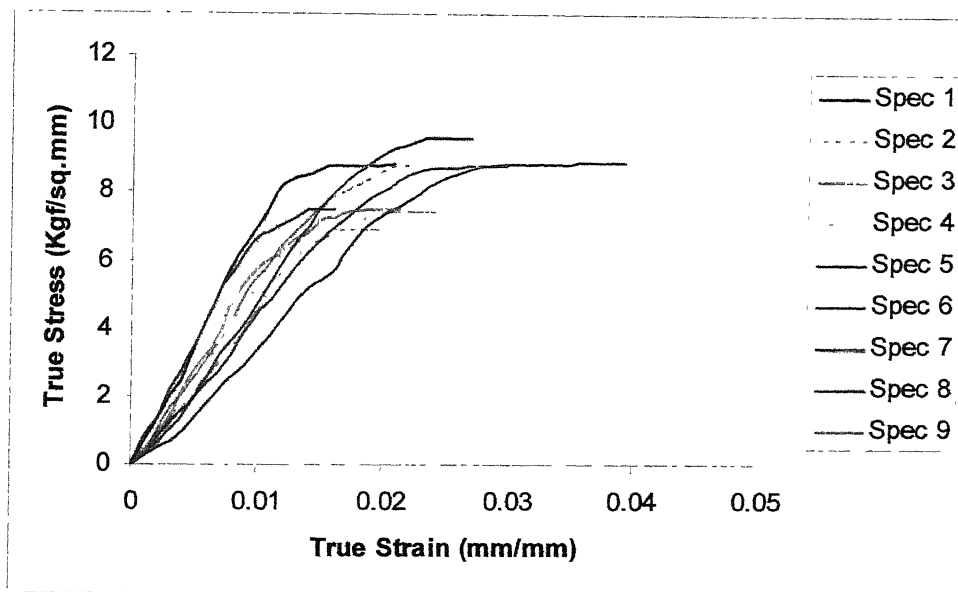


Figure 4.22. True Stress-Strain Curves at 350°C.

[A flat region is seen at higher strain values beyond 0.015 strain.]

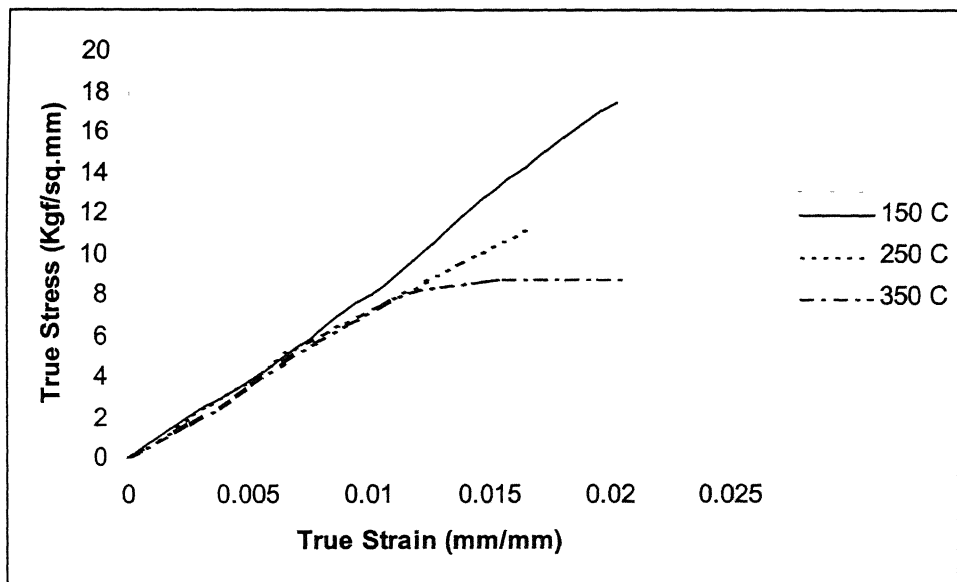


Figure 4.23. True Stress vs True Strain at Different Temperatures

For Specimen 1

[Stress values at higher temperatures are lower than that at lower temperatures. Also the gap between stress values at different temperature increases with increasing strain.]

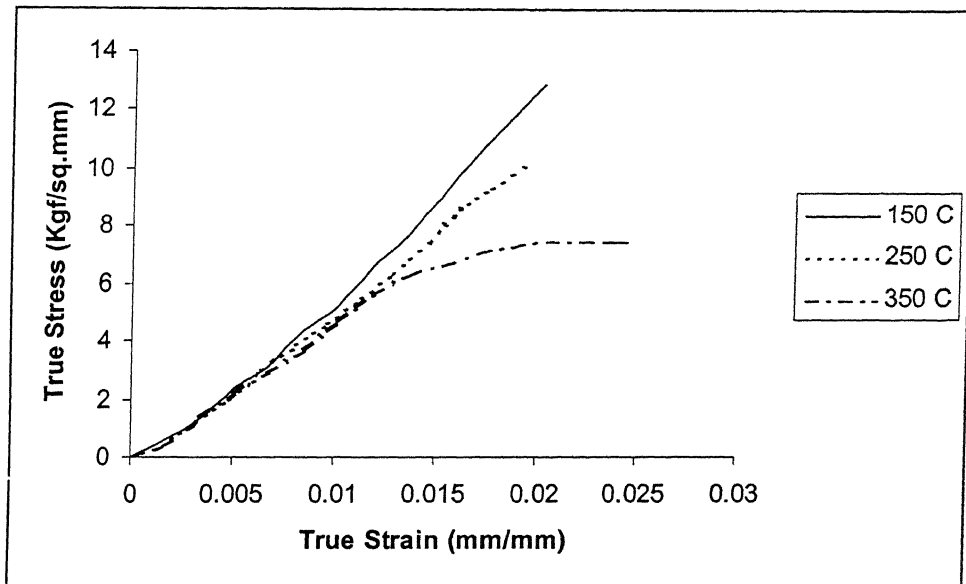


Figure 4.24. True Stress vs True Strain at Different Temperatures
For Specimen 2.

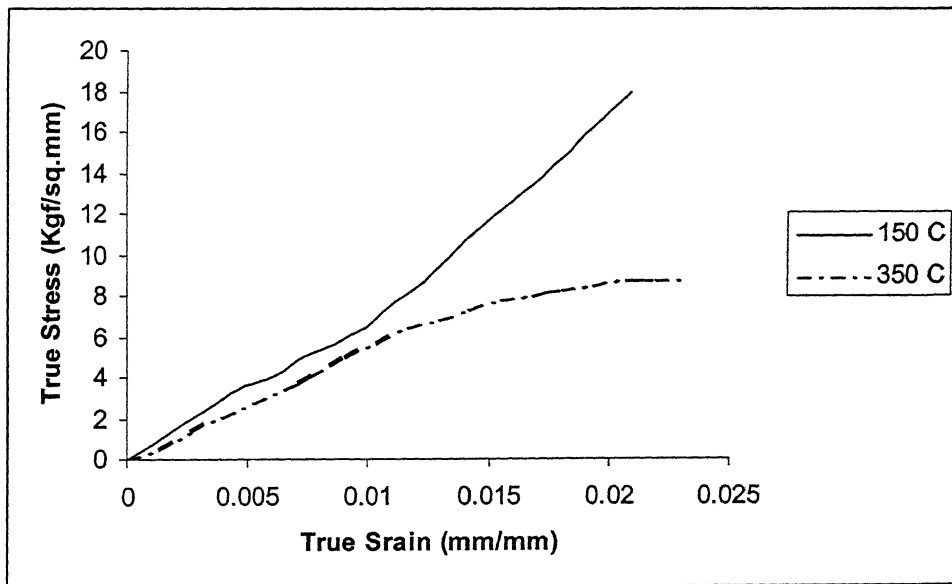


Figure 4.25. True Stress vs True Strain at Different Temperatures
For Specimen 3.

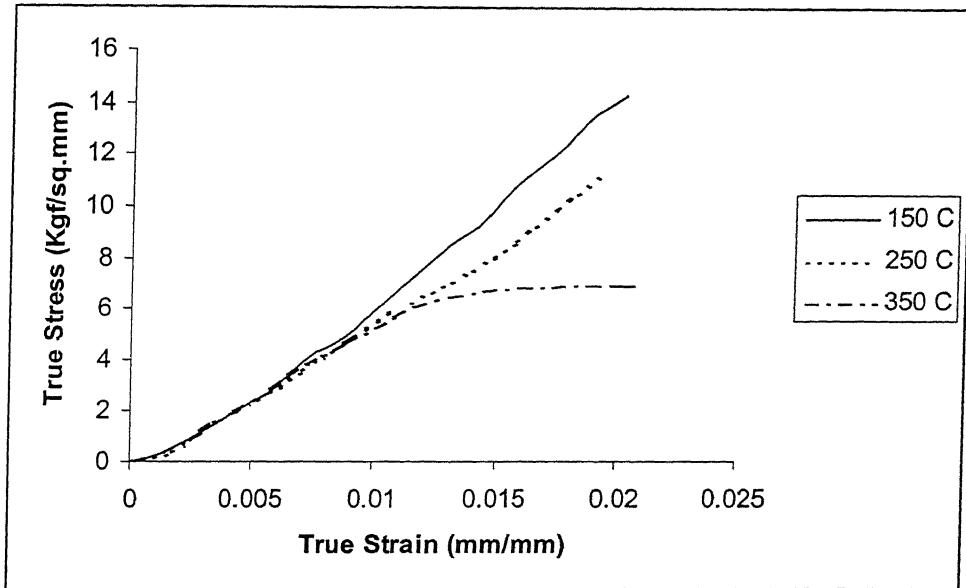


Figure 4.26. True Stress vs True Strain at Different Temperatures

For Specimen 4.

[Initial portion of the stress strain curve is almost similar but with increase in strain the gap between stress values increases]

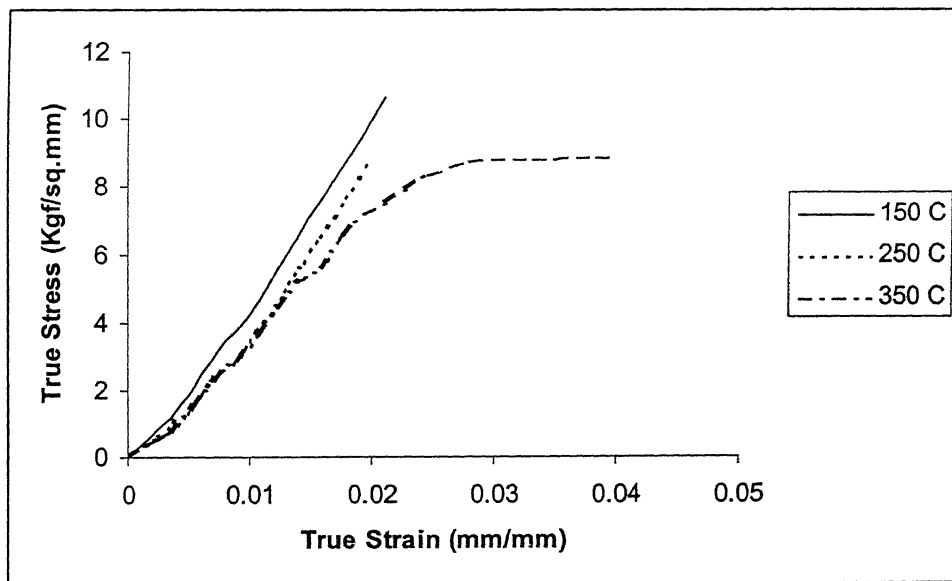


Figure 4.27. True Stress vs True Strain at Different Temperatures

For Specimen 5.

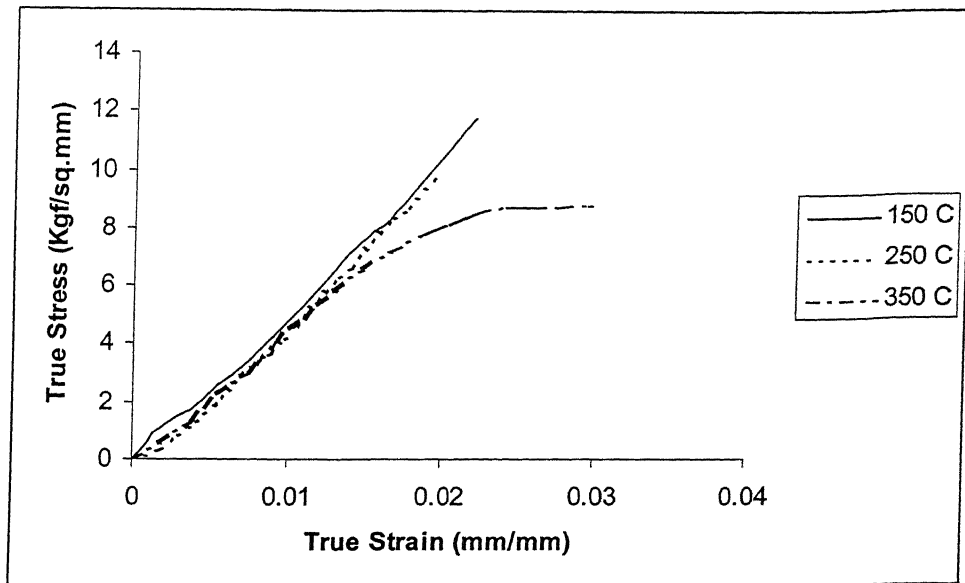


Figure 4.28. True Stress vs True Strain at Different Temperatures
For Specimen 6.

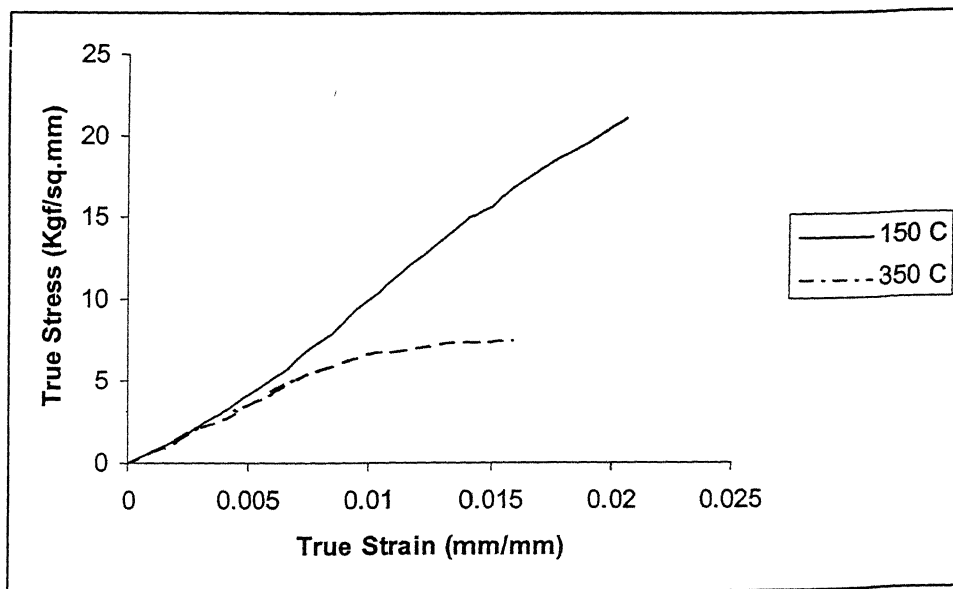


Figure 4.29. True Stress vs True Strain at Different Temperatures
For Specimen 7.

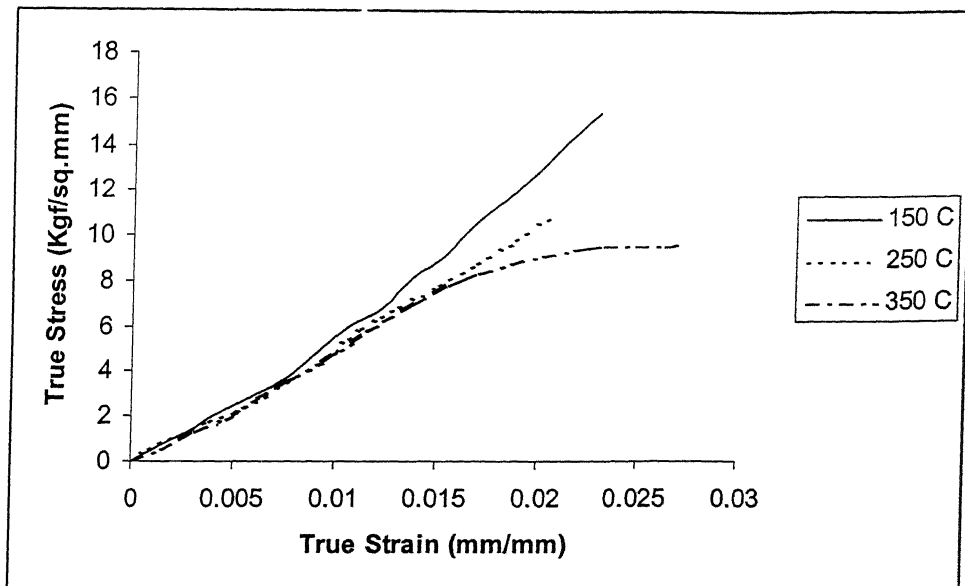


Figure 4.30. True Stress vs True Strain at Different Temperatures
For Specimen 8.

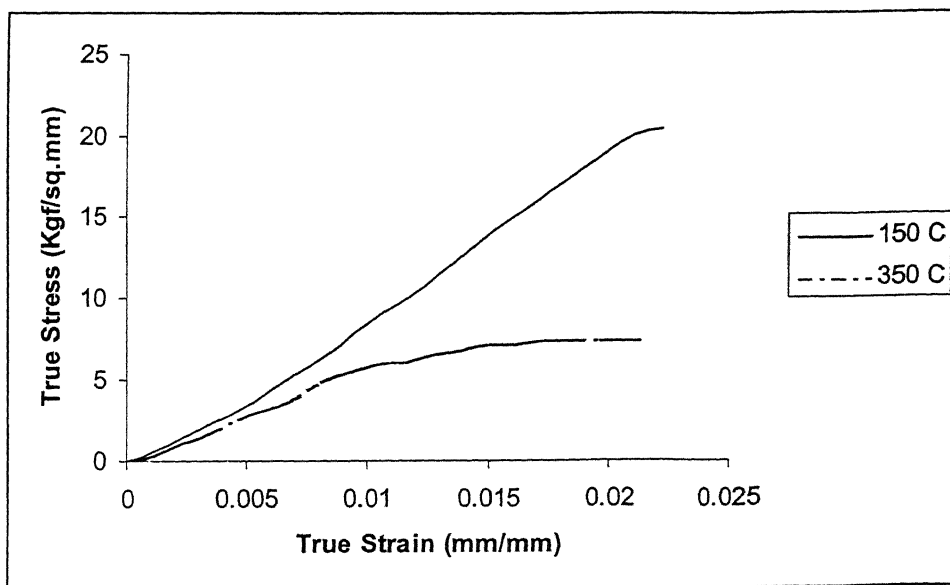


Figure 4.31. True Stress vs True Strain at Different Temperatures
For Specimen 9.

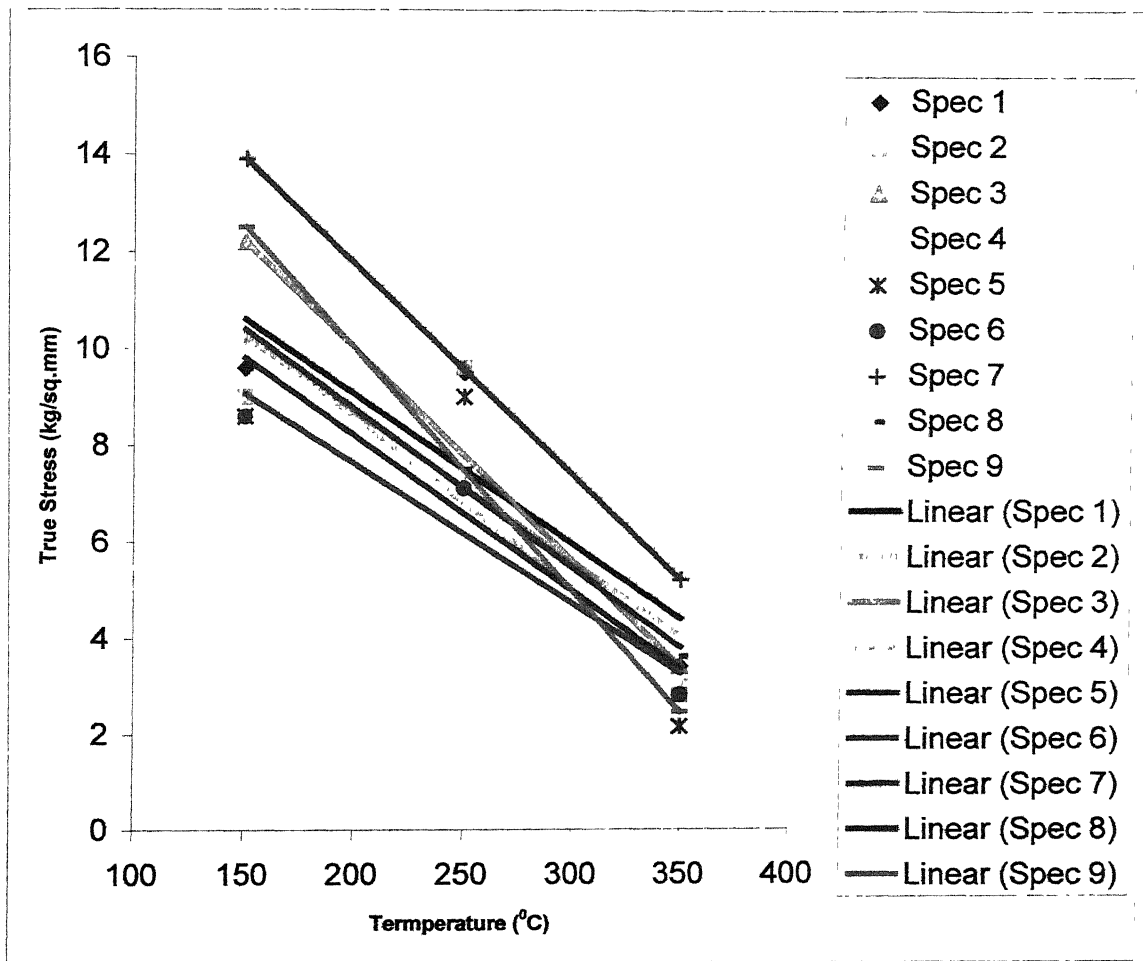


Figure 4.32. Variation of Stress with Temperature at a strain of 0.015 mm (the flat portion of the stress-strain curves).

[With increase in temperature the stress decreases. The slopes of the curves are almost similar. The difference between stress values narrows down with rise in temperature]

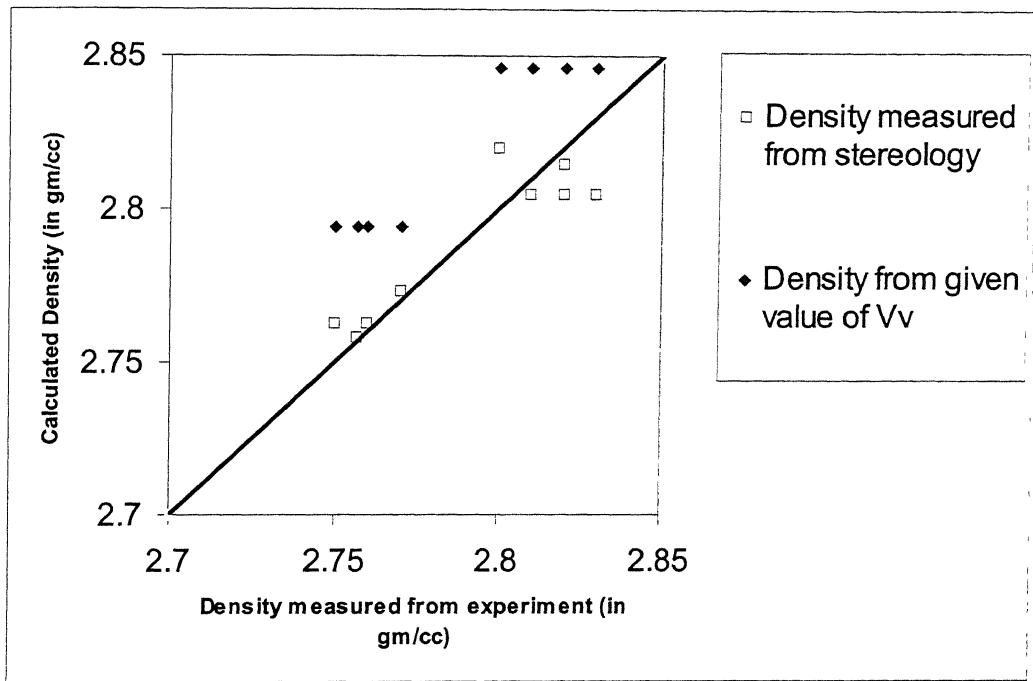


Figure 4.33. Comparison between Calculated density and Experimentally measured density.

[The density calculated from V_v of Stereology is well correlated with the density measured from experiment. Reported densities are away from the trend]

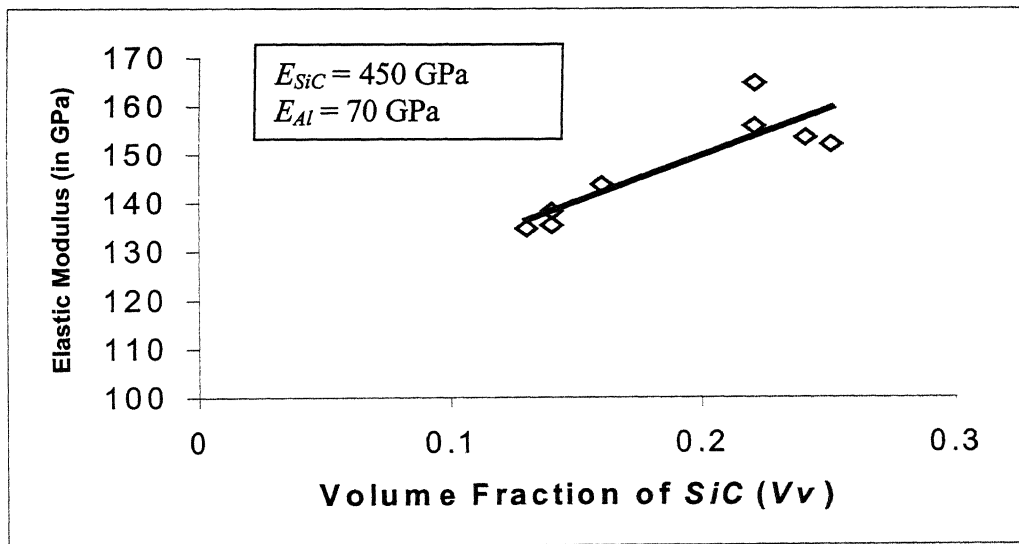


Figure 4.34. Variation of Elastic Modulus with Volume Fraction.

[All the points fit into the trend. It can be seen that as the volume fraction increases the Elastic Modulus of the material increases]

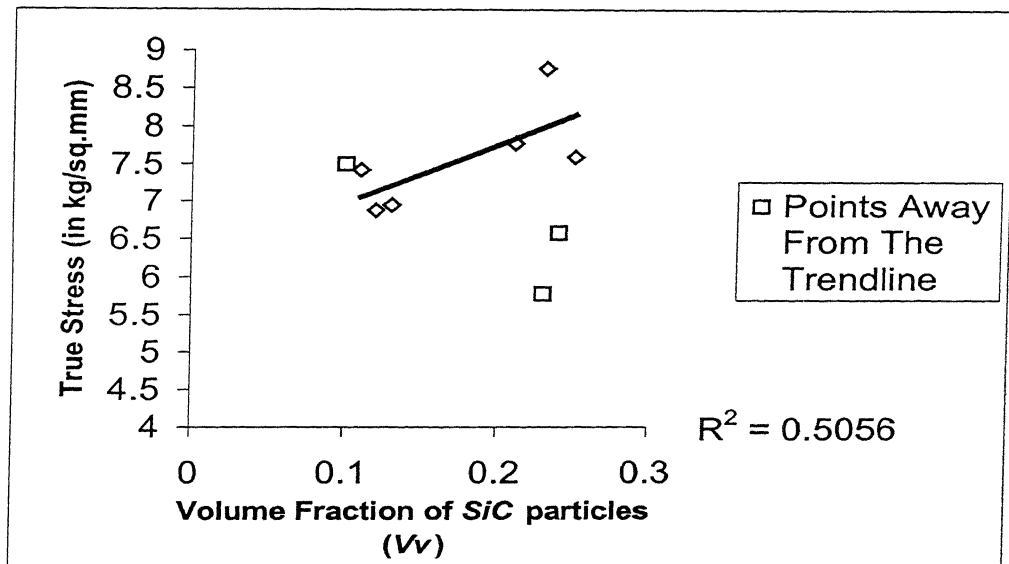


Figure 4.35. Variation of True Stress at 350°C at a strain of 0.015 (corresponding to the flat region of the stress-strain curves) with Volume Fraction.

[It can be seen that as volume fraction increases flow stress increases. Three points corresponding to specimen 7, 5 and 6 are away from the trend]

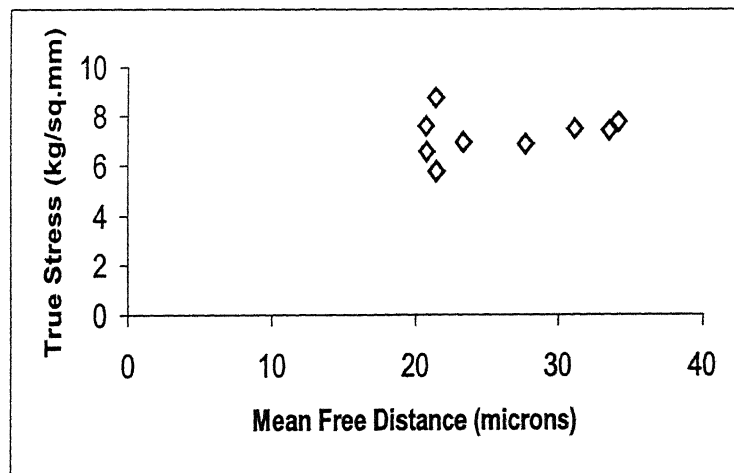


Figure 4.36. Variation of stress at a strain of 0.015 (corresponding to the flat region of the stress-strain curves) with Mean Free Distance (λ).

[It can be seen that the values are not well correlated. There is a very slight variation in the flow stress with mean free distance between particles]

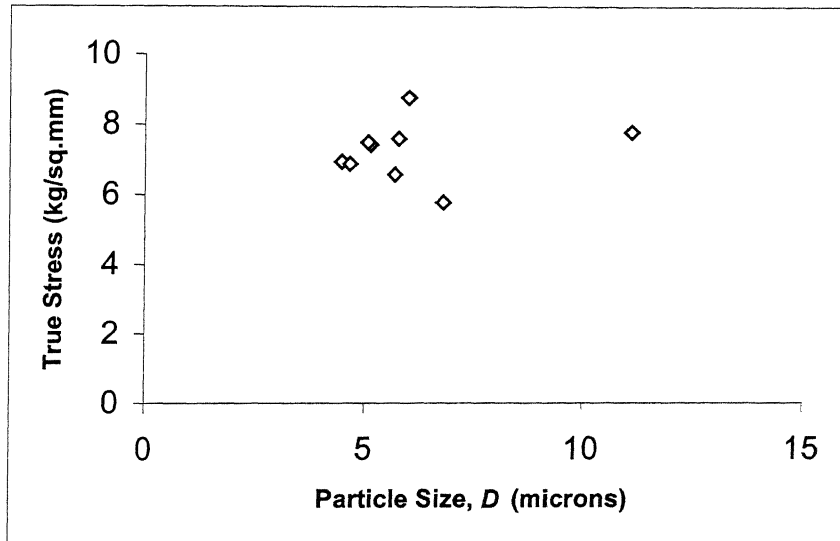


Figure 4.37. Variation of Stress with Particle Size (D) of SiC particles at a strain of 0.015 (corresponding to the flat region of the stress-strain curves)

[It can be seen that the values are not well correlated. There is a very slight variation in the flow stress with mean particle size]

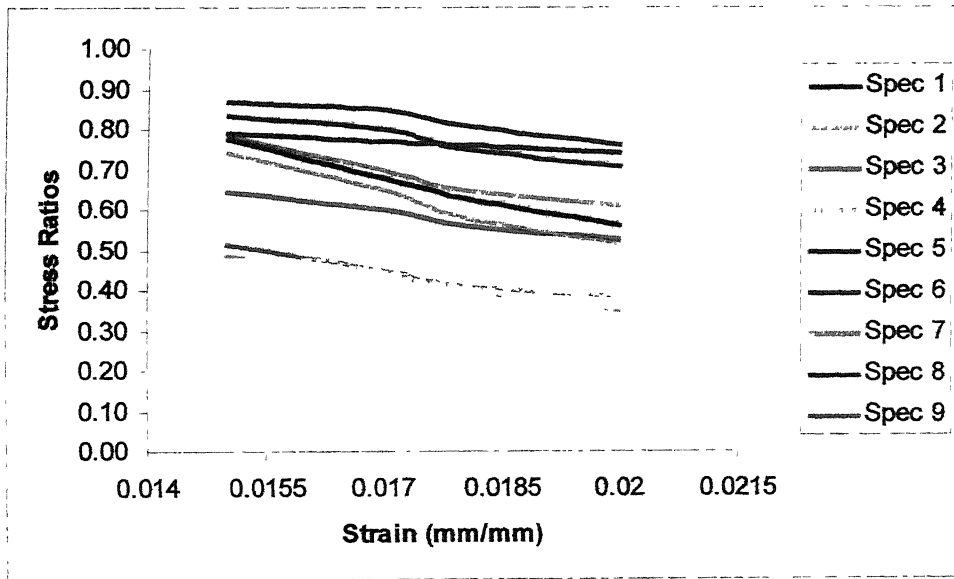


Figure 4.38. Variation of Stress Ratios ($\sigma_{350^{\circ}\text{C}} / \sigma_{150^{\circ}\text{C}}$) with increase in strain

[All the curves have a similar slope. The stress ratios decrease as the strain increase. This reveals that the gap between stress-strain curves at 350°C and 250°C increases]

CHAPTER 5

CONCLUSION

1. Quantitative Stereological Measurements gave an appropriate estimate of the volume fraction of the composites. The volume fraction from Stereology matched with that calculated from the density measurements.
2. The microstructure of the composites consisted of three phases, the Al matrix, The *SiC* particles and the *Si* rich phase. The microstructure also showed non uniform distribution of *SiC* particles.
3. Stress values for the composites decreased with increase in temperature. At higher temperature amount of reinforcement had a little effect on the stress value of the composites.
4. Elastic modulus of the composites is dependent on the volume fraction of the *SiC* particles and is higher for higher volume fraction but was not affected by λ or D .
5. With increase in volume fraction the stress values for the composite rises. However, some samples showed different results. This was attributed due to some of the microstructural feature, which resulted during the fabrication process of the composites.
6. The particle size and the mean free distance (λ) have least effect on the stress value of the composites.
7. The Stress ratios ($\sigma_{350^{\circ}\text{C}} / \sigma_{150^{\circ}\text{C}}$) for strains greater than 0.015 (corresponding to the flat portion of the Stress-Strain curves decreases with increasing strain. This indicates that the gap between stress-strain curves at temperatures 350°C and 150°C increases. This may be attributed to the fact that with the rise in temperature the material exhibit a progressive transition from local plastic flow to bulk flow [11]. Also the rate of strain hardening decreases with the rise in temperature due to increase in the dislocation mobility. In other words, the material undergoes dynamic recovery.

REFERENCE

1. M. Taya, R.J. Arsenault, Metal Matrix Composites- Thermomechanical Behavior, Pergamon Press, Oxford OX3 OBW, England, 1989.
2. K. G. Krieder, Metal Matrix Composites, Academic Press Inc, NY, USA.
3. W. C. Harrigan, Jr., "Metal matrix composites," Metal Matrix Composites-Processing and interfaces, R. K. Everett, and R. J. Arsenault, Academic Press Inc., San Diego, USA, 1991, pp. 1-16.
4. T. W. Clynes, and P. J. Withers, An Introduction to Metal Matrix Composites, Cambridge University Press, UK, 1993.
5. R. B. Bhagat, " Casting fibre reinforced metal matrix composites," Metal Matrix Composites-Processing and interfaces, R. K. Everett, and R. J. Arsenault, Academic Press Inc., San Diego, USA, 1991, pp. 43-84.
6. R. K. Everett, " Deposition technologies for MMC Fabrication," Metal Matrix Composites-Processing and interfaces, R. K. Everett, and R. J. Arsenault, Academic Press Inc., San Diego, USA, 1991, pp. 103-120.
7. D. Lewis, III, " In situ reinforcement of metal matrix composites," Metal Matrix Composites-Processing and interfaces, R. K. Everett, and R. J. Arsenault, Academic Press Inc., San Diego, USA, 1991, pp. 121-150.
8. R. K. Everett, " Diffusion Bonding," Metal Matrix Composites-Processing and interfaces, R. K. Everett, and R. J. Arsenault, Academic Press Inc., San Diego, USA, 1991, pp. 17-42.
9. Z. Wang and R. J. Zhang, " Mechanical behavior of cast particulate SiC/Al (A356) Metal matrix composites," *Metallurgical Transaction A*, 1991, v. 22A, pp. 1585-1594.
10. J. Yang, S. M. Pickard, C. Cady, A. G. Evans and R. Mehrabian, " The stress-strain behavior of aluminium matrix composites with discontinuous reinforcements," *Acta Metallurgica et. Materialia*, 1991, v. 39, n. 8, pp. 1863-1869.
11. P. B. Pragnell, T. Downes, W. M. Stobbs, P. J. Withers, " The deformation behavior of discontinuously reinforced MMCs-I-the initial yielding behavior," *Acta metallurgica and materialia*, 1994, v. 42, n. 10, pp. 3425-3436.

12. R. J. Arsenault, "Tensile and compressive properties of metal matrix composites," Metal Matrix Composites-Mechanism and Properties, R. K. Everett, and R. J. Arsenault, Academic Press Inc., San Diego, USA, 1991, pp. 133-168.
13. D. L. McDanel, "Analysis of stress-strain, fracture, and ductility behavior of aluminium matrix composites containing discontinuous silicon carbide reinforcement," *Metallurgical Transaction A*, 1985, v. 16A, pp. 1105-1115.
14. S. Das, K. Hatsukano, D. P. Mondal, A. H. Yegneswaran, and K. Aoi, "Deformation behavior of aluminium composites: Upsetting and cold indirect extrusion," State of Art in Cast Metal Matrix Composites in the Next Millenium, P.K. Rohatgi, The Minerals, Metals and Material Society, Warendale, Pennysylvania, USA, 2000.
15. D. L. Davidson, "Fracture toughness of particulate metal matrix composites," ,
Metal Matrix Composites-Mechanism and Properties, R. K. Everett, and R. J. Arsenault, Academic Press Inc., San Diego, USA, 1991, pp. 217-234.
16. F. Delannay, "Thermal Stresses and thermal expansion in MMCs," Comprhensive Composite Materials, v. 3, T. W. Clyne, Cambridge University Press, U. K. , 2000, pp. 341-370.
17. D. L. Davidson, "Tensile deformation and fracture toughness of 2014+15vol pct. SiC particulate composites," *Metallurgical Transaction A*, 1991, v. 22A, pp. 113-123.
18. N. Kanetake, M. Narmura, and T. Choh, "Continuous observation of microstrutural degradation during tensile loading in particle reinforced aluminium matrix composites," *Material Science and Technology* , 1995, v.11, pp. 1246-1252.
19. C. P. You, A. W. Thompson, and I. M. Bernstein, "Proposed failure mechanism in discontinuously reinforced aluminium alloy," *Scripta metallurgica*, 1987, v. 21, pp. 181-185.
20. S. V. Kamat, J. P. Hirth, R. Mehrabian, "Mechanical properties of particulate reinforced aluminium matrix composites," *Acta Metallurgica*, 1989, v. 37, n. 9, pp. 2395-2402.
21. M. Manoharan, and S. V. Kamat, "On fracture toughness of particulate metal matrix composites," *Acta Metallurgica*, 1991, v. 25, pp. 2121-2125.

22. H. K. Ahn, and T. Kobayashi, "Fracture toughness evaluation in particulate reinforced aluminium alloy composites," *Scripta Metallurgica*, 1997, v. 37, n. 12, pp. 1973-1978.
23. N. Chawla, C. Andres, J. W. Jones, J. e. Allison, "Effect of SiC volume fraction and particle size on the fatigue resistance of a 2080 Al/SiC composites," *Metallurgical and Materials Transactions A*, 1998, v. 29A, pp. 2843-2854.
24. G. E. Dieter, Mechanical Metallurgy, Mc GrawHill Book Company, UK.
25. J. N. Hall, J. W. Jones, and A. K. Sachdev, "Particle size, volume fraction and matrix strength effects on the fatigue behavior and particle fracture in 2124 Al-SiCp composites," *Material Science and Engineering*, 1994, A183, pp. 69-80.
26. R. J. Arsenault and S. B. Wu, "A comparison of PM vs melted SiC/ Al composites," *Scripta Metallurgica*, 1988, v. 22, pp. 767-772.
27. V. C. Nardone, and K. M. Prewo, "On strength of discontinuous silicon carbide reinforced aluminium composites," *Scripta Metallurgica*, 1986, v. 20, pp. 43-48.
28. C. W. Nan, and D. R. Clarke, "The influence of particle size and particle fracture on the elastic/plastic deformation of metal matrix composites," *Acta Metallurgica*, 1996, v. 44, n. 9, pp. 3801-3811.
29. Y. Flom, and R. J. Arsenault, "Effect of particle size on fracture toughness of SiC/Al composite materials," *Acta Metallurgica*, 1989, v. 37, n. 9, pp. 2413-2423.
30. M. S. Hu, "Some effects of particle size on the flow behavior of Al-SiCp composites," *Scripta Metallurgica*, 1991, v. 25, pp. 695-700.
31. J. J. Lewandowski, "Fracture and fatigue of particulate MMCs," Comprehensive Composite Materials, v. 3, T. W. Clyne, Cambridge University Press, U. K. , 2000, pp. 151-188.
32. S. G. Sang, N. Shi, G.T. Gray III, and J. A. Roberts, "Reinforcement shape effects on the fracture behavior and ductility of particulate reinforced 6061-Al metal matrix composites," *Metallurgical and Materials Transaction A*, 1996, v. 27A, pp. 3739-3746.
33. J. D. Boyd, and D. J. Lloyd, "Clustering in particulate MMCs," Comprehensive Composite Materials, v. 3, T. W. Clyne, Cambridge University Press, U. K. , 2000, pp. 139-150.

34. J. Boselli, P. D. Pitcher, P. J. Gregson, and Sinclair, "Quantitative Assessment of particle distribution effects on short crack growth in SiCp reinforced Al-alloys," *Scripta Materialia*, 1998, v. 30, n. 5, pp. 893-844.
35. I. C. Stone, and P. Tsakiropoulos, "Characterization of spatial distribution of reinforcement in powder metallurgy route Al-SiCp metal matrix composites," *Material Science and Technology*, 1995, v. 11, pp. 213-221.
36. C. W. Nan, R. Birringer, and H. Gleiter, "On effect of particle size distribution on elastic/plastic deformation of metal matrix composites," *Scripta Materialia*, 1997, v. 37, n. 7, pp. 969-976.
37. T.H. Yip, and Z. Wang, "Effect of particle distribution on the deformation behavior of particulate metal matrix composites," *Material Science and Technology*, 1997, v. 13, pp. 125-134.
38. M. Geni, and M. Kikuchi, "Damage analysis of aluminium matrix composites considering non-uniform distribution of SiC particles," *Acta Materialia*, 1998, v. 46, n. 9, pp. 3125-3133.
39. M. Manoharan, and J.J. Lewandowski, "Crack initiation and growth toughness of an aluminium metal matrix composites," *Acta Metallurgica and Materialia*, 1990, v. 38, n. 3, pp. 489-496.
40. J. J. Lewandowski, C. Liu, And W. H. Hunt, Jr, "Effect of matrix microstructure and particle distribution on the fracture toughness of an aluminium metal matrix composites," *Material Science and Engineering*, 1989, A107, pp. 241-255.
41. D. J. Lloyd, and I. Jin, "Melt processed aluminium matrix particle reinforced composites," *Comprehensive Composite Materials*, v. 3, T. W. Clyne, Cambridge University Press, U. K. , 2000, pp. 555-578.
42. P. Rohatgi, "Cast Metal Matrix Composites," *Metals Handbook*, ASM International, v.15, pp.840-845.
43. D. J. Lloyd, H. Lagace, A. McLead, and P. I. Morris, "Microstructural aspects of aluminium-silicon carbide particulate composites produced by a casting method," *Material Science and engineering*, 1989, A107, pp. 73-80.

44. S. Lee, D. kwan, D. Suh, “ Microstructure and fracture of SiC-particulate reinforced cast A356 Aluminium alloy composites,” *Metallurgical and Materials Transaction A*, 1996, v. 27A, pp. 3893-3901.
45. Y. H. Kim, S. Lee, N. J. Kim, and K. Cho, “Effect of microstructure on the tensile and fracture behavior of cast A356 Al/SiCp composites,” *Scripta Metallurgica and Materillia*, 1994, v. 31, n. 12, pp. 1629-1634.
46. P. A. Karnezis, G. Durrant, B. Cantor, and E. D. Palmiere, “ Mechanical properties and microstructure of twin roll cast Al-7Si/SiC MMCs,” *Mqterial Science and Technology*, 1995, v. 11, pp. 741-751.
47. C.S. Park, M. H. Kim, and A. Lawly, “Microstructure and wear response of spray cast Al-Si/SiCp composites,” *The International Journal of Powder Metallurgy*, 1999, v. 35, n. 1, pp. 41-50.
48. P. A. Karnezis, G. Durrant, and B. Cantor, “ Microstructure and tensile properties of Squeeze cast SiC particulate reinforced Al-7Si alloy,” *Material Science and Technology*, 1998, v. 14, pp. 97-107.
49. I. Georghe, and H. J. Rack, “ Powder Processing of metal matrix composites,” Comprehensive Composite Materials, v. 3, T. W. Clyne, Cambridge University Press, U. K. , 2000, pp. 679-700.
50. M. K. Jain et. al, “ Processing , microstructure, and properties of 2124 Al-SiCp composites,” *The International Journal of Powder Metallurgy*, 1993, v. 29, n. 3, pp. 267-275.
51. Ervin. E. Underwood, Quantitative Stereology, Addison-Wesley Publishing Company, 1970.

ABSTRACT

Silicon Carbide particulate reinforced Aluminium matrix composites comprise a new generation materials whose properties can be tailor made for a particular application. These composites not only possess high specific strength and modulus at room and elevated temperatures but also have excellent wear resistance, high thermal conductivity, low coefficient of thermal expansion, good dimensional stability and low density. These materials also exhibit isotropy unlike continuous fibre reinforced composites. These are much easier and less expensive to fabricate through conventional casting and rolling process. The potential applications for such composites include aerospace, automobile, electronic packaging and sporting goods. Some typical applications include missile fins, inertial guidance control components, precision laser mirror substrate, piston in diesel engines, brake calipers, thermal management materials etc.

One of the major concerns to these materials is the variability in the properties. For example, two composites with same volume fraction may have different mechanical properties, especially the extreme properties like UTS and fracture toughness. This has been attributed to the fact that the flow properties of the matrix are altered by the presence of second phase particles (silicon carbide). Hence the volume fraction, size, shape and spatial distribution (for instance clustering or patches of matrix) of the SiC particles have a considerable effect on the flow properties of the matrix. Some of these microstructural parameters, especially the particle distribution depends on the type of processing used. In order to predict the extreme properties a detailed microstructural characterization is needed.

The present MTech desertation work involves quantitative microstructural characterization and correlation with the mechanical properties of these materials. High temperature compression test and measurement of elastic modulus were performed to determine the mechanical properties of the composites. Microstructure was analyzed

using optical and scanning electron microscope and stereological measurements including volume fraction, surface area per unit volume were carried out.

The composites used for investigation were provided by US industries and were manufactured by patented processes by two different routes- Permanent Mold Casting and Sand Casting. Densities for the sample have been measured using an Analytical Balance by the concept of Archimedes Principle. An Ultrasonic Flaw detector (KRAUTKRAMER-BRANSON USI P12) was used to determine the elastic modulus of the samples. The compression tests were carried out using Material Test System (MTS). The samples were tested at three temperatures of 150⁰C, 250⁰C, and 350⁰C and Stress-Strain Plots were obtained. The specimens were prepared by advanced metallographic specimen preparation techniques for microstructural characterization. The microstructural parameters that have been measured include volume fraction (V_v), surface area per unit volume (S_v), connectivity, mean free path, and particle size. All these parameters have been measured using Digital Image Analysis. The project work aims at correlating the above mentioned microstructural parameters with Elastic Modulus and Yield Stress of the composites under study.

A 137955

137955

Date Slip

The book is to be returned on
the date last stamped.

| | |
|--|--|
| | |
| | |
| | |
| | |
| | |
| | |
| | |
| | |
| | |
| | |
| | |
| | |
| | |
| | |
| | |

